A: ALPHA ACTIVITY OF NATURAL SAMARIUM

B: A SEARCH FOR NEUTRONIC NUCLEI

A: ALPHA-ACTIVITY OF NATURAL SAMARIUM

B: A SEARCH FOR NEUTRONIC NUCLEI.

by

MOOLCHAND GUPTA, B.Sc., M.Sc.

A Thesis

Submitted to the Faculty of Graduate Studies

in Partial Fulfilment of the Requirements

for the Degree

Doctor of Philosophy

McMaster University

October 1967

DOCTOR OF PHILOSOPHY (1967)

McMASTER UNIVERSITY
Hamilton, Ontario

TITLE: A: Alpha-activity of Natural Samarium

B: A Search for Neutronic Nuclei

AUTHOR: Moolchand Gupta, B.Sc. (Agra University)

M.Sc. (Rajasthan University)

SUPERVISOR: Dr. R. D. Macfarlane

NUMBER OF PAGES: x, 131

SCOPE AND CONTENTS:

The alpha-activity of natural samarium has been studied using an ionization chamber. A gridless ionization chamber has been developed in order to obtain high resolution and high sensitivity. The half lives and the energies of the alpha decay of Sm^{147} and Sm^{148} were measured where as the alpha-activity of Sm^{149} and Sm^{146} could not be detected.

Experiments were carried out in order to search for the existence of Particle stable neutron clusters in the range of Mass 6-10 as a component of a nuclear reactor flux and as the product of high energy proton spallation of heavy nuclei.

ACKNOWLEDGEMENTS

I wish to express my sincere thanks to Professor Ronald D. Macfarlane for his inspiration and the guidance in the conduct of this research. My thanks are also due to Drs. M. A. Preston and C. J. L. Lock for their time and interest in serving as my thesis supervisory committee.

My thanks are due to the members of the Nuclear Research Shop, in particular Messers. T. Brydon and H. Howell for their help in design and fabrication of the ionization chamber. I would also like to express my appreciation to the members of the Nuclear Reactor for their co-operation.

I also like to acknowledge the contribution of Dr. N. S. Oakey on electronic problems and Mr. H. S. Samant for moral support.

I am grateful to Messers. S. D. Garg and S. D. Gupta for their financial help and encouragement which helped me to come to Canada. My father, Shri Shivcharan D. Goyal deserves thanks for his persistent encouragement and the sacrifices of his own comforts during my studies.

I thank Miss Linda Kisslinger, who was responsible for the typing of this thesis.

Above all I thank God for the blessings of an education and resources bestowed upon me.

TABLE OF CONTENTS

LIST OF TABLES

LIST OF ILLUSTRATIONS

CHAPTER I

INTRODUCTION

1.1 General.

From the study of the mass defect curves it has been noted that most of the isotopes with a mass number greater than 140, are alpha-unstable. Radioactive decay by this mode is commonly observed in both natural and artificial isotopes of the elements with proton number, Z, greater than 82. Prior to 1949, most alpha-decay studies were made for nuclides having $Z \geq 82$. In the region $Z < 82$, Hoffmann (Hof-21) was the first to detect alpha-activity which he believed to be of natural Pt. Alpha-emitting nuclides in the rare earth region were first discovered by Hevesy and Pahl (Hev-32) in 1932. Thereafter the radiations emitted by natural samarium were studied by many workers (Ras-50, Wea-50, Jes-50). Few alpha-emitters are known in the naturally occuring rare earth nuclides because the alpha-decay energy is low and because the decay rate depends on the decay energy in an exponential manner as formulated by Gamow (Gam-29) and Condon and Gurney (Con-29).

Kohman in 1949 (Koh-49) predicted, by the study of alpha-particle binding energies in this region, that the neutron deficient isotopes of medium heavy elements might exhibit alpha-activity. From a study of mass data, it is observed that the alpha-decay

energy increases with decreasing number of neutrons for a given Z and is maximum for the nuclides with 84 neutrons.

In 1949 Thompson and co-workers (Tho-49) discovered alpha-activity in neutron deficient isotopes of Au, Hg, Gd, and Dy. Afterwards much work in this region, was done by Rasmussen, Thompson and Ghiorso (Ras-53). Dunlavey and Seaborg (Dun-53) produced Sm^{146} and Toth and Rasmussen (Tot-60) discovered alpha-emitting isotopes of Dy. Extensive studies were made by Kauw, Porschen and Riezler (Por-54, Rie-57) using the nuclear emulsion technique, by Macfarlane and Kohman (Mac-61) using a cylindrical ion-chamber and by Karras and Siivola (Kar-60, Sii-62) using a gridded ionization chamber.

Artificially prepared nuclides near 82 neutron closed shell have also been investigated by Macfarlane and co-workers (Mac-62, Mac-63, Mac-64, Mac-65). Siivola (Sii-66), Graffe et. al. (Gra-61), Karras (Kar-63) also have made contributions using solid state barrier detectors.

1.2 Objective of the Study.

1.2.1 Development of an Ionization Chamber for studying alpha-emitters of very low specific activity.

The first objective of this work was to develop a technique for studying natural alpha-emitters of very low specific activity; using a large, low background cylindrical ionization chamber. At the same time an attempt was made to achieve a high resolution

and high sensitivity.

1.2.2 To obtain precise measurements of the alpha-particle energy and half life of samarium-147.

It is important to obtain precise half-life and alpha-particle energy for samarium-147, so that it can be used as a standard in studying other alpha-decaying isotopes since in the region of about 2 MeV no other natural alpha-emitters are known.

1.2.3 Search for alpha-activity in samarium-148 and Sm^{149}.

From the mass data (Mat-65) it is possible to evaluate the available alpha-particle energy (E_α) for these isotopes. The results are given below:

$$Sm^{148}\ E_\alpha = 1.950 \pm 0.005 \text{ MeV.}$$

$$Sm^{149}\ E_\alpha = 1.848 \pm 0.002 \text{ MeV.}$$

These results suggest that it might be possible to observe a measurable alpha activity in the isotopes Sm^{148} and Sm^{149}. The alpha-particle energy for these isotopes is smaller than the Sm^{147} alpha-particle energy. Therefore a high energy resolution is needed to resolve these activities from the more prominent Sm^{147} activity.

1.2.4 Search for the evidence of samarium-146 alpha-activity in natural samarium.

Sm^{146} is probably the longest lived extinct natural nuclide. It is beta stable and decays by alpha-emission with a half life of

$(8.5 \pm 1.2) \times 10^7$ years and has an alpha-particle energy of (2.46 ± 0.02) MeV (Fri-63). Its half life suggests that it does not exist in nature, but the recent work of Graeffe et.al. (Gra-64) suggests that though Sm^{146} does not exist in nature there is a possibility of its formation because of Super-nova explosions in our galaxy. Also, the possibility of (n,2n) reactions on Sm^{147} by cosmic-ray neutrons is another way that Sm^{146} would be present in natural samarium in detectable amounts.

1.2.5 Calculations of Alpha-reduced Widths.

A comparison will be made of experimental alpha-reduced widths, using the Bethe formula and different forms of the alpha-nuclear potentials of the isotopes under study.

1.3 Summary of Earlier Investigations on Alpha-activity of Natural Samarium.

1.3.1 Previous results.

The natural radioactivity of samarium was discovered by von Hevesy and Pahl (Hev-32) in 1932. Thereafter the radiations emitted by Sm were studied by several investigators. It was found to be alpha-radioactive and its particle energy and specific activities were measured. All available data about alpha-activity of Sm are presented in Table 1.1 in chronological order, in which the specific activity refers to natural Sm and the half life to Sm^{147}.

1.3.2 Mass Assignment of the Natural Activity of Samarium.

The first attempt of a mass assignment of the samarium alpha-alpha-activity was made by M. Curie and F. Joliot in 1934 (Cur-34).

SUMMARY OF THE EARLY WORK ON Sm ACTIVITY:

TABLE 1.1

Investigators	Alpha-Energy E_α (MeV)	Sp. Activity dis/gm/sec.	Half life x 10^{11} years	Method of investigation	Reference
Hevesy, G. V. Pahl, M.	2.20	75	1.8	Geiger counter	Hev-33
Herzfinkel, M. Wroncberg, A.	2.10	67	2.1	Ion chamber	Her-34
Curie, M. Joliot, F.	2.80	88	1.5	Cloud chamber	Cur-34
Ortner, G. Schintlmeister, J.	2.25			Ion chamber	Ort-34
Mader, M.	2.30	89	1.5	Ion chamber	Mad-34
Lyford, D. Beardon, J.	2.90	102	1.3	Ion chamber	Lyf-34
Libby, W. F.	2.40	140	0.95 ± 0.07	Prop. counter	Lib-34
Tayler, H. J.	2.20			Nuclear Emulsion	Tay-35
Hoseman, R.	2.20	89	1.5	Nuclear Emulsion	Hos-36
Lewin, L.	2.20			Ion chamber	Lew-36
Cuer, F. Lattes, C. M. G.		94	1.3 ± 0.12	Nuclear Emulsion	Cue-46

Investigators	Alpha-Energy E_α (MeV)	Sp. Activity dis/gm/sec.	Half life x 10^{11} years	Method of investigation	Reference
Piccioto, E.		133	1.0 ± 0.06	Nuclear Emul	Pic-49
Haenny, Ch. Najar, M. Gaillourd, M.	2.20			Nuclear Emulsion	Hae-49
Jesse, W. P Saduskis, J.	2.18			Ion chamber	Jes-50
Szteinsznaider, D.	2.12			Nuclear Emulsion	Szt-53
Beard, G. Wiedenbeck, M.		108	1.25 ± 0.06	Prop. counter	Bea-54
Leslie, G. E.	2.18	115	1.15 ± 0.03	Nuclear Emulsion	Les-56
Beard, G. Kelly, W. H.		103	1.28 ± 0.04	Scin. counter	Bea-58
Macfarlane, R. D.	2.24	113	1.18 ± 0.05	Ion chamber	Mac-59
Vorobe'v, A. A. Komar, A. P. Korole'v, V. A. Solyakin, G. E.	2.19			Ion chamber	Vor-60
Karras, M.	2.20	115	1.16 ± 0.05	Ion chamber	Kar-60a
Karras, M. Nurmia, M.	2.20	117	1.14 ± 0.05	Ion chamber	Kar-60b

Investigators	Alpha-Energy E_α (MeV)	Sp. Activity dis/gm/sec.	Half life x 10^{11} years	Method of investigation	Reference
Macfarlane, R. D. Kohman, T. P.	2.23	116	1.15 ± 0.05	Ion chamber	Mac-61
Graeffe, G. Nurmia, M.	2.23		1.14	Ion chamber	Gra-61
Wright, P. M. Steinberg, E. P. Glendnin, L. E.		125	1.051 ± 0.02	Scin.counter	Wri-61
Siivola, A.	2.23			Ion chamber	Sii-62
Donhoffer, D.		126.93	1.04 ± 0.03	Scin. counter	Don-64
Valli, K. Aaltonen, J. Nurmia, M. Poyhonen, R.	2.231	122	1.08 ± 0.02	Ion chamber and Scin. counter	Val-65

From mass data they concluded that most likely the alpha-emitting isotope is Sm^{148}.

In 1938 Wilkings and Dempster (Wil-38) reported that the alpha-tracks from various separated isotopes laid down on a photographic plate appear to start from mass 148. In 1948 Dempster (Dem-48) reported that the active isotope was mass 152.

The possibility of samarium-146 being the active isotope in natural samarium was ruled out by Ingrahm, Hess and Hayden (Ing-48). They observed mass spectroscopically that Sm^{146} in natural Sm was less than 0.002 percent.

In 1949 Dempster (Dem-49) again carried out the mass assignment and reported that the alpha-emitting isotope is almost certainly the isotope at mass-147. In 1950 Weaver (Wea-50) by the study of alpha-activity of enriched isotopes of samarium concluded that the alpha-activity of natural samarium is because of mass-147.

In 1950 Rasmussen and co-workers (Ras-50) obtained an isotopically pure Sm^{147} by an ion-exchange separation from Pm^{147} (β^- -emitter). The samarium sample was then analysed in an optical spark spectrograph to establish its purity (to ensure it was pure Sm). The alpha-activity of this sample was measured by an ionization chamber. An alpha-activity with the same energy, as obtained for natural samarium, was observed.

1.3.3 Previous results on the alpha-activity of Sm^{148} and Sm^{149}.

The alpha-activity of natural samarium was shown to be caused primarily by Sm^{147}. However, systematics predict that Sm^{148} and Sm^{149} might also be alpha-active.

Macfarlane and Kohman (Mac-59 and Mac-61) using an enriched sample of Sm^{148} and Sm^{149} attempted to detect alpha-activity from these isotopes with an ion-chamber but they did not see any activity. In 1960 Karras (Kar-60) also using an ion chamber reported the alpha-particle energies and half lives for these isotopes. Macfarlane et.al. and Karras's results are summarized in Table 1.2.

The mass spectrometric values of the (Mat-65) alpha-particle energies (E_α) of these isotopes are:

Sm^{148} $E_\alpha = 1.95 \pm 0.005$ MeV.

Sm^{149} $E_\alpha = 1.848 \pm 0.002$ MeV.

1.3.4 Previous results of the possibility of the existence of Sm^{146} in natural samarium and alpha-activity of Sm^{146}.

Mass spectrometeric studies were carried out by Inghram Hess and Hayden, in order to detect Sm^{146} in natural samarium. They could not detect and set an upper limit $2 \times 10^{-3}\%$ for its isotopic abundance in nature (Ing-48).

Collins, Rourke and White using a more sensitive mass spectrometer set a limit of less than $8 \times 10^{-5}\%$ (Col-57). In 1952 Long, Pool and Kundu (Lon-52) reported a low intensity alpha-activity in old samples of Nd bombarded with deuterons and

TABLE 1.2

Samarium-148		Samarium-149	
Macfarlane et al	Karras	Macfarlane et al	Karras
$T_{1/2} > 2.4 \times 10^{14}$ years for $1.5 < E < 2.0$ MeV.	$T_{1/2} = (1.2 \pm 0.3) \times 10^{13}$ years	$T_{1/2} > 1.1 \times 10^{15}$ years for $1.5 < E < 2.0$ MeV.	$T_{1/2} = (4 \pm 2) \times 10^{14}$ years
$T_{1/2} > 2.4 \times 10^{13}$ years for $2.0 < E < 2.14$ MeV.	$E_\alpha = 2.14 \pm 0.03$ MeV.	$T_{1/2} > 1.1 \times 10^{14}$ years for $2.0 < E < 2.14$ MeV.	$E_\alpha = 1.84 \pm 0.05$ MeV.

suggested that it was caused by Sm^{146}. They calculated its half life to be between 10^4 and 10^6 years.

In 1953, Dunlavey and Seaborg (Dun-53) succeeded in producing Sm^{146} by bombarding natural Nd with 40 MeV alpha-particles. They reported that it emitted alpha-particles of 2.55 MeV and its half life was $\sim 5 \times 10^7$ years.

In 1959, Macfarlane and Kohman (Mac-59, Mac-61) searched for Sm^{146} alpha-activity in natural samarium using a large cylindrical ionization chamber. No activity was found and an upper limit of 1.3×10^{-2} dis/(gm x sec) was set for the specific activity in natural samarium. Vorobev, Komar, Korolev and Solyakin (Vor-60) reported an indication of its existence although it was not statistically significant. They established an upper limit 0.03 dis/(gm x sec) for its specific activity in natural samarium.

Macfarlane repeated his work (Mac-60) using an isotopically enriched sample but could not detect any activity. Karras and Nurmia (Kar-60b) using nuclear abundance systematics calculated the half life of Sm^{146} and gave the most probable value of 3×10^8 years. Friedman, Milstead, and Harkness (Fri-63) reported it to be 8.5×10^7 years.

Recently Nurmia et.al. (Nur-64) redetermined the Sm^{146} alpha-particle energy and the half life. Sm^{146} was produced by (n,2n) and (γ,n) reactions on Sm^{147}. The reported half life and alpha-particle energy were $(7.4 \pm 1.2) \times 10^7$ years and 2.46 MeV

respectively. It was concluded that the half life of Sm^{146} is too short to be present in nature. Friedman et.al. (Fri-66) reported that the half life of Sm^{146} determined by the isotope dilution method is $(1.026 \pm 0.048) \times 10^8$ years.

1.4 Kinetics of Alpha-decay

1.4.1 Introduction

The quantum theory of alpha decay was treated independently by Gamow (Gam-29) and Condon and Gurney (Con-29). Their one body model treatment gave quite adequate results on half lives of even-even nuclei. Half lives for alpha transitions proceeding from even-even nuclei to the ground state of the daughter nuclei in heavy elements agree well with this 'one body' model. A similar treatment can be applied in rare earth region.

In this simple theory, the barrier is pictured as a potential made up of a Coulomb potential,

$$V = \frac{2Ze^2}{r}$$

where Z is the proton number of the daughter nucleus, e is electronic charge and r is the distance between the alpha-particle and daughter nucleus with a sharp cut off at a certain radius. The alpha-particle confined in a barrier makes frequent collision with the wall and has a probability for penetrating the barrier. The decay constant λ is expressed as

$$\lambda = f.P$$

where f is the frequency factor, expressed as collisions per second with the wall of the barrier, P is the quantum probability factor. The penetration factor, P, has been evaluated quite extensively. In this work the Bethe formula (Bet-37) has been used.

1.4.2 The Bethe Formula

In Bethe's derivation, using the WKB approximation the penetration factor P for a definite angular momentum ℓ is given by

$$P = \exp\left[-\frac{2}{\hbar}\int_{R}^{R_E}\left(2M\left(\frac{2Ze^2}{r} + \frac{\ell(\ell+1)\hbar^2}{2Mr^2} - Q_{eff.}\right)\right)^{1/2} dr\right]$$

where Z is the atomic number of the daughter nucleus and

$Q_{eff.}$ = Total effective decay energy of the bare nucleus. This is the alpha-particle energy plus recoil energy plus electron screening correction. The electron screening correction is given by

$$E_{sc} = 65.3\ (Z+2)^{7/5} - 80\ (Z+2)^{2/5}\ eV \qquad 1.4.1$$

M = Reduced mass of the system.

R_E = Outer classical turning point and is evaluated from

$$\frac{2Ze^2}{R_E} + \frac{\ell(\ell+1)h^2}{2MR_E^2} - Q_{eff.} = 0$$

Before P can be evaluated numerically R (effective radius) must be known and is assumed to be $\sim 1.5 \times A^{1/3}$.

1.4.3 Nuclear potential

The Coulomb potential with a sharp cutoff at some effective radius is not a realistic potential. To obtain a more significant treatment of alpha decay data, Rasmussen (Ras-59) used a potential derived from alpha-scattering. The potential used was deduced by Igo from an optical model analysis of alpha-scattering data (Igo-58). The nuclear potential V(r) consists of an exponential expression for the real part of the nuclear potential valid in the surface region for

$$|V| \leq 10 \text{ MeV}$$

$$V(r) = -1100 \exp\left(-\left(\frac{r-1.17A^{1/3}}{0.574}\right)\right) \text{ MeV} \qquad 1.4.2$$

where r is in fermis.

Using this nuclear potential Rasmussen calculated the probability, P,

$$P = \exp\left(-\frac{2}{\hbar}\int_{R_i}^{R_E}\left(2M\left(V(r) + \frac{2Ze^2}{r} + \frac{l(l+1)\hbar^2}{2Mr^2} - Q_{eff.}\right)\right)^{1/2}dr\right) \qquad 1.4.3$$

The quantity R_i, is the inner classical turning point and is calculated by equating the expression within the integral to zero.

However, Poggenberg (Pog-65) has questioned the representation of the alpha nuclear potential by Igo potential because the Igo potential is a well of infinite depth which does not connect reasonably with the form of the usual shell model nuclear potentials. Therefore, he has used the Woods-Saxon potential

having for the real part the usual form

$$V(r) = - \frac{74}{(1+\exp(\frac{r-R_o}{0.565}))} \qquad 1.4.4$$

In the above equation the parameter R_o is taken to be $(1.17\ A^{1/3} + 1.6)$ fm where 1.6 fm is the alpha size. For the calculation of P from equation (1.4.3), V(r) is replaced by equation (1.4.4).

1.4.4 Momentum Dependance of Nuclear Potential

The nuclear part of the barrier, in the above calculations of P, has been considered to be purely static; while Chaudhury (Cha-63) has suggested that the nuclear potential is momentum dependent. He has taken a interaction kernel possessing a non-local part which is approximated by a delta δ_b function and is represented by Gaussian,

$$\delta_b = \pi^{-3/2}\ b^{-3}\ \exp(-(r-r')/b)^2$$

where b is the extent of non-locality and is chosen to be 0.902×10^{-13} cm.

Using the approximation Chaudhury calculated the penetrability factor,

$$P = \exp\left[-\frac{2}{\hbar}\int_{R_i}^{R_E}\left[2M((V(r) + \frac{2Ze^2}{r} - Q_{eff.}) \cdot c\ (r) + \frac{(l(l+1)\hbar^2)}{2Mr^2}\right]^{1/2} dr\right] \qquad 1.4.5$$

where $c\ (r) = (1 + \omega.V(r))^{-1}$. In this expression ω is defined as

$$\omega = \frac{Mb^2}{2\hbar^2}$$

and V(r) is taken as the Igo-Potential (equation 1.4.2).

1.4.4 The Reduced Alpha-Width

Rasmussen (Ras-59) has defined the quantity δ^2 which is called the reduced alpha-width or in short reduced width. δ^2 is given by

$$\delta^2 = \frac{h\lambda}{P} .$$

The reduced width δ^2 as a first approximation, should be constant for even (ground state transitions) and favoured alpha-decay. The experimental δ^2 is evaluated by computing P from equations (1.4.3, 1.4.4, and 1.4.5) and the experimental half life.

For odd mass nuclides, the hindrance factor, F, is defined as:

$$F = \frac{\delta_1^2 + \delta_2^2}{2\delta_{odd}^2}$$

where δ_1^2 and δ_2^2 are the reduced widths for ground state transitions for nearest or next nearest even nuclei and δ_{odd}^2 is the reduced width for odd mass in question with $\ell = 0$. The hindrance factor is a factor by which a given alpha group decays more slowly than would be calculated by barrier penetration theory normalized to the ground state transition rates of even nuclei.

CHAPTER II

DESCRIPTION OF THE APPARATUS

2.1 Ionization Chamber

2.1.1 General Considerations:

Naturally occuring rare earth alpha-emitting nuclides have a very low specific activity. Therefore for a detectable count rate it is necessary to use a source of the order of a few milligrams. Of the many available methods of alpha-spectrometry only pulse ionization chambers are capable of accommodating more than a few milligrams of material. The achievement of high energy resolution requires the use of a very thin source, i.e. of the order of 10 micro-grams per cm^2. Therefore the area of the chamber should be made large in order to achieve high resolution and measurable count rates.

Parallel plate, gridded-pulse ionization chambers and cylindrical chambers using large area have been described by many authors, (Hil-61, Osb-64, Mac-61, Bun-49 and Wil-50). For the present work an ionization chamber with and without a grid was designed.

In principle gridded ionization chambers are used to minimize the positive ion effect. But with a concentric arrangement of electrodes, however, the need for a grid as a means of reducing positive ion-effect can be largely obviated if the

Figure 2.1 Diagram of ionization chamber.

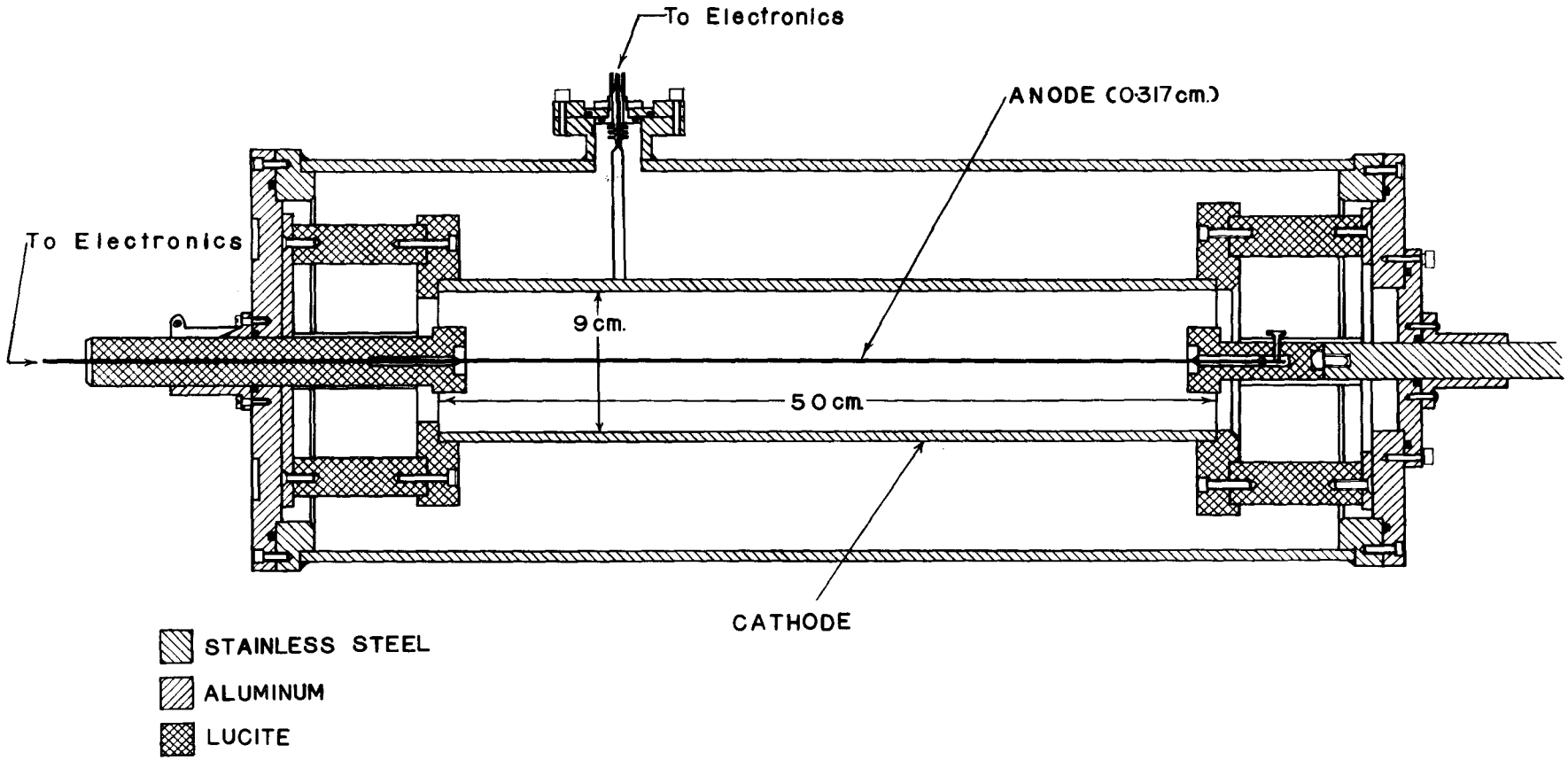
To Electronics
ANODE (0·317cm.)
To Electronics
9 cm.
50 cm.
CATHODE
STAINLESS STEEL
ALUMINUM
LUCITE

alpha tracks and associated positive ion column can be confined to the region of comparatively low field close to the negative electrode. Therefore, an ionization chamber with the above requirements was designed.

2.1.2 Description of the Counter

(a) Ionization Chamber with out Grid:

This instrument consists of two concentric cylindrical electrodes of length 50 cm. The outer electrode (cathode) is a stainless steel cylinder of diameter 9 cm and the collector electrode a stainless steel rod of diameter 3.17 mm. The ionization chamber is shown in figure 2.1.

The total effective area of the cathode is about 1400 cm^2. The collector electrode is strung through the full length and runs through the axis of the cathode cylinder. The cathode is supported by lucite rings inside a steel cylinder of 25.4 cm diameter and 65 cm length. The lucite rings are supported on both ends by four lucite rods of 2.54 cm diameter which are screwed on the aluminium end plates of the outer cylinder. The collector is supported on one side by a lucite rod and on the other side by a stainless steel rod of diameter 2.54 cm.

The aluminium end plate, on the stainless steel rod side, has an opening of 10 cm diameter for the insertion of the sample. After introducing the sample this is closed by another aluminium end plate which is held vacuum tight by

means of 'O' -Rings. The stainless steel supporting rod is fixed to the base of the counter. On one side there is an outlet of 0.625 cm diameter with a Hoke valve for continuous flow operation.

The lucite rod supporting the collector is held vacuum tight by an 'O' -Ring. The collector protrudes through the rod and is sealed by "epoxy cement". The collector is directly connected to the preamplifier. At this end, there is a 3.75 cm diameter outlet with a flange for evacuating the counter.

The cathode is connected by means of phosphore bronze strip to the high voltage terminal (BNC-UG634/U at the top of the counter and is held vacuum tight by 'O' -Rings.

(b) Ionization Chamber with Grid:

A grid which fits in the dimensions of the ionization chamber was also built. It is a cylindrical wire grid and surrounds the collector electrode. The distance between grid and collector is 1.3 cm. The grid is made of nichrome wires with diameter 0.100 mm and spaced 0.315 mm apart. Both ends are connected to lucite plates and are held inside the chamber by lucite rods in a manner similar to that used for the collector electrode.

The grid can be easily installed or removed from the ionization chamber.

2.2 Counting Gas:

When high energy charged particles, e.g. alpha-particles, interact with gases, they expend most of their energy by exciting and ionizing the atoms or molecules. The average energy expended in producing an ion-pair (W) for most gases is between 20 to 40 eV. In alpha-spectroscopy, argon is generally used which has a value of 26.4 eV. (Ionization potential of Ar = 15.5 eV).

It has been reported that the convenient method for converting excited Ar atoms into ion-pairs is by adding a gas with a lower ionization potential than the energy of the 1^{st} excited state of the argon atoms, i.e. a gas with lower ionization potential than 11.6 eV. The ionization potentials of C_2H_2 and C_2H_4 are 11.40 and 10.80 eV respectively (Bor-63, Vor-63).

The work of Bortner et. al. (Bor-63) have shown that addition of 0.5% acetylene to argon reduces W to 20.35 eV.

The pertinent processes in argon and its additive gases are given in Appendix I.

Most commercial source of gases are contaminated with traces of oxygen or other electronegative impurities which result in the loss of electrons because of capture by these impurities. Facchini et. al. (Fac-56) have suggested the addition of small amounts of nitrogen, which reduces the capture cross-section of electrons by oxygen or other

Figure 2.2 Effect of the concentration of

(a) acetylene

(b) nitrogen

on the resolution of the ion-chamber.

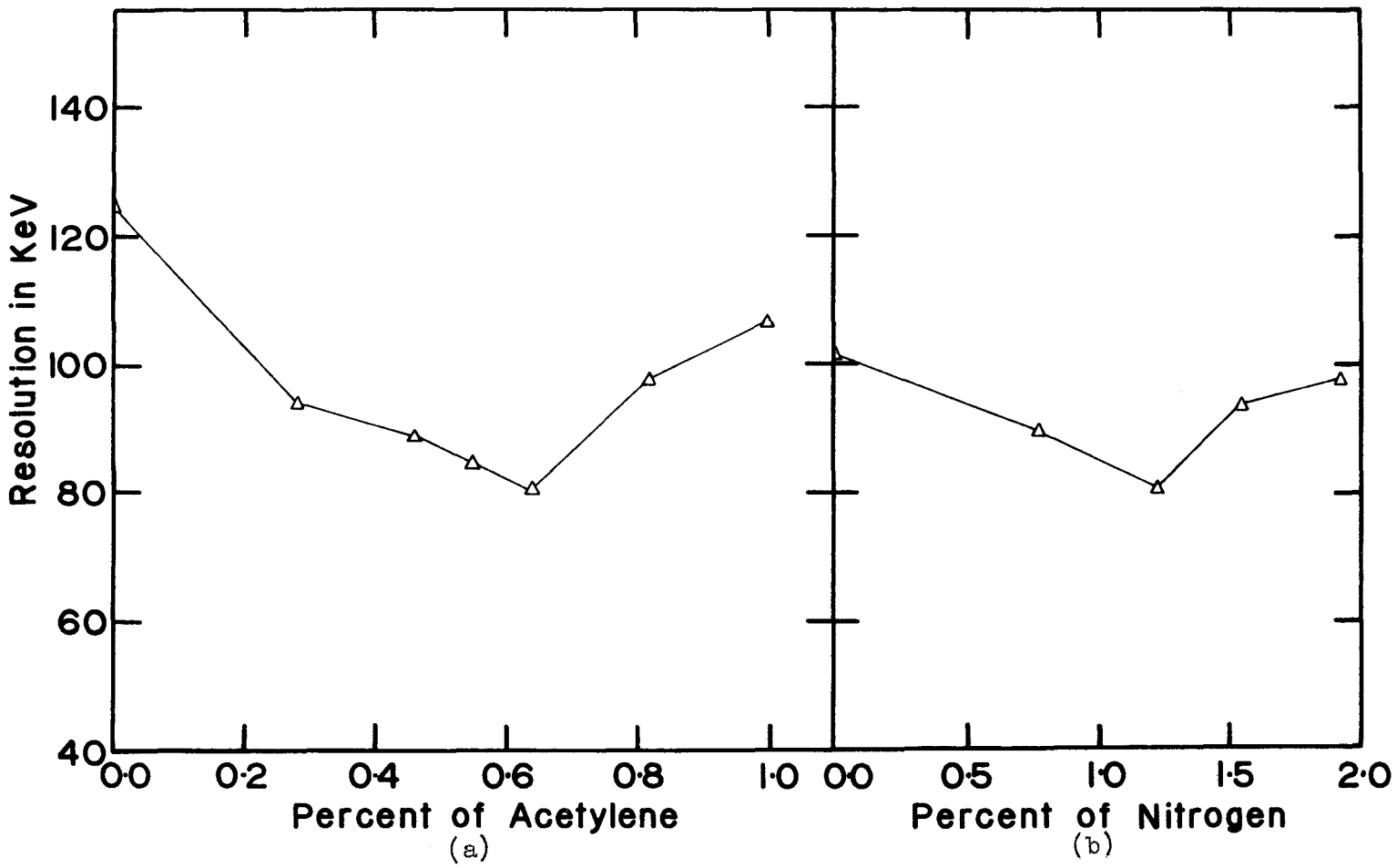
Resolution in KeV
140
120
100
80
60
40
0·0
0·2
0·4
0·6
0·8
1·0
Percent of Acetylene
(a)
0·0
0·5
1·0
1·5
2·0
Percent of Nitrogen
(b)

electronegative impurities by controlling the velocity of the electrons.

In order to achieve good energy resolution a mixture of argon, acetylene and nitrogen was used. The results of various concentrations of acetylene and nitrogen are shown in figure 2.2. The resolution of the counter is determined by using U^{235} and U^{236} and the counter was operated at a total pressure of 226 cm. It was found that the best resolution is achieved when the gas mixture consists of 0.64% acetylene and 1.2% nitrogen and the balance argon.

2.3 Operation of the Counter:

The operation of the counter was studied by using Am^{241} and Ra^{226} sources at various pressures. Am^{241} and Ra^{226} spectra were recorded for the argon, acetylene and nitrogen gas mixture and a 90% argon and 10% methane gas mixture. The results for various pressures are shown in figure 2.3. The alpha-spectra for Ra^{226} and Am^{241} are given in figure 2.4 (a) for 10% methane and 90% argon and in figure 2.4 (b) for 0.6% acetylene, 1% nitrogen and 98.4% argon.

At a pressure of 400 cm, the best resolution is achieved for both gases. The operating voltages were adjusted such that ion-recombination is a minimum and no electron multiplication occurs. An anode voltage of 1500 volts and a cathode voltage of-1445 volts were used. At higher pressures recombination becomes a serious problem.

Figure 2.3 Effect of pressure on resolution, using

□ 10% methane and 90% argon

Δ 0.6% acetylene, 1% nitrogen and 98.4% argon

as counting gas.

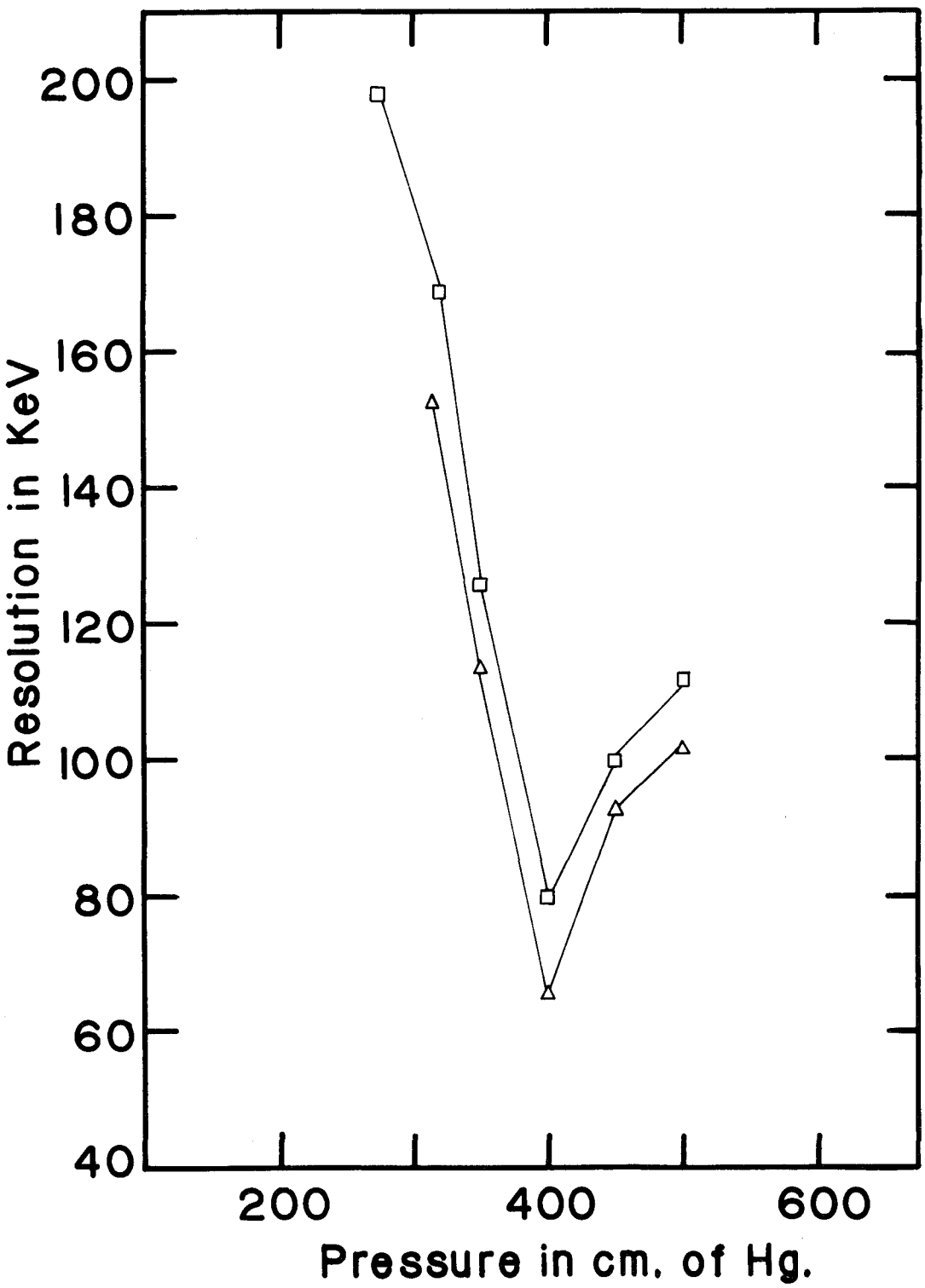
200
180
160
140
120
100
80
60
40
Resolution in KeV
200
400
600
Pressure in cm. of Hg.

Figure 2.4 Alpha spectrum of Ra^{226} and Am^{241} obtained by using

(a) 0.6% acetylene, 1% nitrogen and 98.4% argon gas mixture

(b) 10% methane and 90% argon mixture at 400 cm pressure.

A and C - Ra^{226}

B and D - Am^{241}

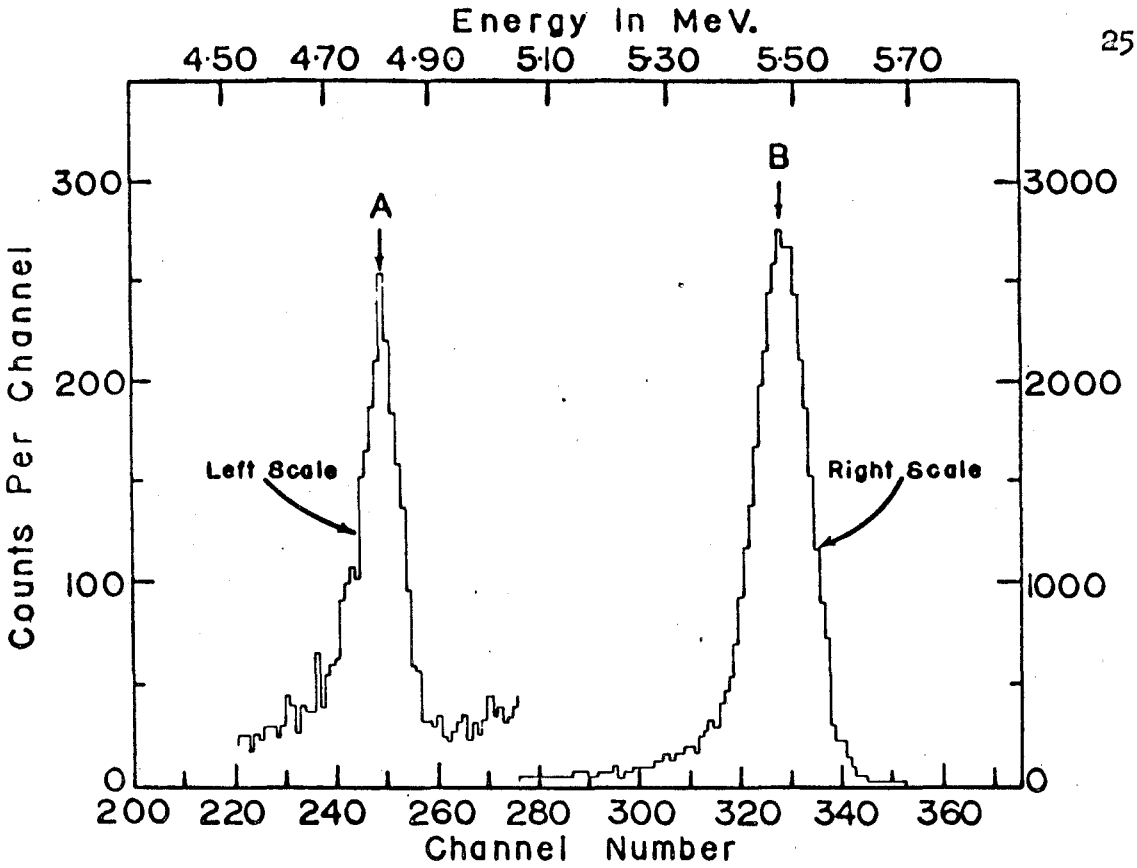
Energy In MeV.
4·50 4·70 4·90 5·10 5·30 5·50 5·70
A
B
Left Scale
Right Scale
Counts Per Channel
300
200
100
0
3000
2000
1000
0
200 220 240 260 280 300 320 340 360
Channel Number

(a)

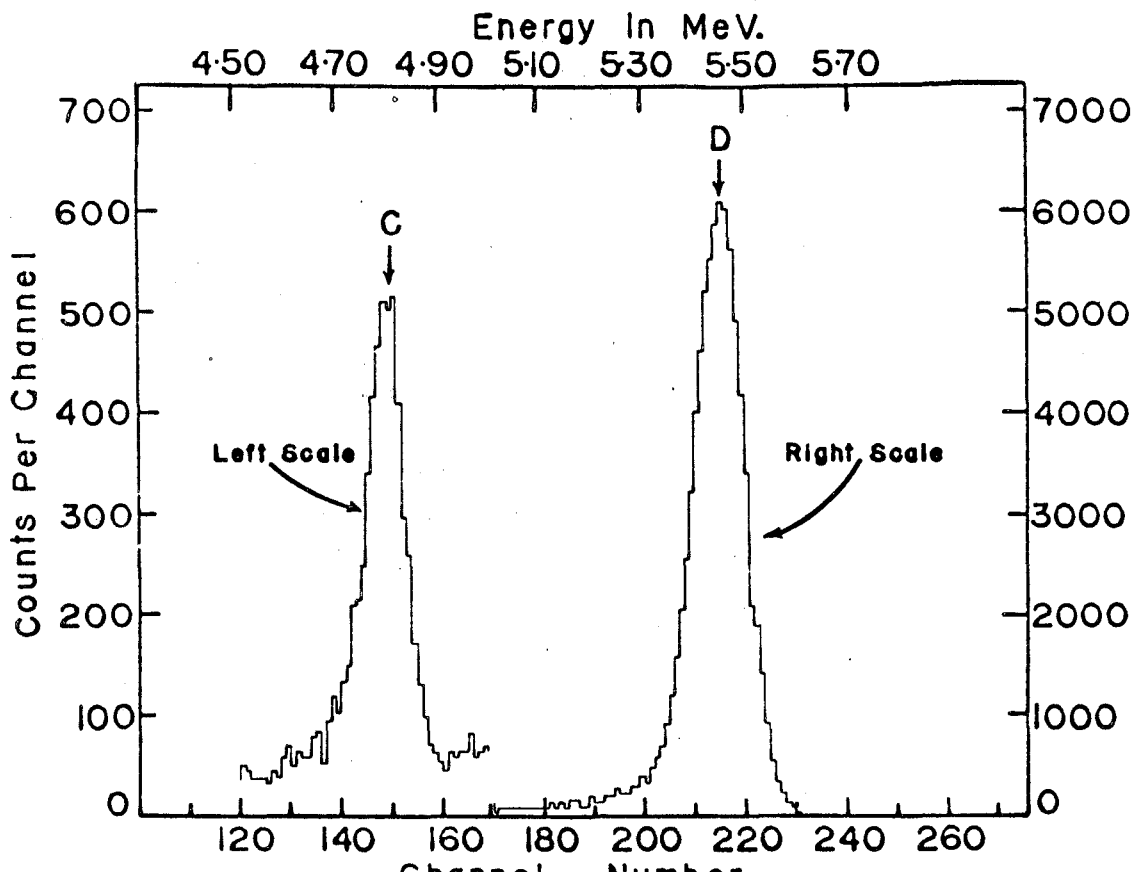
Energy In MeV.
4·50 4·70 4·90 5·10 5·30 5·50 5·70
C
D
Left Scale
Right Scale
Counts Per Channel
700
600
500
400
300
200
100
0
7000
6000
5000
4000
3000
2000
1000
0
120 140 160 180 200 220 240 260
Channel Number

(b)

There is, however, an advantage in operating the ionization chamber at higher pressures because the radial distribution of the tracks is smaller and there is a decrease positive-ion effect.

For Sm^{147} and other rare earth alpha-emitters the counter was operated at a relatively low pressure (226cm of Hg) because the range of alpha-particles of Sm^{147} is much shorter than those of Am^{241} or Ra^{226}. The results for samarium-147 with and without a grid are shown in figure 2.5. The resolution obtained for the gridded ion-chamber was 60 KeV where as for un-gridded chamber it was 48 KeV.

Experiments were also performed to determine its drift stability. Operating under static conditions for a period of 2 days it drifted in energy about 10 KeV, i.e., 0.5% of its original value. This slight drift may be caused by oxygen out gassing from the sample. If the counter is operated as a flow counter at pressure 226cm with a flow rate 8 cc/min, no detectable drift is observed.

2.4 Pulse Shapes:

In order to determine the important characteristics of the counter a study was made of the characteristic pulse shapes. A 100-C Tennelec preamplifier, which has no internal pulse shaping, was used to study the pulse shapes of the alpha-pulses in the chamber. Pulse shapes were first recorded for the gridded ion chamber.

Figure 2.5 Alpha spectrum of Sm^{147} from

(a) without grid

(b) with grid ion-chamber.

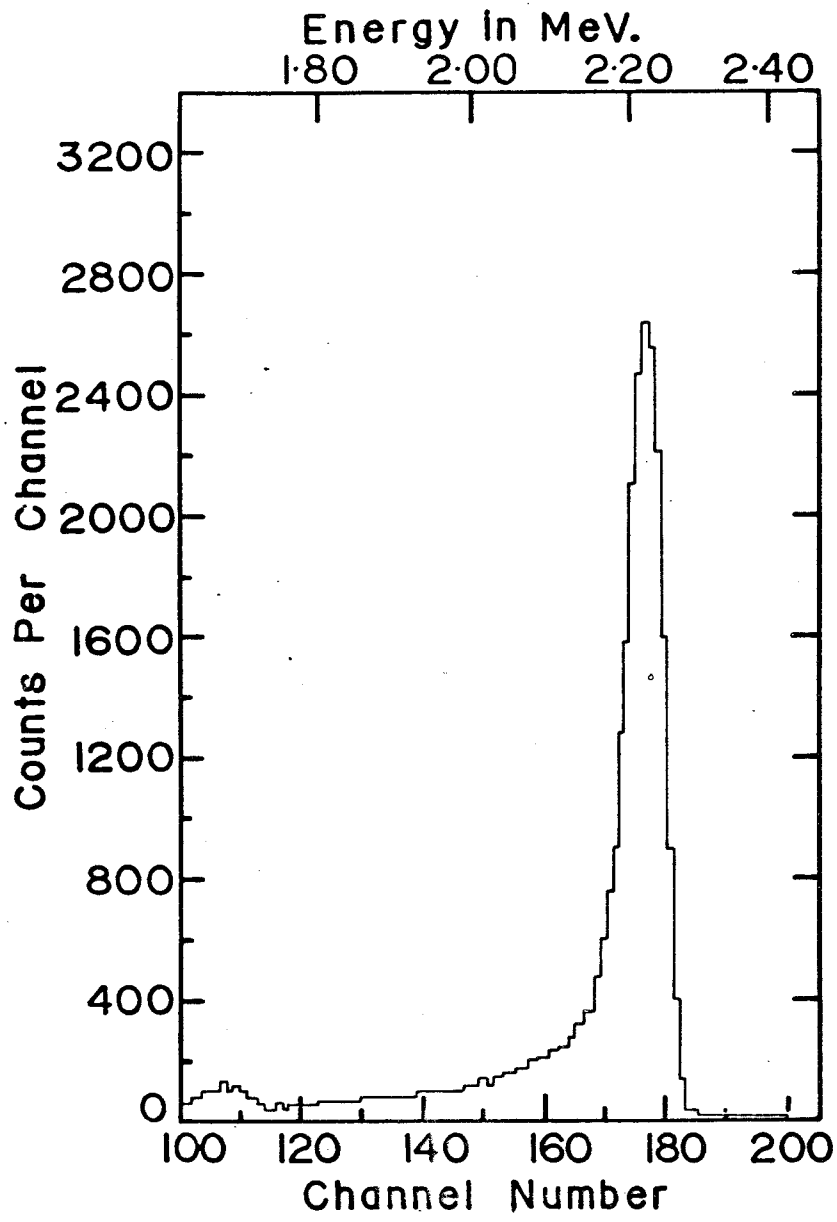
Energy in MeV.
1·80
2·00
2·20
2·40
3200
2800
2400
2000
1600
1200
800
400
0
Counts Per Channel
100
120
140
160
180
200
Channel Number

(a)

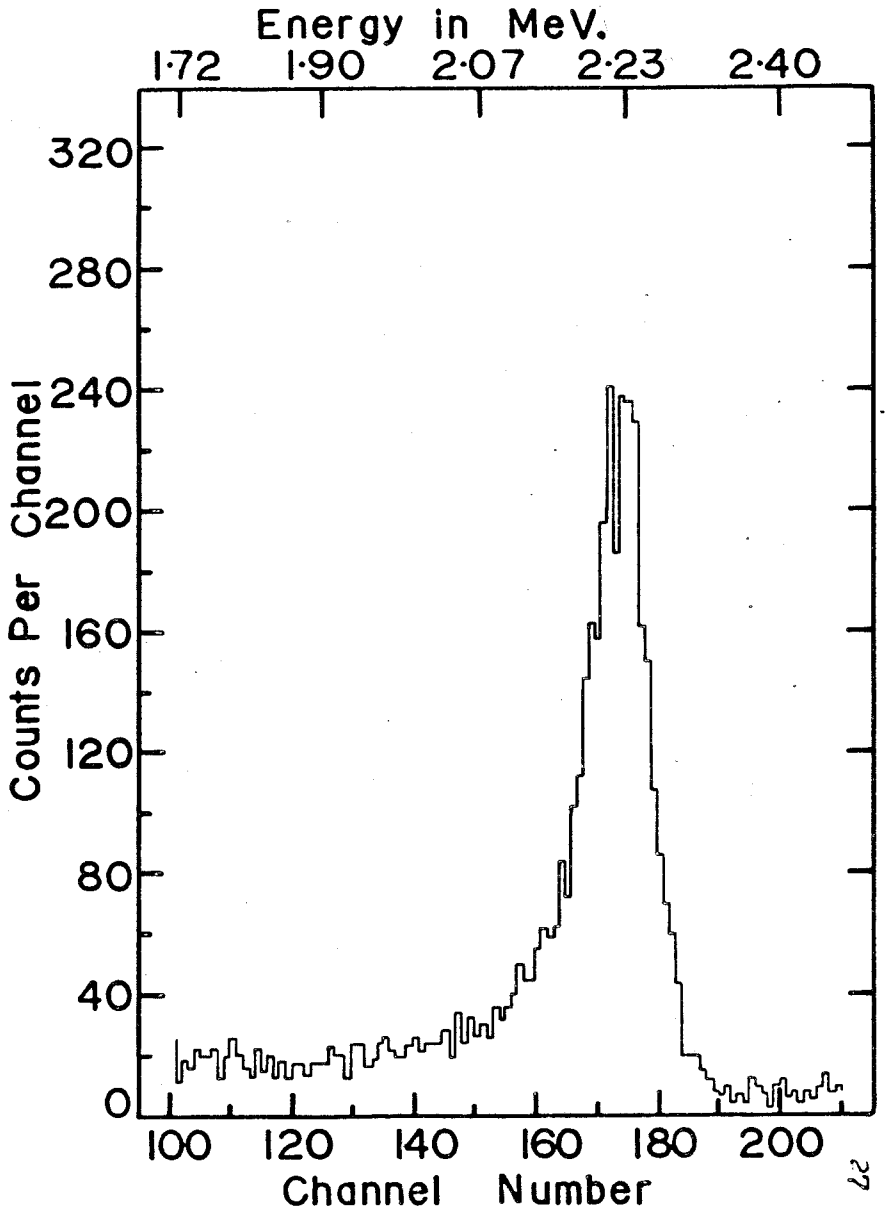
Energy in MeV.
1·72
1·90
2·07
2·23
2·40
320
280
240
200
160
120
80
40
0
Counts Per Channel
100
120
140
160
180
200
Channel Number

(b)

The pulse shapes are shown in figure 2.6. Figure 2.6 (a) shows the pulse shape using a 10% methane and 90% argon mixture. Figure 2.6 (b) for a 0.6% acetylene, 1% nitrogen and 98.4% argon mixture.

The pulse shape for the ungridded ion chamber are shown in figure 2.7 for the two different gas mixtures.

The pulse shape in the gridded ion chamber is much smaller than the chamber without the grid. This is because the total capacitance of the ungridded chamber is smaller than that of the grid system. Also there is a small amount of charge collection on the grid which tends to reduce the pulse height.

For a cylindrical geometry, the maximum pulse obtainable from the chamber $P(\tau)$ in terms of τ is

$$P(\tau) = \frac{2}{3 \ln b/a} \cdot \ln\left(\frac{1}{1-\tau}\right)$$

where a and b are the radii of inner and outer electrodes and on the τ scale the pulse height is now approximately unity and the biggest value of $\tau = \left[1-\left(\frac{a}{x_o}\right)^{3/2}\right]$.

x_o = distance of the center of gravity of the alpha tracks from the axis of the chamber.

If $x_o >> a$, the value of τ will be nearly unity.

$P(\tau)$ varies logarithmically with x_o. Therefore, if radial distribution of the tracks is small, the pulses will have a small rise time. Under this condition there would be minimum positive ion effect. For ionization chambers with cylindrical geometry, operating at high

Figure 2.6 Pulse shapes in the ionization chamber with grid.

(a) Pulse shape in 10% methane and 90% argon mixture.

(b) Pulse shape in 0.6% acetylene, 1% nitrogen and 98.4% argon mixture.

PULSE SHAPES IN THE IONIZATION CHAMBER WITH GRID

Scale

Horizontal	1 microsec/div
Vertical	0.05 volts/div

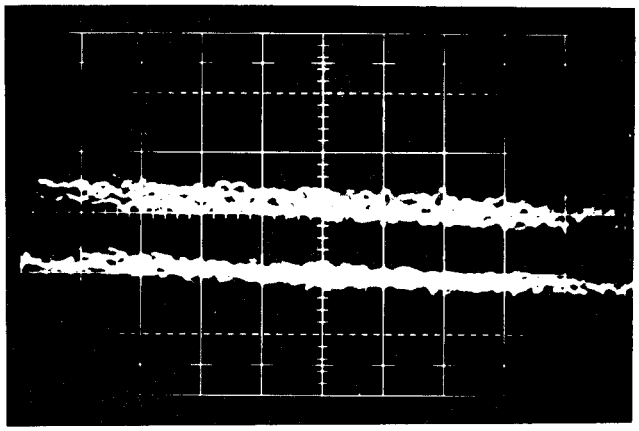

Pulse shapes in 90% Argon and 10% Methane

(a)

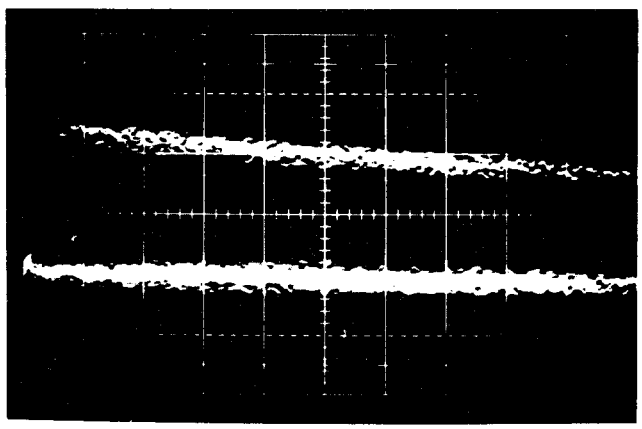

Pulse shapes in 0.6% Acetylene, 1.0% Nitrogen and 98.4% Argon

(b)

Figure 2.7 Pulse shapes in the ionization chamber without grid.

(a) Pulse shapes in 10% methane and 90% argon mixture.

(b) Pulse shapes in 0.6% acetylene, 1% nitrogen and 98.4% argon mixture.

PULSE SHAPES IN THE IONIZATION CHAMBER WITHOUT GRID

Scale

Horizontal	1 microsec/div
Vertical	0.1 volts/div

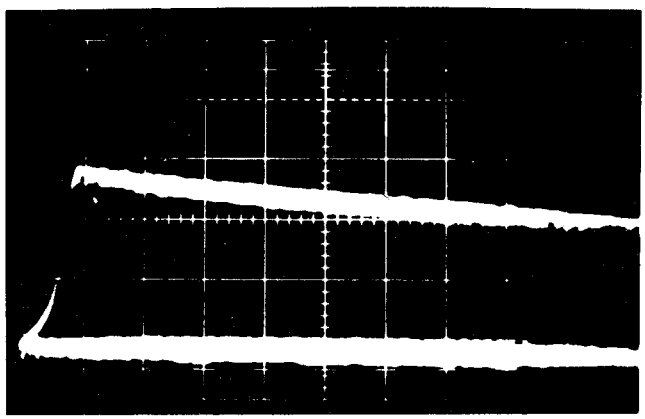

Pulse shape in 90% Argon and 10% Methane

(a)

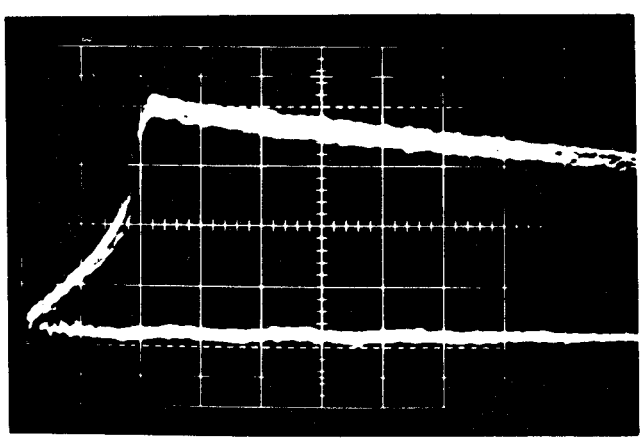

Pulse shape in 0.6% Acetylene, 1.0% Nitrogen and 98.4% Argon

(b)

pressures has the same effect as operating with a grid.

From the measured pulse shapes it is also apparent that the pulse height is higher for the $Ar-C_2H_2-N_2$ mixture by a factor of about 1.25. This is a result of the increase of ionization caused by interactions of C_2H_2 with metastable Ar atoms.

2.5 Resolution of the Counter System

2.5.1 Resolution of the Ion-Chamber.

The ion-chamber produces pulses of variable size having a Poisson distribution. This distribution arises from several effects which will be treated separately. The difference between the observed resolution and that which we shall calculate represents, for the most part, the contribution from fluctuations due to positive ions produced in the initial ionization.

Figure 2.8 (a) Alpha-spectra shapes as calculated from equation (II-4) for different source thickness.

(b) Shift of line peak as a function of source thickness.

In (a), the values of h/R corresponding to

A 0.001

B 0.002

C 0.003

D 0.004

E 0.006

F 0.008

G 0.01

H 0.02

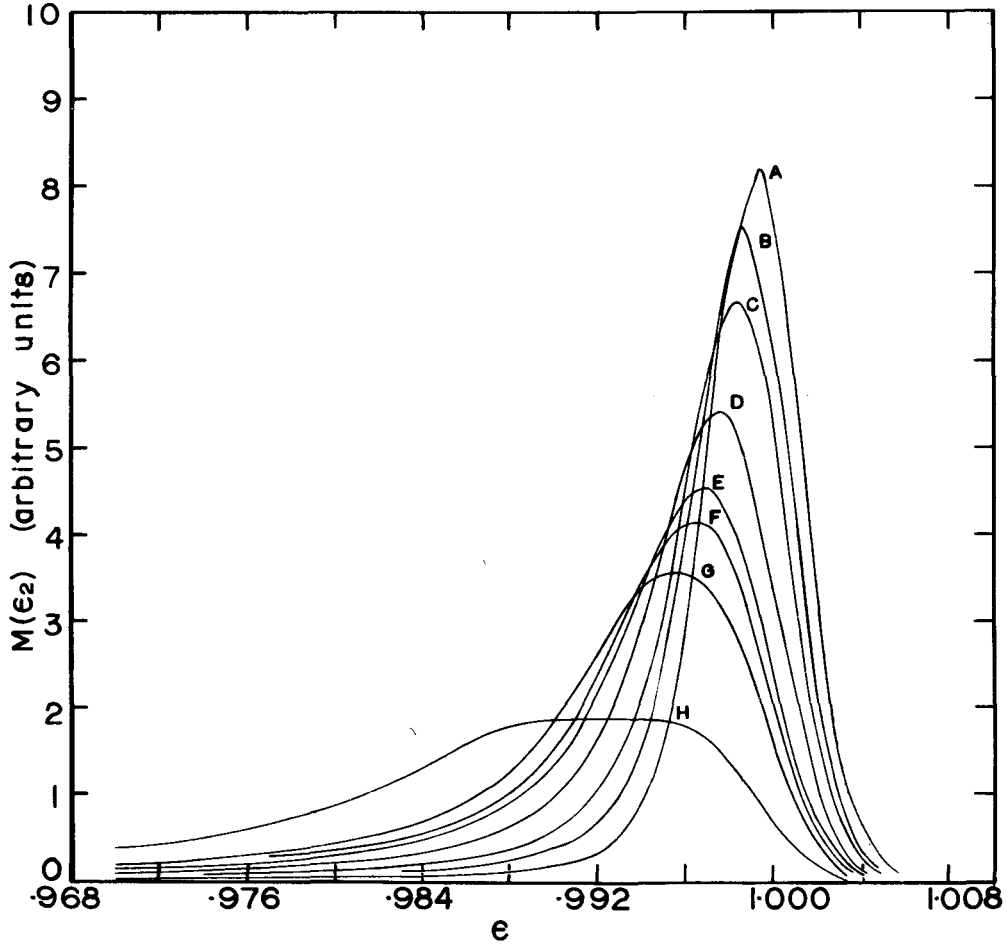

(a)

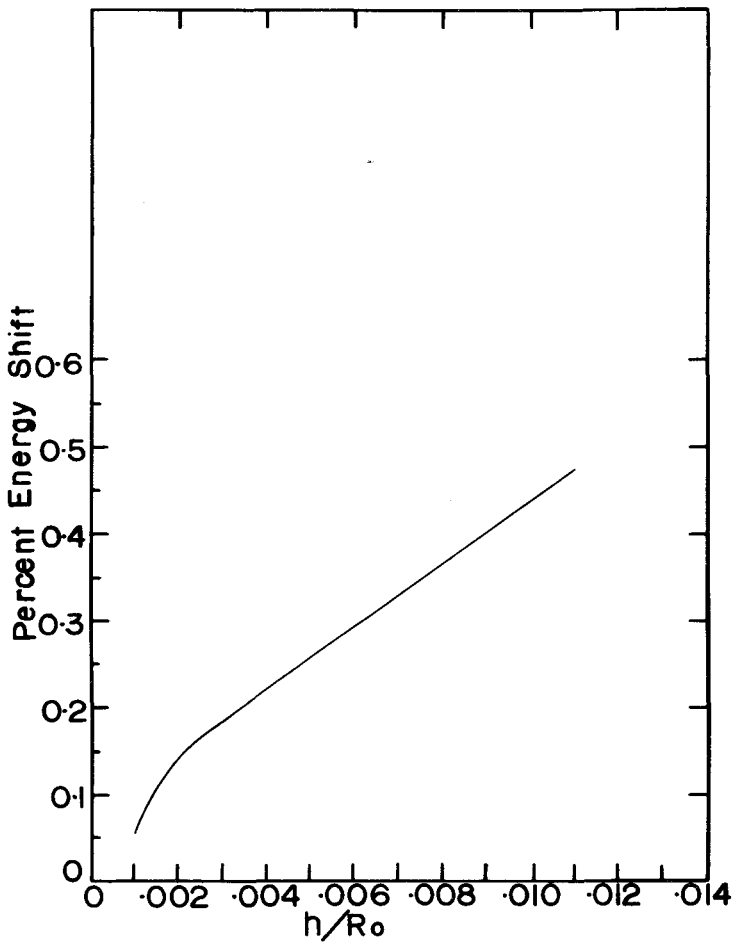

(b)

2.5.2 Total Resolution of the Alpha-Spectrometer

Poor resolution may be caused by effects other than the intrinsic statistical resolution of the chamber. These include the following:

(a) Statistical variation in the energy of alpha-particles leaving the sample.

A detailed study of this was made by Kocharov et. al. (Koc-61). Calculations of the effect of the source thickness on the resolution are given in Appendix II. The experimentally observed spectrum, $M(\epsilon_2)$, can be expressed analytically and is given by equation (II-4)

$$M(\epsilon_2) = \frac{N_o n}{4\sqrt{2\pi}\,\sigma}\left[\frac{h}{R_o}\int_o^{\epsilon} \exp(-(\epsilon_2-\epsilon_1)^2/2\sigma^2)\cdot \frac{\epsilon_1^{n-1}}{(1-\epsilon_1^{n})^2}\cdot d\epsilon_1 + \frac{R_o}{h}\int_{\epsilon}^{1} \exp(-(\epsilon_2-\epsilon_1)^2/2\sigma^2)\cdot \epsilon_1^{n-1}\cdot d\epsilon_1\right] \quad \text{II-4}$$

where

N_o = Total number of radioactive atoms in a sample of of thickness h mg/cm^2.

σ = Standard deviation.

R_o = Range of the alpha-particles at full energy.

ϵ = Ratio of the energy E to full energy E_o.

n = 1.5

Equation II-4 has been numerically integrated for different values of h using an IBM 7040 computer. The σ is taken to be the spread due to the noise and the rise time. The integration was performed from 0 to ϵ by Simpson's rule taking 250

intervals at each value of ϵ_2 and for ϵ to 1 by the Gauss quadrature method in 140 intervals at each value of ϵ_2. $M(\epsilon_2)$ has been calculated as a function of ϵ_2 for different values of h. The results are shown in figure 2.8 (a).

In figure 2.8 (b) the energy shift is plotted as a function of h/R_o. From this, for a known value of h, the energy spread due to finite source thickness can be estimated.

An experimental alpha-spectrum of Sm^{147}, using a $26.68 \mu g/cm^2$ thick sample is shown in figure 2.5 (b). The energy spread caused by this source thickness is calculated to be 15 KeV.

(b) Statistical variation of the number of ion-pairs formed in an ion-chamber.

When an alpha-particle enters the ion-chamber, a number of ion-pairs are produced in the sensitive volume of the chamber. Actually the total ionization produced by an alpha-particle fluctuates. Fano (Fan-47) estimated the mean square fluctuation in the number of ion-pairs and he gave the equation

$$\delta_N^2 = F N_o$$

δ_N^2 is the mean square fluctuation in ionization, N_o is the total number ion-pairs formed and F is the Fano-factor. For an acetylene-argon mixture F = 0.09 (Vor-63). Therefore, $\Delta E = 2.35 \times (F.E.W)^{1/2}$ for Sm^{147} alpha-particles.

$$\Delta E = 6 \text{ KeV}.$$

(c) Finite rise time of alpha-pulses.

If the amplifier contains a smoothing time constant t_1, differentiation time constant t_2 and the rise time of the pulses is T, then the energy spread because of this finite rise time is given by

$$\frac{\Delta E}{E} = \frac{T^2}{24 t_1 \cdot t_2} \qquad \text{(Han-59)}$$

For our experiments with Sm^{147}, T = 2 μ sec and for the TC 110 Tennelec preamplifier used, $t_1 = t_2 = 4$ μ sec. Therefore, ΔE, because of the finite rise time of the alpha-particles is 22 KeV.

(d) Electronic noise.

This is an important factor affecting the energy resolution. It was estimated from the energy spread of a pulse from a pulser. It was found that this factor contributes 35 KeV.

The contribution of all the factors to the energy resolution is shown in Table 2.1.

The total energy resolution is given by:

$$E_T = (E_I^2 + E_S^2 + E_f^2 + E_t^2 + E_N^2)^{1/2}$$

where E_I = Measured Energy resolution of the ion-chamber (48 KeV for Sm^{147}).

Therefore,

$$E_I = (E_T^2 - (E_f^2 + E_S^2 + E_t^2 + E_N^2))^{1/2} = (48^2 - (45.1)^2)^{1/2} \text{ or } 16.4 \text{ KeV.}$$

This value probably represents the contribution from positive ion effects.

TABLE 2.1

	FACTOR	SYMBOL	ENERGY SPREAD
1.	Source Thickness	E_S	15 KeV
2.	Statistical Fluctuation	E_f	6 KeV
3.	Finite rise time	E_t	22 KeV
4.	Electronic noise	E_N	35 KeV
	Total	E_T	48 KeV

Figure 2.9 Block diagram of the electronics.

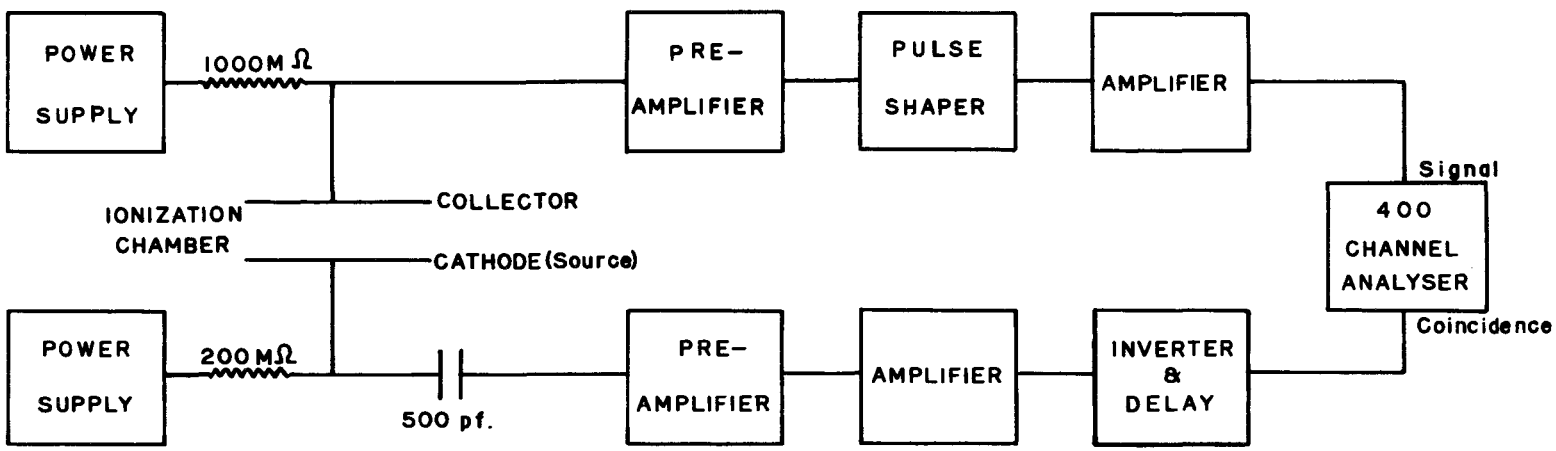
POWER SUPPLY
1000M Ω
PRE-AMPLIFIER
PULSE SHAPER
AMPLIFIER
Signal
400 CHANNEL ANALYSER
IONIZATION CHAMBER
COLLECTOR
CATHODE (Source)
POWER SUPPLY
200 MΩ
500 pf.
PRE-AMPLIFIER
AMPLIFIER
INVERTER & DELAY
Coincidence

2.6 Electronic Equipment

A Tennelec TC 110 preamplifier was directly connected to the collector electrode of the ion-chamber. The integration and differentiation time constants were optimized at 4μsec. After amplification, the pulses were fed to a pulse shaper which has a rise time of 1.5 μ sec and an amplification factor of 2. The pulses were further amplified by an ORTEC TC 201 Low-noise amplifier and then analysed by a Model 34-12B RIDL pulse-height analyser.

The electrode potentials were chosen to minimize ion-electron recombination. The high voltage supplies used were a RIDL 40-12B and an Atomics Super Stable Model 312.

The cathode was connected to a RIDL power supply through a UG-634/U and a 200 M Ω resistor. The Super Stable Power supply was connected to the collector through the preamplifier.

The cathode was connected to a RIDL Model 31-18 Nuvistor preamplifier through a 500 pf capacitor. After further amplification, the cathode pulses were led to delay and inverter circuit.

The cathode pulses were used to generate -10V pulse and were delayed by 1.5 μ sec. This was then used to gate on the analyser through the delayed coincidence mode. The block diagram of the electronics is shown in figure 2.9. The purpose of this coincidence requirement is described in the next section.

CHAPTER III

BACKGROUND IN THE REGION OF ALPHA-ENERGIES

3.1 General.

A factor limiting the sensitivity of an ion chamber for detecting weak alpha-activities is the level of the background-activity. In this work it had to be reduced to a level where an activity of only a fraction of a count per hour could be detected from the background. The alpha-energy spectrum is always superimposed on the background activity. By improving the resolution and by reducing the useless cathode area exposed to the counting volume, it is possible to achieve a very low background activity. The resolution is the other factor effecting the sensitivity of the counter. The smaller the width of the peak (or better resolution) the lower will be the effective background under the peak. The details of the resolution of ion chamber have been given in Chapter II. Now the question is from where does the background come?

3.2 Factors Contributing to the Background.

3.2.1 Natural Activity of the Construction Material.

The main source of alpha-radiation other than samples which can contribute to the background is from the material used for construction of the counter. Traces of natural U, Th and their decay products are present in materials in varying amounts.

Therefore by choosing the material which is known to have low background, its contribution can be minimized. Devoe (Dev-61) has given a list of construction materials commonly used with their alpha-backgroud. Among the metals stainless steel is considered to be one of the best.

3.2.2 From the Electrodes Exposed to the Counting Volume in the Chamber.

The material used for electrodes also has background activity. Stainless steel was selected as a construction material for the electrodes.

3.2.3 The Chamber Gas.

The counting gas also contributes some activity from the small amount of radon which is introduced in the counting gas as a decay product of U^{238} and Th^{232}. This is present in the walls of the gas cylinder. This does not present a great problem, because the energy region of the interest in this work is from 1.5 to 2.5 MeV and the alpha-particles from Rn can be easily resolved from the low energy alpha-particles.

3.2.4 Natural Radioactive Contamination of Samples.

The rare earths are always accompanied by traces of U and Th. It does not however, present any serious problem because very thin sources are used and low-energy tailing of the alpha-spectrum from these elements is negligibly small and can be easily resolved in the energy region of interest, i.e. from 1.5 to 2.5 MeV.

3.2.5 External Radiations

The contribution caused by natural activity of the environment is negligibly small. Certain components of cosmic radiation will be detected by the chamber i.e., protons, μ-meson, etc. The recoil protons or any other nuclear reactions produced by the fast neutrons of cosmic rays will also give rise to a low energy background.

3.2.6 Electrical Disturbances.

The electrical noise, pick-up or hum can be a serious problem for systems in which high gain is used. To reduce the noise level and hum, a very low noise preamplifier Tennelec TC 110 was used. The first tube of the preamplifier which may be a major cause of noise was carefully chosen to give the minimum noise.

The pick-up was minimized by careful shielding of the sensitive parts of the ion chamber and preamplifier. The noise level was carefully monitored and the first tube was changed periodically.

3.3 Methods Used to Reduce the Background.

The contribution to the background by activities in the walls of the outer cylinder and electrodes, and external radiations, is reduced to some extent by the use of high pressure. The background counts caused by the sample backing can be reduced by plating a thick copper film over the sample backing. However, since the sample after depositing over the backing requires heating at relatively high temperature, the copper becomes oxidized and forms a layer of oxide giving a large effective sample thickness.

The main cause of the background is the surface layer of the

Figure 3.1 Alpha background of

(a) bare stainless steel sheet

(b) after cleaning the stainless steel electo-analytically

(c) after cleaning the sheet electro-analytically plus the cathode collector coincidence.

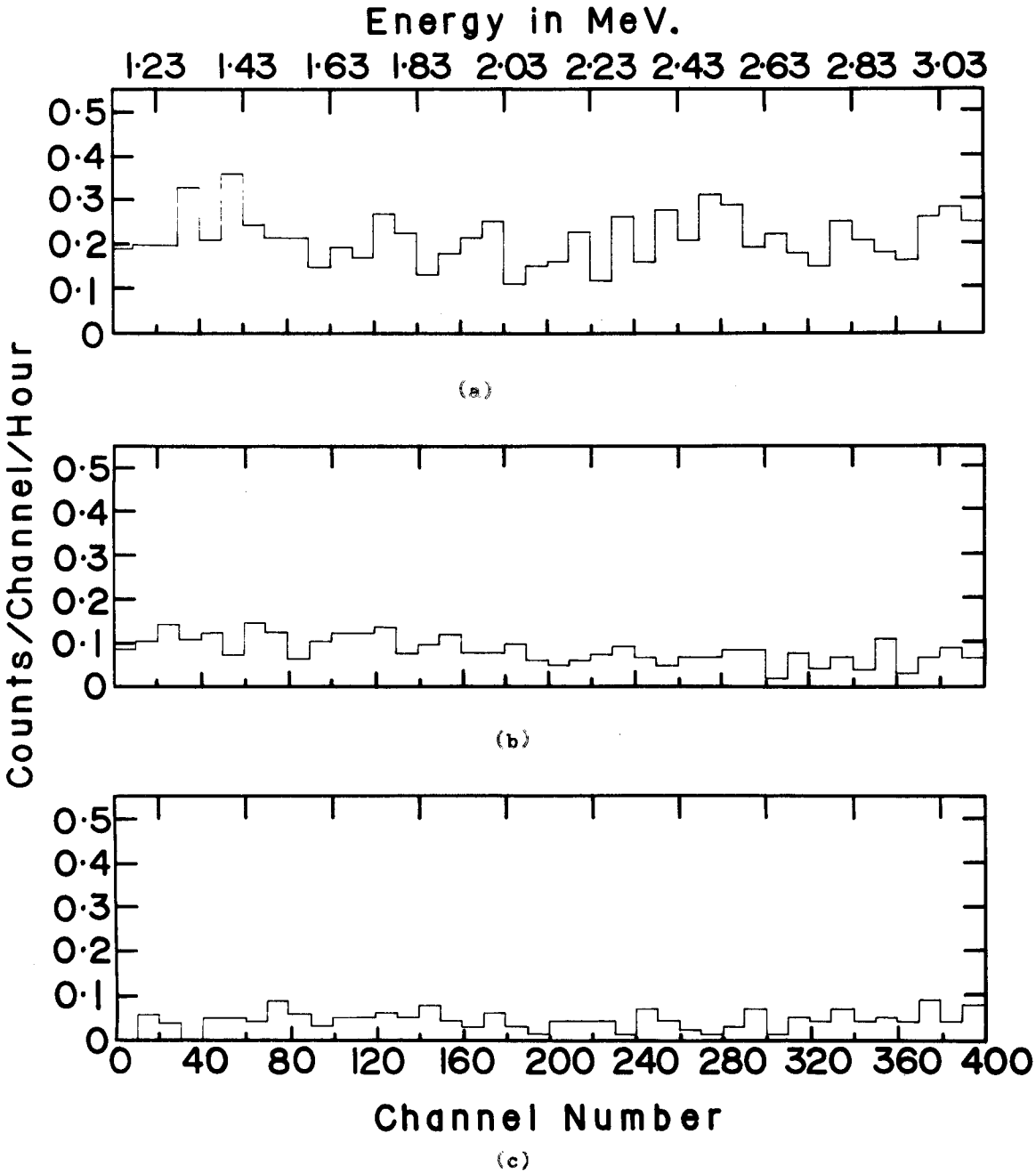
Energy in MeV.
1·23 1·43 1·63 1·83 2·03 2·23 2·43 2·63 2·83 3·03
0·5
0·4
0·3
0·2
0·1
0
(a)
(b)
(c)
Counts/Channel/Hour
0 40 80 120 160 200 240 280 320 360 400
Channel Number

sample backing. It was found that if the surface was electro-polished, the background can be reduced considerably. To do this the stainless steel cylinder was dipped in $FeSO_4$ solution. The sample backing (stainless steel cylinder) was made an anode and another stainless steel rod served as cathode. This was electrolysed for 5 hours at a current density of $2mA/cm^2$.

A background count was made for a 10 hours period on an untreated stainless steel cylinder. This gave a count rate of 20 count/hr/500 KeV interval. The result is shown in figure 3.1(a).

After cleaning electrolytically, the background was measured again and found to have a count rate of 8 counts/hr/500 KeV; a reduction of a factor of 2.5. The result is shown in figure 3.1(b). The background caused by the electrodes and other chamber walls, except the cathode, can be eliminated by the use of the time delay of the voltage pulse induced on the collector from the starting time of the voltage pulse induced on the cathode. For this the coincidence circuit with a time delay of 1.5 μ sec. was used. The background using the cathode-anode pulse coincidence method was reduced to 3 counts/hr./500 KeV. The results are shown in figure 3.1(c).

CHAPTER 4

SAMPLE PREPARATION

4.1 General.

4.1.1 Source of Samples.

(a) Natural samarium - A sample of samarium oxide of 99.9% purity was obtained from the Lindsay Rare-earth Chemical Company, West Chicago, Illinois, U.S.A.

(b) Samarium sample enriched in mass 146 - The sample was supplied by Oak Ridge National Laboratory and was obtained at the mass 146 position of a calutron collection plate which had been used in the separation of Macro-amounts of Sm isotopes from natural samarium.

(c) Enriched samples - All the enriched isotopes samples used in this study were obtained from the isotopes division of the Union Carbide Corporation, Oak Ridge National Laboratory, Oak Ridge, Tenn., U.S.A.

Table 4.1 shows the isotopic composition of each sample as given by the Isotopes Division of Union Carbide Corporation.

4.1.2 Sample Deposition

In alpha-spectroscopy, it is necessary to have very sharp spectra so that the energies can be measured precisely. This can be achieved if the source is thin and uniform.

To obtain a thin and uniform deposition over a large area

TABLE 4.1

ISOTOPIC COMPOSITION OF THE SAMPLES

ISOTOPE SAMPLE	ISOTOPIC COMPOSITION	PERCENT
	Sm-144	0.08
Sm-147	Sm-147	97.8 ± 0.1
	Sm-148	0.91 ± 0.05
	Sm-149	0.51 ± 0.05
	Sm-150	0.17 ± 0.05
	Sm-152	0.34 ± 0.05
	Sm-154	0.21 ± 0.05
Sm-148	Sm-147	0.026
	Sm-148	99.941 ± 0.01
	Sm-149	0.032
Sm-149	Sm-144	<0.08
	Sm-147	0.33 ± 0.05
	Sm-148	0.55 ± 0.05
	Sm-149	97.46 ± 0.05
	Sm-150	0.65 ± 0.05
	Sm-152	0.70 ± 0.05
	Sm-154	0.34 ± 0.05

of 1400 cm^2 the method of evaporation was found to be useful. It consists of spreading an alcoholic solution of nitrate of sample and evaporating off the alcohol.

4.2 Preparation of Sample Backing.

The stainless steel backing was used in the measurements. For the studies of Sm-147 and Sm-146 a stainless steel sheet, measuring 28.6 cm wide, 50 cm long and 0.050 cm thick, was used. The sheet was cleaned with dilute nitric acid and then with distilled water. The sheet was also thoroughly rubbed with steel wool to reduce the gloss which prevents the solution from wetting the surface of the backing. Afterwards the backing was cleaned with absolute alcohol.

The sheet was wrapped in paper and then rolled into a cylindrical shape 50 cm long and 9 cm diameter and again cleaned with absolute alcohol.

For studies of Sm^{148} and Sm^{149} a stainless steel cylinder of diameter 9 cm and 1.6 mm thickness was used. This was cleaned with nitric acid and then electrolytically etched as described in Chapter 3. Afterwards, it was washed with absolute alcohol.

4.3 Deposition of Samarium - Procedure

(1) A weighed amount of oxide was dissolved in a minimum amount of nitric acid in 50 ml beaker.

(2) The solution was evaporated to dryness using infrared heat lamps. Five ml of distilled water was added and again evaporated to dryness. The procedure was repeated until nitric acid was removed.

(3) The residue was dissolved in 30 ml of absolute alcohol and a small amount of polyethylene glycol solution (so as to give .1% solution of polyethylene glycol in alcohol) was added.

(4) The sample backing was placed on a 'V' shaped wooden stand to keep the backing horizontal. The stainless steel sheet was placed inside an aluminium cylinder of 9 cm diameter and 50 cm length. The backing was heated at both ends by infrared heat lamps.

(5) The alcohol solution was then spread over the stainless steel backing and the cylinder was rotated slowly so that the alcohol solution spread out evenly over the area to about 3 cm from the ends.

(6) When all the solution was transferred, the backing was heated by heat lamps for about 30 minutes.

(7) The sample backing was removed from the stand and the entire surface was ignited with a Fisher burner. Upon ignition the polyethylene glycol and other organic materials disappear and the nitrate changes to the oxide.

While the backing is still hot, it is placed inside the ionization chamber.

CHAPTER V

ANALYSIS OF DATA

5.1 General.

For nuclides which are alpha-active, the observed activity gives information about the alpha-particle energy and specific activity. From this data the half-life, alpha-decay energy and specific activity can be calculated. For precise energy measurements, the functional form of the calibration curve must be known.

5.2 Linearity of the Alpha-Spectrometer.

5.2.1 General.

Energy measurements using an ionization chamber are generally relative. The unknown spectrum is measured together with some standard spectrum. The unknown energy is obtained by interpolation from the standards.

The linearity of an ion chamber has been studied quite thoroughly by many investigators. Jesse and co-workers (Jes-50, Jes-51) investigating the ionization vs. energy relationship for argon, up to 1.5 MeV came to the conclusion that the total ionization produced is very accurately proportional to the energy of the alpha-particles causing ionization.

Cranshaw and Harvey (Cra-48) obtained different results using argon in an electron-collecting chamber. They found that

the pulse height vs. energy relation was linear from 5 MeV. to 9 MeV and had a zero pulse height energy of 85 KeV. They suggested that the average energy, W, required to produce an ion-pair depends on the alpha-particle energy as

$$W = W_{\infty}(1-0.069\ E^{-1/2}) \qquad 5.1$$

where W_{∞} is the average energy required to produce an ion-pair at high energy, and E is the energy of the alpha-particles in MeV.

Harvey, Jacskon, Eastwood and Hanna (Har-57) confirmed the results of Cranshaw and Harvey (Cra-48), using 6% methane and 94% argon gas mixture in a gridded-ionization chamber.

Macfarlane (Mac-59), using 94% argon, 5% ethylene and 1% nitrogen mixture confirmed the linearity between the pulse height and the energy. In the work described here, it was also found that for argon, acetylene and nitrogen gas mixture the same relationship holds, i.e., there is a linear relationship between pulse height and the energy of the alpha-particle.

5.2.2 The Linearity of the System.

The linearity of the electronics associated with the alpha-spectrometer was studied employing a Victoreen pulser (Model-PPG1). The pulser was normalized to the Sm^{147} peak channel. Spectra for various pulse heights were obtained as a function of the channel number for different bias levels of the post amplifier. Each spectrum was assumed to have a Gaussian shape

$$N(x) = A\ \exp(-(x-x_0)^2/2\sigma^2)$$

Figure 5.1 Plot of pulse height vs. peak positions at different bias levels

A. 0.90

B. 0.75

C. 0.65

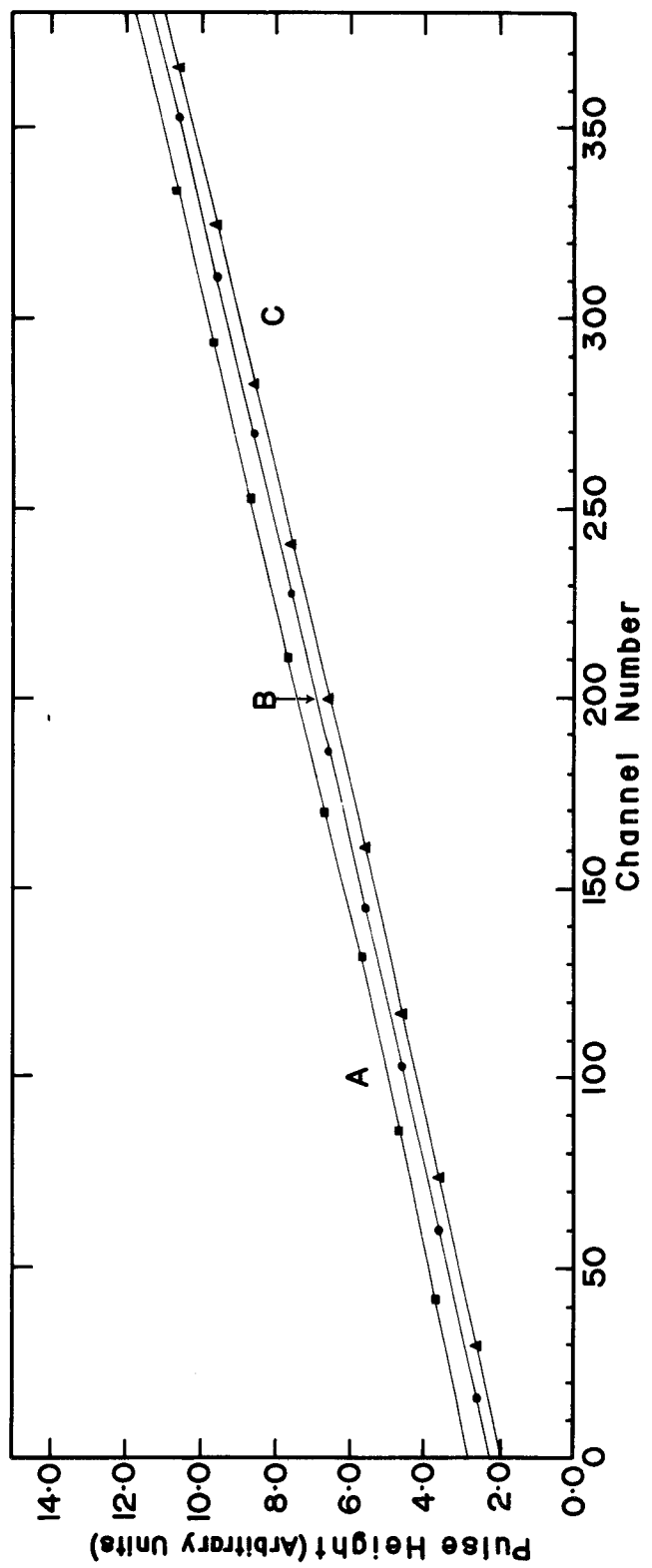
Pulse Height (Arbitrary Units)
0·0
2·0
4·0
6·0
8·0
10·0
12·0
14·0
0
50
100
150
200
250
300
350
Channel Number
A
B
C

where

$N(x)$ = Number of the counts in channel x.

A = Amplitude of the distribution.

x_0 = Peak channel.

σ = Standard deviation.

A non-linear weighted least square fit was perforemed using the IBM 7040 computer at McMaster University, in order to determine the precise peak position x_0, amplitude A and standard deviation σ.

After evaluating x_0 another least square's fit of

$$V = a + b\, x_0 + c\, x_0^2 \qquad 5.2$$

where V is the pulse height and a,b and c are constants,was performed in order to determine whether there was any non-linearity for different bias levels. The results of this least square's fit are recorded in Table 5.1.

Figure 5.1 shows a plot of V vs. x_0 for different bias levels.

5.3 Method used to Determine the Alpha-particle Energy.

The unknown spectrum is measured together with the sample.

When an alpha-spectrum was obtained, the precise peak position of each spectrum was determined by a non-linear least square fit of

$$N(x) = A \exp(-(x - x_0)^2/2\sigma^2). \qquad 5.3$$

TABLE 5.1

Bias	a	b	c
0.65	$1.90 \pm .025$	$(2.281 \pm .034) \times 10^{-2}$	$(2.776 \pm .92) \times 10^{-6}$
0.75	$2.23 \pm .013$	$(2.286 \pm .02) \times 10^{-2}$	$(2.638 \pm .06) \times 10^{-6}$
0.90	$2.703 \pm .05$	$(2.30 \pm .06) \times 10^{-2}$	$(2.496 \pm 1.6) \times 10^{-6}$

Then from known energies of the standards, a and b of the equation

$$E = a + b\,(x_0 + \frac{c}{b}\,x_0^2) \qquad 5.4$$

are computed. $\frac{c}{b}$ was taken from the linearity measurements and has been shown to be independent of the gain of the amplifier.

In the rare earth region i.e., in the region of 1.5 to 2.5 MeV., only alpha arising from Li^6 (n,α) H^3 and B^{10} (n,α) Li^{7*} with thermal neutrons are accurately known. Therefore, to determine Sm^{147} alpha-energy these two standards are used. For the energies of other isotopes of samarium, Sm^{147} was taken as a standard. For these isotopes, to find a and b the pulser was first normalized to the Sm^{147} peak and at different energies the pulser peaks were produced. These peaks were used to calculate b and $\frac{c}{b}$. Then the Sm^{147} peak was used to calculate a.

From known values of a and b the energy of the peak at x_0 was computed.

5.4 Determination of the Specific Activity and the Half-life.

If a sample contains two alpha-emitters and if the half-life of one of the alpha-emitter is known precisely, then it is convenient to calculate the half-life of one relative to the other.

In this method if the count rate of the standard alpha-emitter be $(\frac{dN}{dt})_s$ and that of unknown be $(\frac{dN}{dt})_x$, then

$$(\frac{dN}{dt})_x \Big/ (\frac{dN}{dt})_s = \frac{N_x \lambda_x}{N_s \lambda_s} \qquad 5.5$$

where N_x/N_s is the ratio of the number of atoms of the unknown

and the standard in the sample, and λ is the decay constant.

The count rate was calculated by assuming that the ratio $(\frac{\Delta E}{\sqrt{E}})$ is constant; where ΔE is given energy interval over which the spectrum is investigated and E is the alpha energy, i.e.,

$$(\frac{\Delta E}{\sqrt{E}})_s = (\frac{\Delta E}{\sqrt{E}})_x$$

The total number of counts in a particular energy interval in the standard spectrum were measured. Then the total number of counts in the same relative energy interval of the unknown peak were counted. In practice, however, the practical resolution was taken into account, i.e., the number of counts in the channels covering full width at half maximum were calculated for their count rates. From known data λ_x can be evaluated.

From the decay constant, λ_x, of the alpha-emitter, the specific activity a_o may be calculated according to the general law of radioactive disintegration, i.e.,

$$a_o = N\lambda$$

where N is the total number of the radioactive atoms and is given by $\frac{P.N_o}{A}$, where

P = abundance of the radioactive nuclide in the natural sample

A = atomic weight of the element

N_o = Avogadro's number.

The specific activity is expressed as dis/(gm x sec).

The half-life of Sm^{147} was determined by taking Th^{232} as a standard source and for other isotopes of samarium, Sm^{147} was taken as standard. From the data $(T_{1/2})_x$ can then be calculated.

5.5 Establishing an Upper Limit on Specific Activity.

In cases where no alpha-activity was observed, only an upper limit on specific activity could be established.

To set the upper limit, the count rate within a energy interval which should include the activity, if it were present, was obtained and an average count rate per channel for the minimum count rate above background in any one channel which would give a significant peak in this energy region. This was usually several times the standard deviation of the average count rate per channel. This estimate depends upon the average count rate per channel and on whether it was constant or there was some variation caused by tailing from a high energy activity. This estimate, which is an upper limit of the count rate in one channel was then converted to an upper limit for the absolute count rate by determining the fraction of the total activity in one of the channels containing the peak of the spectrum of a known alpha-emitter of approximately the same energy and sample thickness.

5.6 Calculations of the Penetrability and the Reduced Width.

To compute the barrier penetrability, different forms of nuclear potentials were used for the rare earth alpha-emitters.

The barrier penetration factor is given by equations (1.4.3 and 1.4.4)

$$P = \exp\left(-\frac{2}{\hbar}\int_{R_i}^{R_E}\left(2M(V(r) + \frac{2Ze^2}{r} + \frac{\hbar^2}{2Mr^2}\ell(\ell+1) - Q_{eff.}\right)^{1/2} dr\right).$$

The symbols have the same meaning as in equations (1.4.3 and 1.4.4). The WKB integral was evaluated at inner and outer classical turning points where the integrand vanishes.

The integration was carried out numerically by the use of and IBM 7040 Fortran IV computer. The outer turning point R_E found by the solution of a quadratic equation and the inner turning point was found by a simple Newton's iterative method.

The barrier integral was evaluated by a modified Simpson's rule (Ras-59) with a summation over the barrier region divided into 128 equal intervals. Simpson's rule was modified at the ends to take better account of the fact that the integrand is zero at the turning points and behaves there as $C\left|r-R_t\right|^{1/2}$; where C is constant and R_t is the turning point radius.

The form of Simpson's rule which was applied is

$$I_{128} = \frac{h}{3}\left(3y_1 + 2(y_3+y_5+\ldots+y_{125}) + 4(y_2+y_4+\ldots y_{126}) + 3\,y_{127}\right) \quad 5.6$$

where h is the magnitude of the interval.

Using the experimental half-life, the reduced alpha-emission width δ^2 was computed, from the expression

$$\delta^2 = \frac{h\cdot 0\cdot 693}{T_{1/2}\cdot P} \quad 5.7$$

where $T_{1/2}$ is the half-life of the alpha-emitter and h is Planck's constant. Knowing the reduced width a hindrance factor F was calculated according to the equation

$$F = \frac{\delta_1^2 + \delta_2^2}{2\delta_{odd}^2}$$

where δ_1^2, δ_2^2 are the reduced widths of the nearest even-even nuclei and δ_{odd}^2 for the odd nucleus in question.

CHAPTER VI

EXPERIMENATAL RESULTS

6.1 Samarium-147

6.1.1 Alpha-particle energy measurement

(a) Experimental details

To measure precisely the energy of the alpha-particles of Sm^{147}, a mixed source containing 0.03530 mg lithium carbonate (99.0% Li^6), 0.0690 mg borax and 1.0 mg Sm_2O_3 (enriched in Sm^{147}) was prepared. $Li^6(n,\alpha)H^3$ and $B^{10}(n,\alpha)Li^{7*}$ act as a standard calibrating source. The McMaster University nuclear reactor was used as a source of neutrons. The ion chamber was placed in front of a neutron beam which was controlled by a slit, so that a flux of 1000 neutrons/sec/cm^2 could be obtained. In this case the coincidence circuit used for background reduction was not used. The range of the H^3(2.74 MeV) is very large and was not fully stopped in the chamber at the pressure used.

(b) Results

Figure 6.1 shows the energy spectra obtained from the source. It shows the Sm^{147} peak as well as the $Li^6(n,\alpha)H^3$ alpha peak at 2.051 $\pm$ 0.0012 MeV and the 1.472 $\pm$ 0.0014 MeV peak from $B^{10}(n,\alpha)Li^{7*}$.

A least squares fit to a Gaussian distribution (equation 5.3) was performed and the peak positions and corresponding energies

Figure 6.1 Energy spectrum of Sm^{147}, $Li^{6}(n,\alpha)H^{3}$ and $B^{10}(n,\alpha)Li^{7}$ *.

A - $B^{10}(n,\alpha)Li^{7}$ * peak.

B - Position of $B^{10}(n,\alpha)Li^{7}$ peak.

C - $Li^{6}(n,\alpha)H^{3}$, alpha-peak.

D - Sm^{147} peak.

E - Position of $Li^{6}(n,\alpha)H^{3}$, Tritium peak.

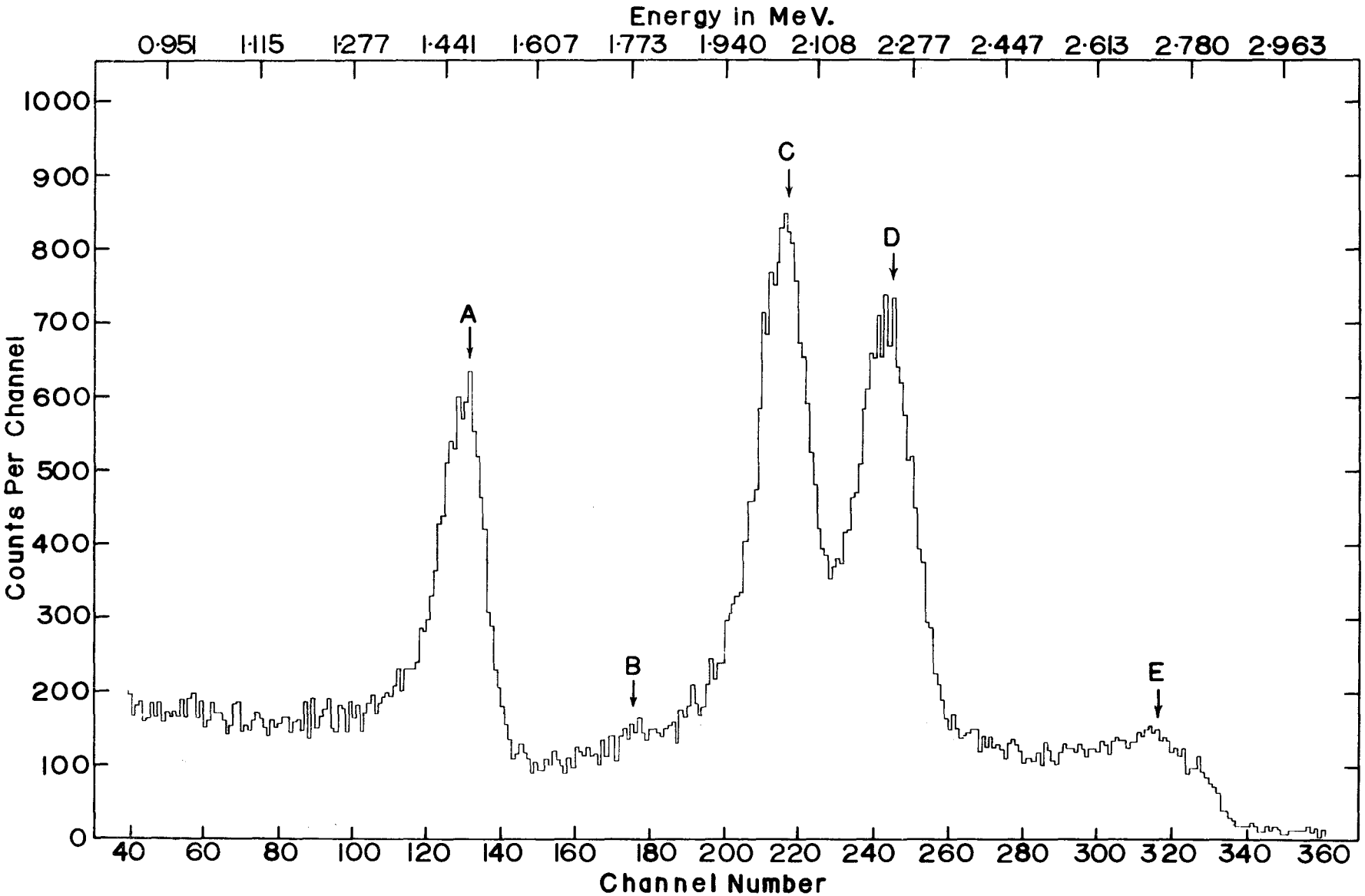
Energy in MeV.
0·951
1·115
1·277
1·441
1·607
1·773
1·940
2·108
2·277
2·447
2·613
2·780
2·963
Counts Per Channel
0
100
200
300
400
500
600
700
800
900
1000
A
B
C
D
E
40
60
80
100
120
140
160
180
200
220
240
260
280
300
320
340
360
Channel Number

TABLE 6.1

Nuclear reaction	Peak position	Alpha-energy (MeV)
$B^{10}(n,\alpha)\ Li^{7*}$	129.644 ± 0.09	1.472 ± 0.0014
$Li^{6}(n,\alpha)\ H^{3}$	216.586 ± 0.100	2.051 ± 0.0012
Sm^{147} (alpha-decay)	243.534 ± 0.150	to be determined

are given in Table 6.1

The alpha-particle energy of Sm^{147} was calculated as follows

First the $Li^6(n,\alpha)H^3$ and $B^{10}(n,\alpha)Li^{7*}$ peaks were used to evaluate 'a' and 'b' in equation (5.4).

$$E = a + b\left(x + \frac{c}{b} x_o^2\right)$$

$\frac{c}{b}$ was taken as 1.21685×10^{-5} for a bias level of 0.65 which gives 'a' as 0.630 ± 0.0014 MeV and 'b' as 6.394 ± 0.025 MeV/channel. Using the values of 'a' and 'b' and equation (5.4) again the energy of Sm^{147} peak was calculated. For Sm^{147}

$$E_\alpha = 2.233 \pm 0.005 \text{ MeV}$$

and

$$Q_\alpha = 2.295 \pm 0.005 \text{ MeV}.$$

6.1.2 Determination of the specific activity

(a) Experimental details

To determine the specific activity of Sm^{147} a mixed source of Sm^{147} and Th^{232} was prepared in which the ratio of the Sm^{147} atoms to Th^{232} atoms was 2.2644. The sample was counted for 12 hours. Another sample containing natural neodymium and Th^{232} in the same ratio was also counted for a period of 12 hours.

(b) Results

Figure 6.2 shows the alpha-spectrum from a mixed sources of Sm^{147} and Th^{232} and figure 6.3 that of natural neodymium and Th^{232}. During counting coincidence circuit was not used.

Figure 6.2 Alpha-spectrum of Sm^{147} and Th^{232}

B - Sm^{147} peak.

A - Th^{232} peak.

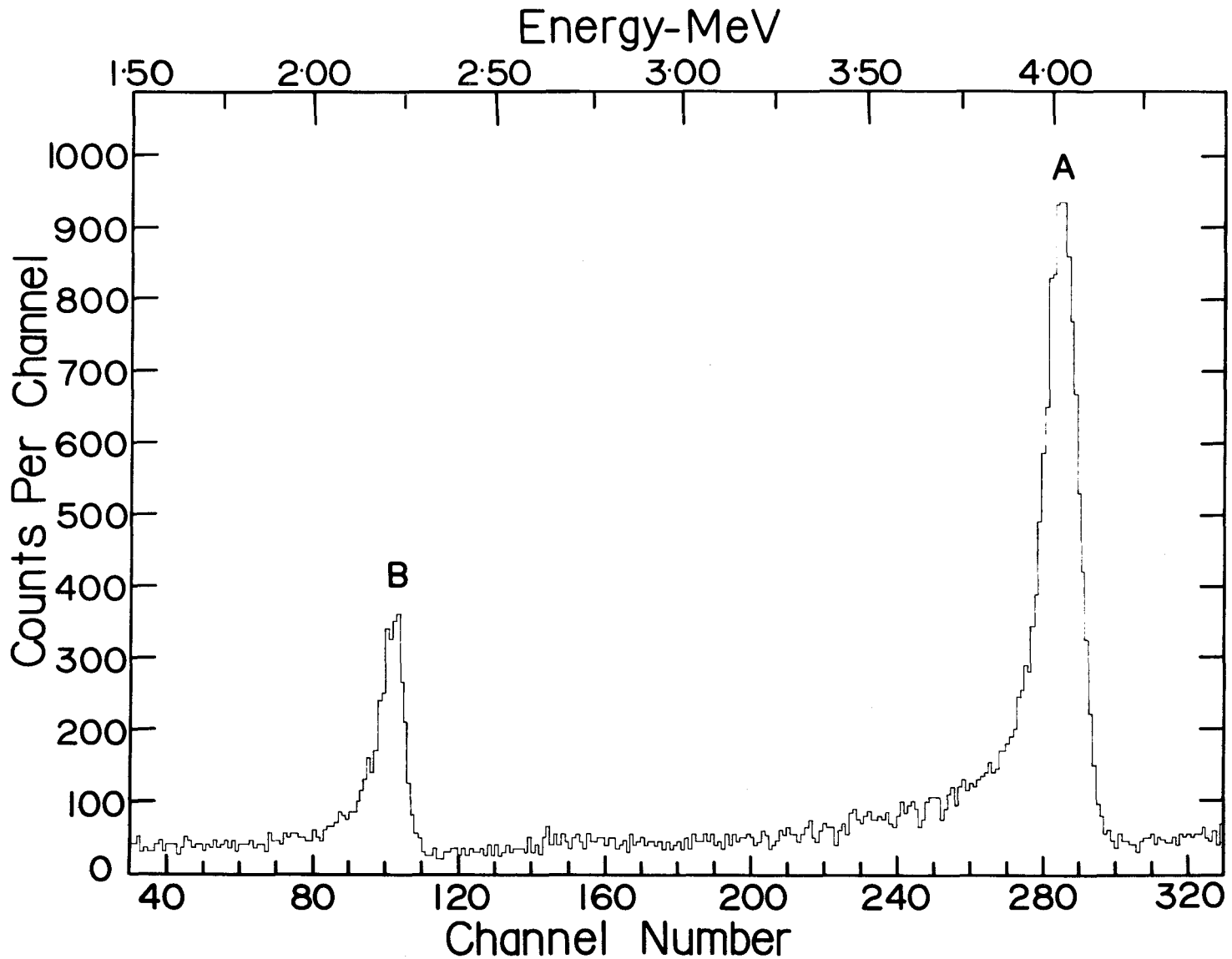
Energy-MeV
1·50
2·00
2·50
3·00
3·50
4·00
Counts Per Channel
1000
900
800
700
600
500
400
300
200
100
0
A
B
40
80
120
160
200
240
280
320
Channel Number

Figure 6.3 Alpha-spectrum of natural neodymium and Th^{232} sample.

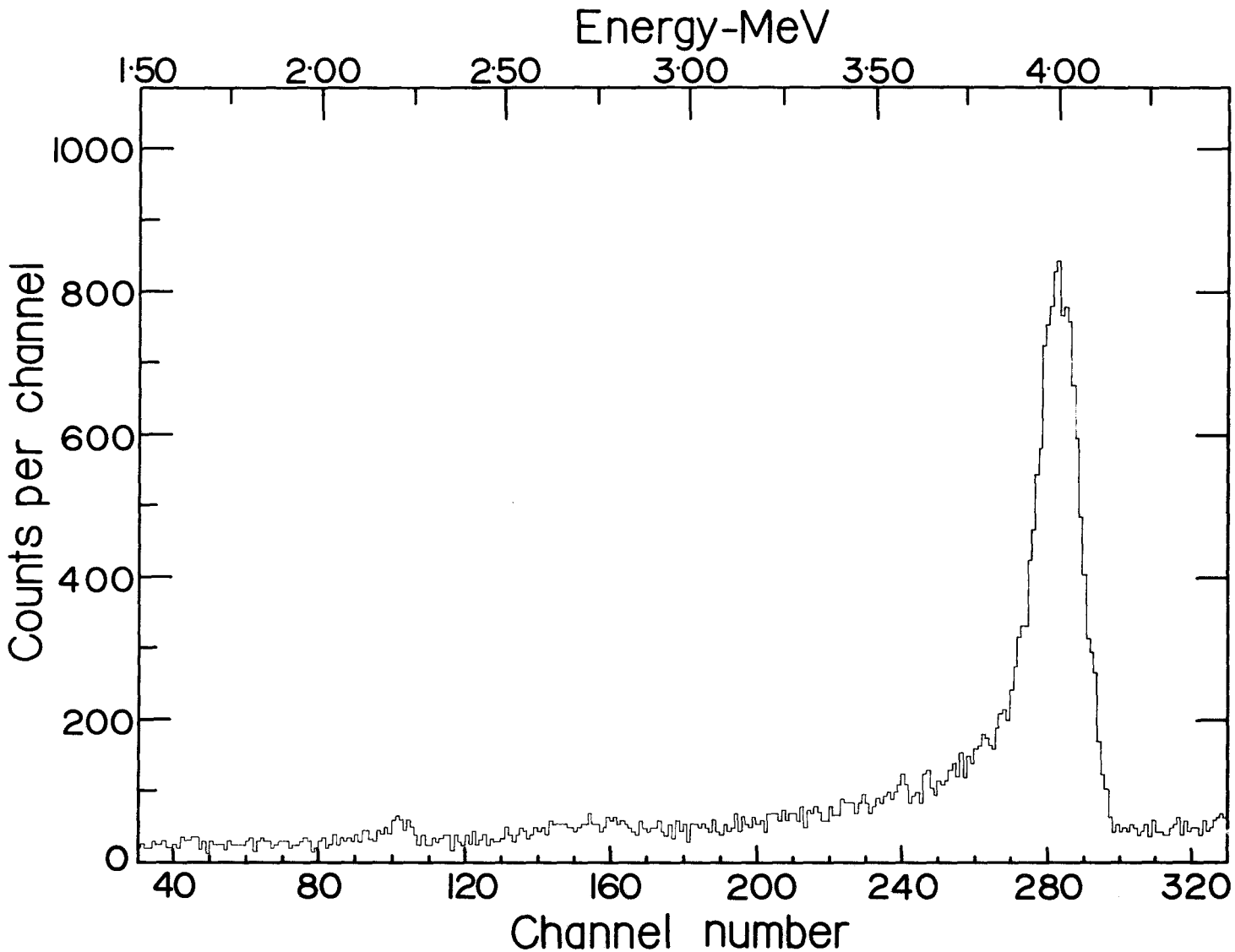
Energy-MeV
1·50
2·00
2·50
3·00
3·50
4·00
1000
800
600
400
200
0
Counts per channel
40
80
120
160
200
240
280
320
Channel number

(i) Total number of the counts in the channel covering FWHM (12 channels of 3.95 to 4.06 MeV) in Th^{232} peak = 9026 ± 95

(ii) Estimated background in the same energy interval = 600 ± 24

(iii) Net number of counts in Th^{232} peak at FWHM = 8426 ± 98

(iv) Total number of counts in the channels covering FWHM (9 channels or 2.164 to 2.26 MeV) in Sm^{147} peak = 2810 ± 53

(v) Estimated background in the above energy interval (from figure 6.3) = 275 ± 17

(vi) Net number of the counts in the Sm^{147} peak = 2535 ± 55

Now,

$$\frac{(\frac{dN}{dt})_{Sm^{147}}}{(\frac{dN}{dt})_{Th^{232}}} = \frac{(N\lambda)_{Sm^{147}}}{(N\lambda)_{Th^{232}}}$$

Therefore,

$$\lambda_{Sm^{147}} = \frac{(\frac{dN}{dt})_{Sm^{147}}}{(\frac{dN}{dt})_{Th^{232}}} \times \frac{N_{Th^{232}}}{N_{Sm^{147}}} \times \lambda_{Th^{232}}$$

$(T_{\frac{1}{2}})_{Sm^{147}} = (1.061 \pm 0.019) \times 10^{11}$ years.

$= (6.53 \pm 0.16) \times 10^{-12}$ years.

Specific activity of $Sm^{147} = \frac{6.023 \times 10^{23} \times 6.534 \times 10^{-12}}{147 \times 3.155 \times 10^{7}}$

or 847 ± 20 dis/(gm x sec).

Specific activity of natural samarium = 124.2 ± 3.0 dis/(gm Sm x sec).

6.2 Samarium-146

6.2.1 Natural samarium sample.

(a) Experimental details

A sample containing 60.18 mg natural samarium oxide was prepared and counted for a period of 489.11 hours. The chamber gas was replaced every week and the spectra were summed using the Sm^{147} peak to account for small shifts and the coincidence circuit was used.

(b) Results

Figure 6.4 shows the spectrum obtained from the sample. On the high energy side there is no indication of the activity.

(c) Calculations of an upper limit to the specific activity

The average number of counts per channel from 2.36 to 2.68 MeV, for a period of 489.11 hours equals 47.5 c/ch. The estimated counts per channel above the background necessary to give a noticeable peak of Sm^{146} activity = 16 c/ch.

The average count rate = 0.037 counts/ch/hr.

From the Sm^{147} ground the percent count in the peak channel = 1.62 % of the total Sm^{147} activity.

There fore the upper limit of the absolute disintegration rate

$$= \frac{0.0327}{0.0162} \text{ dis/hr}$$

or 5.6×10^{-4} dis/sec.

Figure 6.4 Alpha-spectrum of natural samarium.

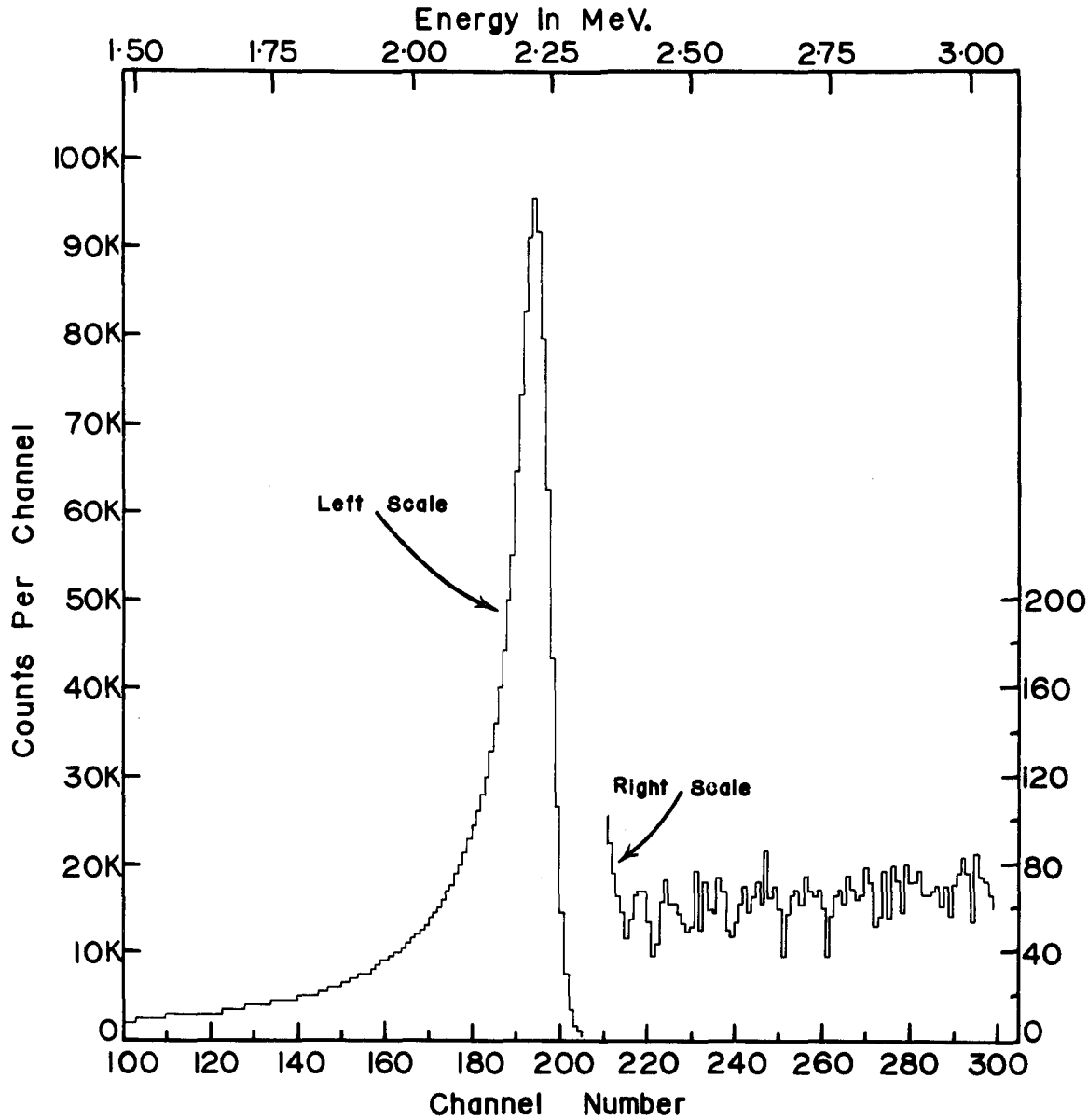
Energy in MeV.
1·50
1·75
2·00
2·25
2·50
2·75
3·00
100K
90K
80K
70K
60K
50K
40K
30K
20K
10K
0
Counts Per Channel
Left Scale
Right Scale
200
160
120
80
40
0
100
120
140
160
180
200
220
240
260
280
300
Channel Number

The upper limit of the specific activity of Sm^{146} is

$$\left[a_o\right]^{natural}_{Sm} < \frac{R}{W_s \cdot f_{Sm}}$$

where R = absolute disintegration rate

W_s = weight of the sample

f_{sm} = fraction of the samarium in the sample. Or

$$\left[a_o\right]^{natural}_{Sm} < \frac{5.6 \times 10^{-4}}{0.06018 \times 864} \text{ or } 0.0108 \text{ dis/gm x sec.}$$

6.2.2 Sample Enriched in Mass-146

(a) Experimental details

A 17.0 mg sample of samarium oxide, enriched in mass-146, was prepared. The sample was counted for 269 hours. The gain shift was corrected by peak to peak adding of the Sm^{147} spectrum.

(b) Results

Figure 6.5 shows the spectra of the sample. It was determined from the Sm^{147} specific activity that the enrichment of Sm^{147} in the sample is ∿70.16%. If we assume that if Sm^{146} is present, it is enriched by the same factor, then we can calculate a limit for a naturally-occurring sample of the amount of Sm^{146} present in nature. In order to calculate a specific activity, we estimated the isotopic composition on the basis of the known performance of the isotope separation and the observed Sm^{147} enrichment.

(c) Calculation of an upper limit to the specific activity.

The average number of counts per channel between 2.35 to 2.65 MeV = 45.75 counts per channel. Estimated counts per channel to give a noticeable peak above the background = 16 counts/channel or 0.06 c/ch/hr. The Sm^{147} peak channel consists of 2.4% of the total Sm^{147} activity. Therefore, the upper limit of absolute disintegration rate for Sm^{146} = [illegible] or 6.9×10^{-4} dis/sec.

Figure 6.5 Alpha-spectrum of the samarium sample enriched in Mass 146.

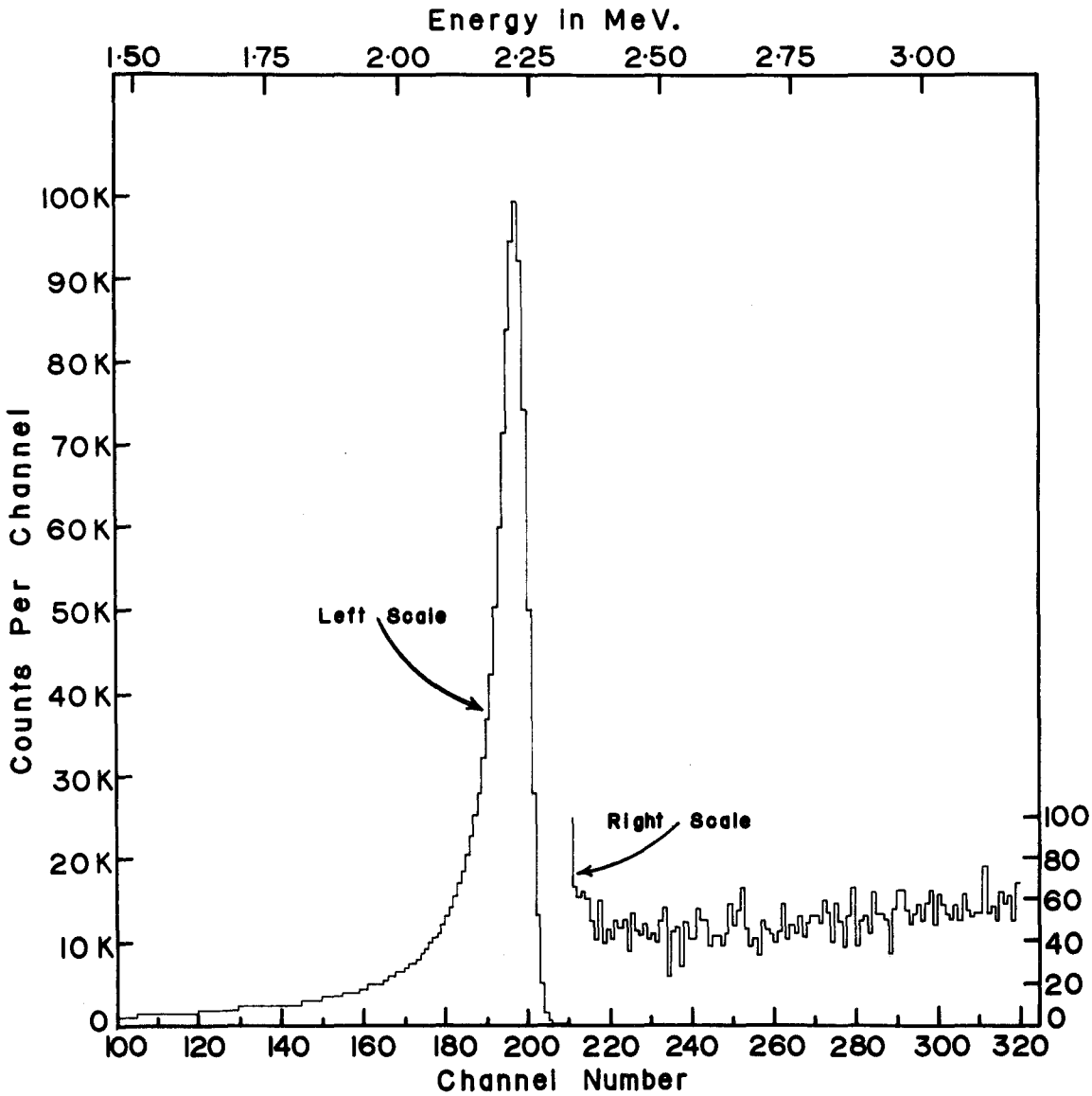
Energy in MeV.
1·50
1·75
2·00
2·25
2·50
2·75
3·00
100K
90K
80K
70K
60K
50K
40K
30K
20K
10K
0
Counts Per Channel
Left Scale
Right Scale
100
80
60
40
20
0
100
120
140
160
180
200
220
240
260
280
300
320
Channel Number

Upper limit to the specific activity of Sm^{146}

$$(a_o)^{enriched}_{Sm} < \frac{6.9 \times 10^{-4}}{0.017 \times 0.995} \text{ or } 4.08 \times 10^{-2} \text{ dis/(gm x sec).}$$

$$(a_o)^{natural}_{Sm} < \frac{4.08 \times 10^{-2} \times 14.97}{70.16 \times 150.35} \times 146.7 \text{ or } 0.0100 \text{ dis/(gm x sec).}$$

Therefore, the upper limit of the specific activity of natural samarium = 0.010 dis/(gm x sec).

6.2.3 An upper limit for the half life of Sm^{146}.

From the knowledge of the upper limit of the specific activity, the age of the element and initial primordial abundance, it is possible to establish the upper limit of the half life.

Nurmia and Karras (Nur-63) have set the primordial abundance of Sm^{146} as 3% by studying the relative abundance of difference nuclides in the rare earth region. The same initial abundance is assumed in the calculations and the age of the elements (T) is assumed to be 4.5×10^9 years (Fri-66). Then the present abundance of Sm^{146} is

$$i(Sm^{146}) = i_o (Sm^{146}) \exp (-\lambda_{Sm^{146}} \cdot T)$$

$$= 0.03 \exp (-\lambda_{Sm^{146}} \cdot 4.5 \times 10^9)$$

where $i(Sm^{146})$ is the present isotopic abundance, $i_o(Sm^{146})$ is the initial isotopic abundance and $\lambda_{Sm^{146}}$ is the decay constant of Sm^{146}.

The present specific activity of Sm caused by Sm^{146} is assumed to be the upper limit and is

$$(a_o)^{natural}_{Sm} < \frac{i(Sm^{146}) \times 6.023 \times 10^{23} \times \lambda_{Sm}146}{150.35}$$

By substituting the values of $(a_o)^{natural}_{Sm}$ and $i(Sm^{146})$ the expression becomes

$$3.155 \times 10^{7} \times 0.01 =$$

$$\frac{0.03 \times 6.023 \times 10^{23} \times \lambda_{Sm}146 \times \exp(-\lambda_{Sm}146 \times 4.5 \times 10^{9})}{150.35}$$

or $\lambda_{Sm}146 \times \exp(-\lambda_{Sm}146 \times 4.5 \times 10^{9}) = 2.625 \times 10^{-15}$.

The equation was solved by iterative method. The solution of the equation is

$$\lambda_{Sm}146 > 3.108 \times 10^{-9} \text{ years}^{-1}.$$

Therefore,

$$(T_{\frac{1}{2}})_{Sm}146 < 2.23 \times 10^{8} \text{ years}.$$

6.2.4 Determination of an upper limit to the present isotopic abundance.

From the value of the decay constant, it is possible to establish an upper limit for the present isotopic abundance. The present isotopic abundance would be

$$i(Sm^{146}) = 3.0 \times \exp(-\lambda_{Sm}146 \times T)$$

or $$2.534 \times 10^{-6}\%.$$

The half life of Sm^{146}, as given by Friedman et. al.

Figure 6.6 Alpha spectra of samarium-148 sample.

A - Samarium-148 peak

B - Samarium-147 peak

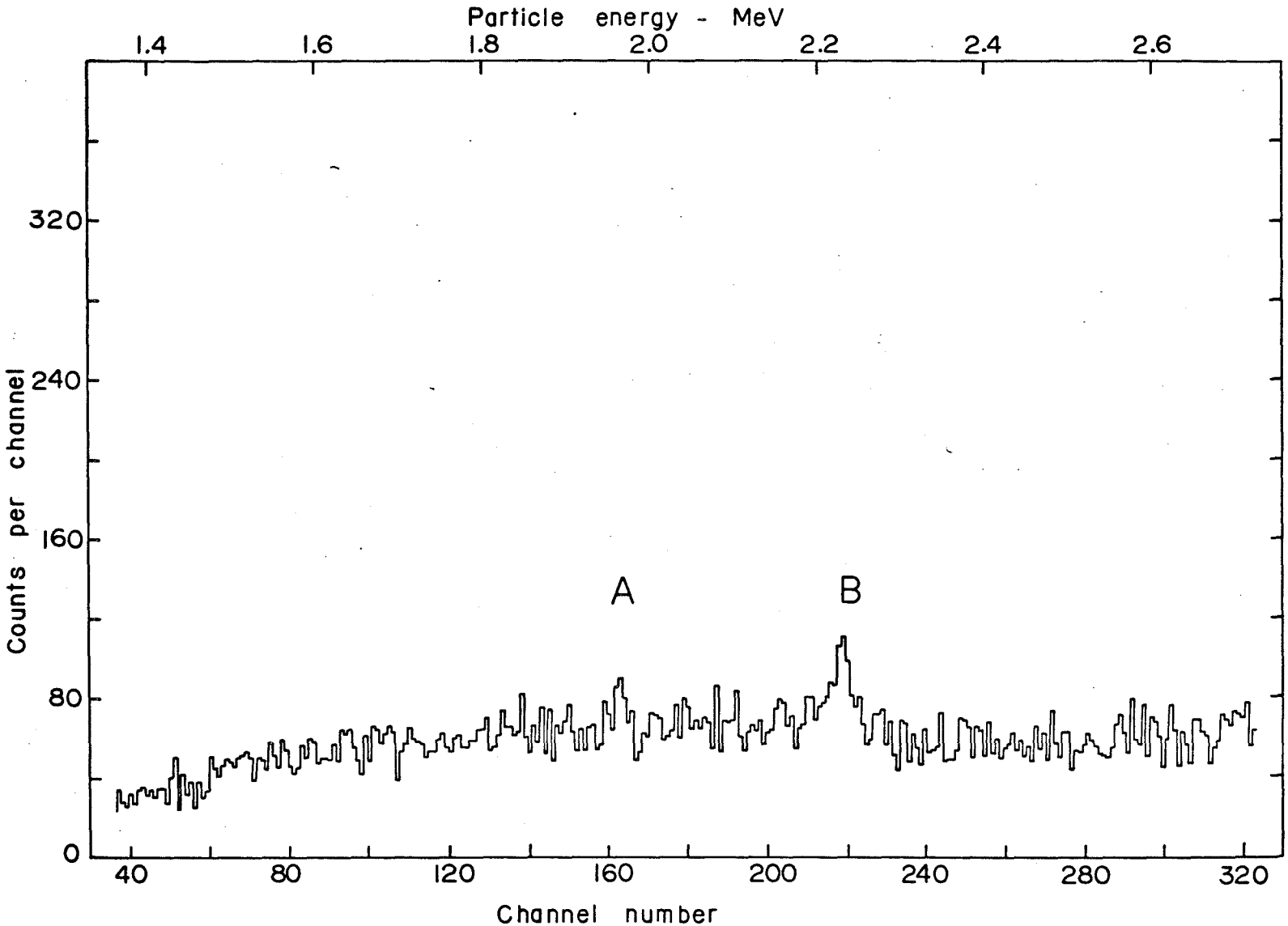
Particle energy - MeV
1.4
1.6
1.8
2.0
2.2
2.4
2.6
320
240
160
80
0
Counts per channel
A
B
40
80
120
160
200
240
280
320
Channel number

(Fri-66) is (1.026 ± 0.048) x 10^8 years. Therefore, the amount of Sm^{146} in natural samarium at present would be about 2.0 x 10^{-15}.

6.3 Samarium-148.

6.3.1 Experimental details.

A 11.6 mg sample of samarium oxide, enriched in Sm^{148} (99.941% enrichment) was prepared. The sample was counted for 1204 hours using the coincidence circuit. The spectra is plotted in figure 6.6. An examination of figure 6.6 shows a peak 'B' which is due to the presence of Sm^{147} in the sample and there is an indication for the presence of an additional peak 'A'. The peak 'A' was consistent in every recorded spectrum and was assigned to Sm^{148} activity.

6.3.2 Experimental results.

(a) Alpha-particle results.

A least squares fit to the Gaussian distribution was performed on both Sm^{147} and Sm^{148} peaks and the calculated peak positions are

Sm^{147}	219.41 ± 0.3
Sm^{148}	163.22 ± 0.5

The alpha-particle energy of the Sm^{148} was calculated as follows:

The pulser was normalized to Sm^{147} peak and other peaks at different energies were generated. A least squares analysis was performed on these peaks, assuming a Gaussian shape. The peak energies and their positions are given in Table 6.2.

The values of c/b and b were calculated from the pulser

TABLE 6.2

Energy of the peak (MeV)	Peak position (channel number)
1.70	112.17 ± 0.08
1.90	153.77 ± 0.10
2.23	221.09 ± 0.08
2.50	275.14 ± 0.08
2.70	316.03 ± 0.07

data and were found to be 7.88×10^{-5} and $(4.755 \pm 0.7) \times 10^{-3}$ MeV/ch respectively. Using the equation (5.4) and the Sm^{147} alpha energy and its peak position, the value of a would be 1.171 ± 0.007 MeV. Substituting the values of a, b and c/b back in equation (5.4) for Sm^{148}, the alpha-particle energy (E_α) of Sm^{148} is found to be 1.958 ± 0.01 MeV.

Therefore, Q_α for Sm^{148} alpha decay = 2.01 ± 0.01 MeV.

(b) Specific activity.

(i) Number of counts between 1.94 and 1.97 MeV = 605 ± 25 counts.

(ii) Average background above 1.97 MeV = 66.3 c/ch.

Therefore, the background in the energy interval of 1.94 and 1.97 MeV = 531 ± 24 counts.

(iii) Net number of counts due to Sm^{148} = 74 ± 33 counts.

(iv) Number of counts between 2.210 and 2.24 MeV = 723 ± 27 counts.

(v) Average background above the energy 2.50 MeV = 57.3 c/ch.

Therefore, the background in Sm^{147} peak = 458 ± 21 counts.

(vi) Net number of Sm^{147} counts in the energy interval of 2.21 to 2.24 MeV = 265 ± 34 counts.

Now

$$\frac{\left(\frac{dN}{dt}\right)_{Sm^{148}}}{\left(\frac{dN}{dt}\right)_{Sm^{147}}} = \frac{W_{Sm^{148}}}{W_{Sm^{147}}} \times \frac{147}{148} \times \frac{\lambda_{Sm^{148}}}{\lambda_{Sm^{147}}}$$

where $\frac{dN}{dt}$ is the count rate, W is the weight and λ is the decay constant. Substituting these values in the above equation,

$$(T_{\frac{1}{2}})_{Sm^{148}} = \frac{99.941 \times 147 \times 1.061 \times 10^{11} \times 265}{2.6 \times 10^{-2} \times 148 \times 74}$$

or $(1.45 \pm 0.60) \times 10^{15}$ years.

Decay constant $(\lambda)_{Sm^{148}} = (4.78 \pm 1.9) \times 10^{-16}$ years^{-1}.

Specific activity of the nuclide = $(6.17 \pm 2.4) \times 10^{-2}$ dis/(gm Sm^{148} x sec)

Specific activity of Sm^{148} in a natural Sm = $(6.8 \pm 2.7) \times 10^{-3}$ dis/(gm Sm x sec).

6.4 Samarium-149.

6.4.1 Experimental details.

A 10.2 mg sample of samarium oxide, enriched in Sm^{149} to 97.45%, was counted in the ion chamber for a period of 480 hours using the coincidence circuit. The sample contained 0.33% Sm^{147}.

6.4.2 Results.

The spectra obtained by counting a Sm^{149} sample is shown in figure 6.7. The peak of Sm^{147} is distinct whereas there is no evidence of any other peak which might be assigned to Sm^{149}. The alpha particle energy of Sm^{149} alpha-decay as calculated from mass data, is 1.848 ± 0.005 MeV. Therefore an upper limit to the specific activity in the region 1.80 to 1.90 MeV is calculated.

Figure 6.7 Alpha-spectra obtained from enriched Sm^{149} sample. The peak is from Sm^{147}.

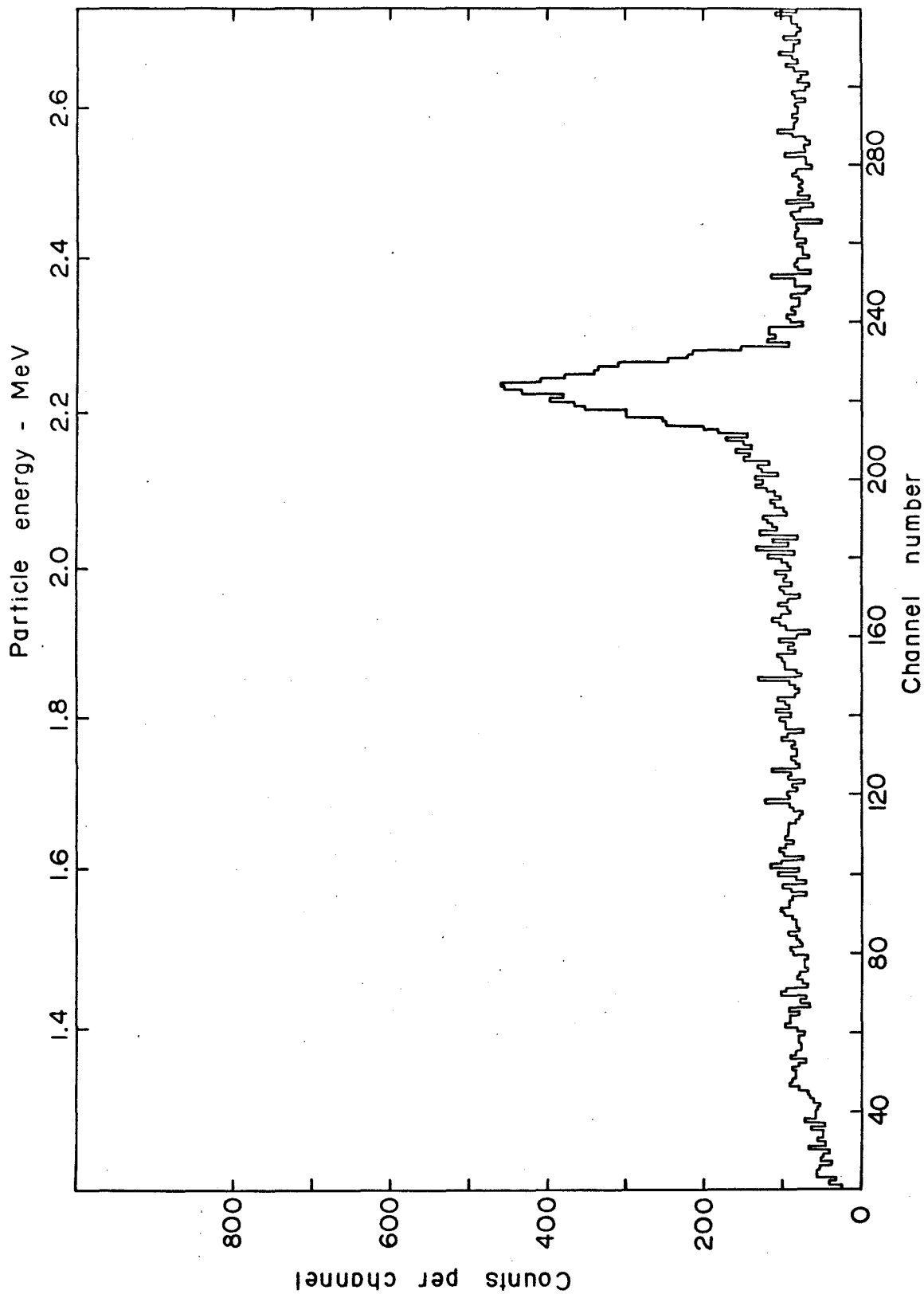
Particle energy - MeV
1.4
1.6
1.8
2.0
2.2
2.4
2.6
Counts per channel
0
200
400
600
800
Channel number
40
80
120
160
200
240
280

6.4.3 Calculation of an upper limit of the decay constant of Sm^{149}.

The number of counts between 1.80 and 1.90 MeV energy interval was 1808 ± 42, giving an average of 90.4 ± 2.2 counts per channel.

The full width of half maximum for Sm^{147} peak was 12 channels. Therefore, if Sm^{149} also has the same FWHM, the total number of counts in this region would be 1082 ± 33. Therefore, the number of counts above this background required to give a noticeable peak were estimated to be 68. The total number of counts in the interval of FWHM in the Sm^{147} peak above the background =

$$4001 \pm 63.$$

Now,

$$\frac{R_{Sm^{149}}}{R_{Sm^{147}}} = \frac{N_{Sm^{149}} \cdot \lambda_{Sm^{149}}}{N_{Sm^{147}} \cdot \lambda_{Sm^{147}}}$$

where R indicates the count rate of the isotope being studied.

Hence,

$$\lambda_{Sm^{149}} < \frac{0.33 \times 149 \times 0.693 \times 68}{97.45 \times 147 \times 1.061 \times 10^{11} \times 4001} \text{ years}^{-1},$$

or $< 3.81 \times 10^{-16}$ years^{-1} for energy interval $(1.80 \leq E_\alpha \leq 1.90)$.

$$(T_{\frac{1}{2}})_{Sm^{149}} > 1.82 \times 10^{15} \text{ years}.$$

6.4.4 Upper limit of the specific activity of Sm^{149}.

$$\text{Specific activity} = \frac{P \times N \times \lambda_{Sm^{149}}}{A}$$

P is the fraction of Sm^{149} in the sample.

$(a_o)_{Sm}^{nuclide} \leq$

$$\frac{0.9745 \times 6.023 \times 10^{23} \times 3.81 \times 10^{-16}}{149 \times 3.155 \times 10^{7}} \text{ dis/(gm } Sm^{149} \text{ x sec)}$$

or 0.0476 dis/(gm x Sm^{149} x sec) for $1.80 \leq E \leq 1.90$)

$$(a_o)_{Sm}^{natural} \leq \frac{0.1383 \times 6.023 \times 3.81 \times 10^{7}}{150.35 \times 3.155 \times 10^{7}}$$

or 6.69×10^{-3} dis/(gm Sm x sec) for $(1.80 \leq E \leq 1.90)$.

Therefore,

the upper limit of the specific activity of Sm^{149} in Natural Sm = 6.69×10^{-3} dis/(gm Sm x sec) for $1.80 \leq E \leq 1.90$.

TABLE 6.3

SUMMARY OF RESULTS

Nuclide	E_α (MeV)	Q_α (MeV)	Specific activity (dis/(gm x sec)		Decay constant	Half life
			Nuclide	Natural	$year^{-1}$	$year^{-1}$
Sm^{146}	-	-	-	< 0.0108	-	-
Sm^{147}	2.233 ± 0.005	2.295 ± 0.005	847 ± 20	124.2 ± 3	$(6.531 \pm 0.12) \times 10^{-12}$	$(1.061 \pm 0.019) \times 10^{11}$
Sm^{148}	1.958 ± 0.010	2.01 ± 0.010	$(6.17 \pm 2.4) \times 10^{-2}$	$(6.8 \pm 2.7) \times 10^{-3}$	$(4.7 \pm 1.9) \times 10^{-16}$	$(1.45 \pm 0.60) \times 10^{15}$
Sm^{149}		-	$< 4.76 \times 10^{-2}$ (for 1.80 MeV < E_α < 1.90 MeV)	$< 6.69 \times 10^{-3}$	$< 3.81 \times 10^{-16}$	$> 1.82 \times 10^{15}$

CHAPTER VII

DISCUSSION AND CONCLUSION

7.1 Discussion of the Results

7.1.1 Sm^{147}

The energy and half-life measurements for Sm^{147} were of considerable importance in this work because this nuclide was employed as an energy and half-life standard in other measurements. The half-life of Sm^{147}, obtained in these measurements is in good agreement with the recent results obtained by scintillation measurements (Don-64, Val-65). This is probably because of several improvements in the experimental technique. The use of a comparative method reduces the error in gravimetric analysis. Also, the uncertainty caused by the 'tail' of the alpha peak was reduced by considering the resolution of the ion chamber. However, the experimental conditions are not completly satisfactory because of the presence of Th^{228} and its decay products in natural thorium, which cause some uncertainty by interference with the Th^{232} peak.

The alpha particle energy of Sm^{147}, 2.233 ± 0.005 MeV, is also in agreement with recent measurements. The latest mass measurements of MacDougall et. al. (Mac -66) give the Q-value for Sm^{147} alpha-decay as 2.295 ± 0.005 MeV, which corresponds to an alpha particle energy of 2.233 ± 0.005 MeV.

Our final results for Sm^{147} are:

Alpha-particle energy (E_α) = 2.233 ± 0.005 MeV

Q-value for alpha-decay (Q_α) = 2.295 ± 0.005 MeV

Alpha-decay constant (λ) = (6.531 ± 0.15) x 10^{-12} $year^{-1}$

Half-life of Sm^{147} ($T_{\frac{1}{2}}$)$_\alpha$ = (1.061 ± 0.019) x 10^{11} years

Specific activity of Sm^{147} = (847 ± 20) dis/(gm Sm^{147} x sec)

Specific activity of natural Sm(a_o) = (124.2 ± 3.0) dis/(gm Sm x sec)

7.1.2 Sm^{146}

An upper limit of 2.23 x 10^{-6}% for the isotopic abundance of Sm^{146} in natural samarium was obtained, whereas the best mass spectrometric limit, obtained by Collins, Rourke, and White (Col-57) is 8 x 10^{-5}%.

The half-life of Sm^{146}, as measured by Friedman et. al. (Fri-66), is (1.026 ± 0.048) x 10^8 years. If one assumes that it was formed in the same manner (and therefore at the same time) as Sm^{144} it would originally have been about 20% of the present abundances of Sm^{147} provided the time interval of formation was short compared to 10^8 years. Now, if the age of the elements is assumed to be 4.5 x 10^9 years, then the abundance of Sm^{146} would be of the order of 10^{-15}. This quantity would be very difficult to detect using an ionization chamber.

7.1.3 Sm^{148}

The results obtained are:

Alpha-particle energy (E_α) = 1.958 ± 0.01 MeV

Q-value for alpha-decay (Q_α) = 2.010 ± 0.01 MeV

Alpha-decay constant (λ) = $(4.71 \pm 1.9) \times 10^{-16}$ year^{-1}

Half-life of Sm^{148} $(T_{\frac{1}{2}})_{\alpha}$ = $(1.45 \pm 0.60) \times 10^{15}$ years

Specific activity of Sm^{148} = $(6.16 \pm 2.40) \times 10^{-2}$ dis/(gm Sm^{148} x sec)

Specific activity of natural samarium (a_o) = $(6.82 \pm 2.7) \times 10^{-3}$ dis/(gm Sm x sec).

The only other results concerning Sm^{148} are those of Karras (Kar-60) and of Macfarlane and Kohman (Mac-61). The reason that Macfarlane et. al. could not detect it was because of the large amount of Sm^{147} in the sample as well as a high background. By using an enriched sample (99.941%) of Sm^{148} and 0.026% Sm^{147}, the low energy tailing was reduced below the activity of Sm^{148}. Also the resolution of the ion chamber and background was much better than that of the previous workers. Hence, this made possible the detection of Sm^{148} activity, which has a rather longer half-life than reported by Karras (Kar-60).

The alpha-particle energy of Sm^{148} is 1.958 ± 0.01 MeV which corresponds to a Q-value of (2.01 ± 0.01) MeV for Sm^{148} alpha-decay. The best Q_{α} from mass data is (2.001 ± 0.005) MeV (Mat-65). The value obtained in the present work is within the error limit of the mass measurements, but is smaller than the value given by Karras (Kar-60).

7.1.4 Sm^{149}

No alpha activity caused by Sm^{149} was observed in these

measurements. It as possible to get an upper limit of the specific activity. The results obtained are:

Specific activity of Sm^{149} < 0.0476 dis/(gm Sm^{149} x sec)

Specific activity of natural samarium < 6.69×10^{-3} dis/(gm Sm x sec) for $(1.80 \leq E \leq 1.90)$

Alpha-decay constant of $Sm^{149}(\lambda) < 3.81 \times 10^{-16}$ year $^{-1}$.

Half-life of Sm^{149} $(T_{\frac{1}{2}})_{\alpha} > 1.82 \times 10^{15}$ years.

The mass value alpha-particle energy of Sm^{149} is 1.847 ± 0.005 MeV (Mat-65). Karras (Kar-60) has reported E_α as being 1.84 ± 0.005 MeV and has determined its half-life to be $(4 \pm 2) \times 10^{14}$ years. Macfarlane and Kohman (Mac-61) did not observe any activity and reported the half-life to be greater than 1.1×10^{15} years for the energy interval $1.5 < E < 2.0$. Our results are not in disagreement with the later workers but the half-life obtained by Karras for Sm^{149} appears to be too short.

From the systematics of the alpha-decay of rare earth nuclei, the samarium-149 alpha-decay would be a favoured alpha-decay. Therefore, if Sm^{149} follows the systematics, the half-life of this nuclide would be of the order of 2×10^{16} years.

7.2 General Discussion

7.2.1 Alpha-decay Rate Correlation.

Half-lives, for alpha-decay transitions proceeding from even

nuclei to ground level in the daughter nuclei in heavy elements, have been found to agree well with those calculated from simple Coulomb barrier penetration theory. The decay rate correlations are based on the fact that the half-life is expressed as

$$\text{Log}\,(T_{\frac{1}{2}}) = C_1(Z_d E_\alpha^{-\frac{1}{2}} - Z_d^{\frac{2}{3}}) - C_2 \qquad 7.1$$

where $T_{\frac{1}{2}}$ is the alpha half-life of the nuclide in years, which has particle energy E_α. Z_d is the atomic number of the daughter nuclei and C_1 and C_2 are constants. The equation was derived by Taagepera and Nurmia (Taa-61) from Bethe's one body model equation. The values of C_1 and C_2 are obtained by fitting to experimental data from heavy elements. The best parameters are:

$$C_1 = 1.61 \text{ and } C_2 = 28.9.$$

Theoretical half-lives of the rare earth alpha-emitters were computed from equation (7.1) and are given in Table 7.1.

A simple examination of the Table 7.1 shows good agreement between the experimental and theoretical half-lives except in few cases, where there is a discrepancy of a factor of 3 to 6. But considering the sensitive dependence of half-life on decay energy the agreement is excellent.

From heavy element data, it is known that the odd mass alpha-emitters have half-lives longer than those calculated from theory. But in the case of odd mass rare earth alpha-emitters of Sm, Gd, Er,

TABLE 7.1

Nuclide	E_α(MeV)	$T_{\frac{1}{2}\alpha}$(exp)	$T_{\frac{1}{2}\alpha}$(theor)	$\frac{T_{\frac{1}{2}\alpha}(\text{exp})}{T_{\frac{1}{2}\alpha}(\text{theor})}$	Ref.
Sm^{146}	2.46 ± .02	(1.026 ± .048) x 10^8y	1.037 x 10^8y	0.989	Fri-66
Sm^{147}	2.233±.005	(1.061 ± .019) x 10^{11}y	1.175 x 10^{11}y	0.903	Present work
Sm^{148}	1.958±.01	(1.45 ± .60) x 10^{15}y	2.912 x 10^{15}y	0.501	Present work
Sm^{149}	1.847±.005	>1.82 x 10^{15}y	3.207 x 10^{17}y	-	Present work
Gd^{148}	3.16 ± .01	97.6 ± 6.5y	71.8 y	1.184	Fri-66
Gd^{149}	3.0 ± .15	3.644 ± 10^3y	3.243 x 10^3y	1.123	Ras-53
Gd^{150}	2.73 ± .01	(1.78 ± .08) x 10^6y	1.78 x 10^6y	1.00	Fri-66
Gd^{151}	2.60 ± .02	4.20 x 10^7y	6.10 x 10^7y	0.688	Sii-64
Gd^{152}	2.14 ± .03	1.1 x 10^{14}y	1.31 x 10^{14}y	0.84	Mac-59
Dy^{150}	4.23 ± .02	44 ± 4 min	14.52 min	3.03	Mac-64a
Dy^{151}	4.06 ± .04	5.085 hr	2.64 hr	1.926	Mac-64a
Dy^{152}	3.65 ± .02	200 days	69 days	2.90	Mac-64a
Dy^{153}	3.48 ± .02	24.35 y	3.78 y	6.44	Mac-64a
Dy^{154}	2.85 ± .05	1.00 x 10^6y	2.393 x 10^6y	0.418	Mac-64a

TABLE 7.1 (cont'd)

Nuclide	E_α(MeV)	$T_{\frac{1}{2}\alpha}$(exp)	$T_{\frac{1}{2}\alpha}$(theor)	$\frac{T_{\frac{1}{2}\alpha}(\text{exp})}{T_{\frac{1}{2}\alpha}(\text{theor})}$	Ref.
Er^{152}	4.80 ± .02	11.9 sec ± 0.5	6.43 sec	1.85	Mac-63b
Er^{153}	4.67 ± .02	37.89 sec ± 0.2	30.02 sec	1.262	Mac-63b
Er^{154}	4.15 ± .02	4.50 min	8.16 hr	?	Mac-63b
Yb^{154}	5.33 ± .02	0.398±.04 sec	0.16 sec	2.49	Mac-64b
Yb^{155}	5.21 ± .02	1.832±.15 sec	0.55 sec	3.33	Mac-64b

and Yb, the theoretical $T_{\frac{1}{2}}$ does not deviate very much from the experimental $T_{\frac{1}{2}}$ and seem to exhibit favoured alpha-decay.

The Coulomb potential with a sharp cut off at some effective nuclear radius is not a realistic nuclear potential. For a more realistic approach an alpha-nuclear potential was introduced (Ras-59, Pog-66, Cho-62), which was derived from alpha scattering data. By using expressions (1.4.3, 1.4.4, 1.4.5) the experimental alpha reduced widths have been computed. The results of these computations are given in Table 7.2.

It is seem from Table 7.2 that where the data is quite certain, the reduced widths for a given neutron number in even-even nuclei are constant except in the case of the Dy isotopes, where a proton subshell (64 protons) closure is reflected. The magnitude of δ^2 is much smaller as compared to other even-even rare earth alpha-emitters because the parent and daughter have different quantum states.

The reduced widths for odd mass nuclei are also of the same order of magnitude as for even-even nuclei. This can be understood as follows:

The odd mass nuclei contain an unpaired nucleon which is less tightly bound than the others and the ground state spin of the parent and the daughter are found to be same. Therefore, when an alpha-particle forms it is not likely to incorporate the odd nucleon, but

TABLE 7.2

Nuclide	$Q_{eff.}$ (MeV)	$T_{\frac{1\alpha}{2}}$ (experimental) sec	Inner turning point fm		Reduced alpha widths (MeV)			Hindrance factor			Ref.
			Igo	Wood-Saxon	Igo	non-local	Wood-Saxon	Igo	non-local	Wood-Saxon	
Nd^{144}	1.92	7.572×10^{22}	8.437	8.304	0.132						Mat-64
Pm^{145}	2.324	1.994×10^{19}	8.455	8.324	0.198	0.148	0.269	1.30	1.052	1.49	Nur-62
Sm^{146}	2.550	3.237×10^{15}	8.466	8.334	0.0955	0.0714	0.130				Fri-66
Sm^{147}	2.316	3.344×10^{18}	8.474	8.340	0.1026	0.077	0.142	1.33	1.34	1.37	Pre-work
Sm^{148}	2.033	4.575×10^{22}	8.480	8.342	0.178	0.135	0.258				Pre-work
Eu^{147}	3.013	9.465×10^{10}	8.486	8.355	0.187	0.138	0.252	0.49	0.493	0.493	Sii-62
Gd^{148}	3.290	3.076×10^{9}	8.500	8.368	0.088	0.0647	0.1185				Fri-66
Gd^{149}	3.105	1.148×10^{11}	8.508	8.375	0.1027	0.756	0.139	1.032	1.03	1.036	Ras-53
Gd^{150}	2.826	5.616×10^{13}	8.514	8.378	0.124	0.0911	0.170				Fri-66
Gd^{151}	2.692	1.325×10^{15}	8.525	8.388	0.158	0.117	0.219	0.785	0.779	0.707	Sii-64
Tb^{149}	4.081	9.135×10^{4}	8.531	8.405	0.0213	0.0156	0.028	3.427	3.439	3.347	Gro-64
Tb^{151}	3.513	2.019×10^{9}	8.541	i.410	0.0083	0.0061	0.0116	10.416	10.385	10.164	Gro-64

TABLE 7.2 (cont'd)

Nuclide	$Q_{eff.}$ (MeV)	$T_{\frac{1}{2}\alpha}$ (experimental) sec	Inner turning point fm		Reduced alpha widths (MeV)			Hindrance factor			Ref.
			Igo	Wood-Saxon	Igo	non-local	Wood-Saxon	Igo	non-local	Wood-Saxon	
Dy^{150}	4.368	2.40×10^{2}	8.545	8.418	0.0580	0.0426	0.0689				Mac-64a
Dy^{151}	4.193	1.830×10^{4}	8.553	8.425	0.0789	0.0577	0.104	0.677	0.678	0.646	Mac-64a
Dy^{152}	3.771	1.728×10^{7}	8.554	8.421	0.0489	0.0356	0.0658				Mac-64a
Dy^{153}	3.596	7.20×10^{8}	8.563	8.429	0.0225	0.0164	0.0289	8.087	8.098	8.843	Mac-64a
Dy^{154}	2.949	3.155×10^{13}	8.556	8.426	0.315	0.230	0.440				Mac-64a
Ho^{151}	4.748	42.0	8.561	8.436	0.104	0.0743	0.133	0.836	0.878	0.830	Mac-63a
Ho^{153}	4.048	1.800×10^{5}	8.567	8.436	0.242	0.175	0.325	0.890	0.898	0.910	Mac-63a
Er^{152}	4.953	11.90	8.572	8.445	0.116	0.0843	0.152				Mac-63b
Er^{153}	4.819	37.89	8.582	8.454	0.161	0.116	0.212	0.512	0.512	0.514	Mac-63b
Er^{154}	4.284	2.70×10^{2}	8.578	8.445	20.09	14.5	27.085				Mac-63b
Tm^{153}	5.271	1.12	8.586	8.459	0.129	0.0936	0.169	0.895	0.894	0.984	Mac-64b
Yb^{154}	5.497	0.398	8.598	8.469	0.115	0.083	0.150				Mac-64b
Yb^{155}	5.373	1.833	8.608	8.479	0.082	0.0593	0.108	1.402	1.400	1.39	Mac-64b

probably consists of protons and neutrons which are already paired. In such transitions, the odd nucleon does not change its quantum state. Therefore, the wave-function of the initial and the final states are very similar leading to a large overlap integral involving the initial and final state wave-functions of the odd nucleon.

If the ground state spins of the parent and the daughter are different δ^2 will be very much smaller and the alpha-decay rate will be unfavoured or hindered. The hindrance factors for odd A nuclei are given in column 7 of the Table 7.2. From the table it is evident that in all cases except Tb^{149}, Tb^{151} and Dy^{153} alpha-decay is favoured. The data on Dy^{153} and Dy^{152} are uncertain and the possibility that even these might be favoured cannot be ruled out. However, the alpha-decay of Tb^{149} and Tb^{151} is hindered because of the closure of subshell 64.

An examination of reduced widths and hindrance factors calculated using different alpha-nuclear potential (Table 7.2) shows (a) that the Woods-Saxon potential results in a 35 - 40% enhancement in reduced widths. (b) The non-local potential can reduce the reduced widths up to 35% as compared to Igo static nuclear potential. Hindrance factors do not change very much. That is, the introduction of these potentials instead of the Igo potential does not effect the relative reduced widths of the rare earth nuclei. The plot of the values of δ^2 (calculated using Igo Potential) are shown in figure 7.1.

Theoretically the reduced widths of the rare earth alpha-emitters were calculated by Macfarlane, Rasmussen and Rho (Mac-64b).

Figure 7.1 Plot of the experimental reduced alpha width as a function of parent proton number for 84 neutron nuclei.

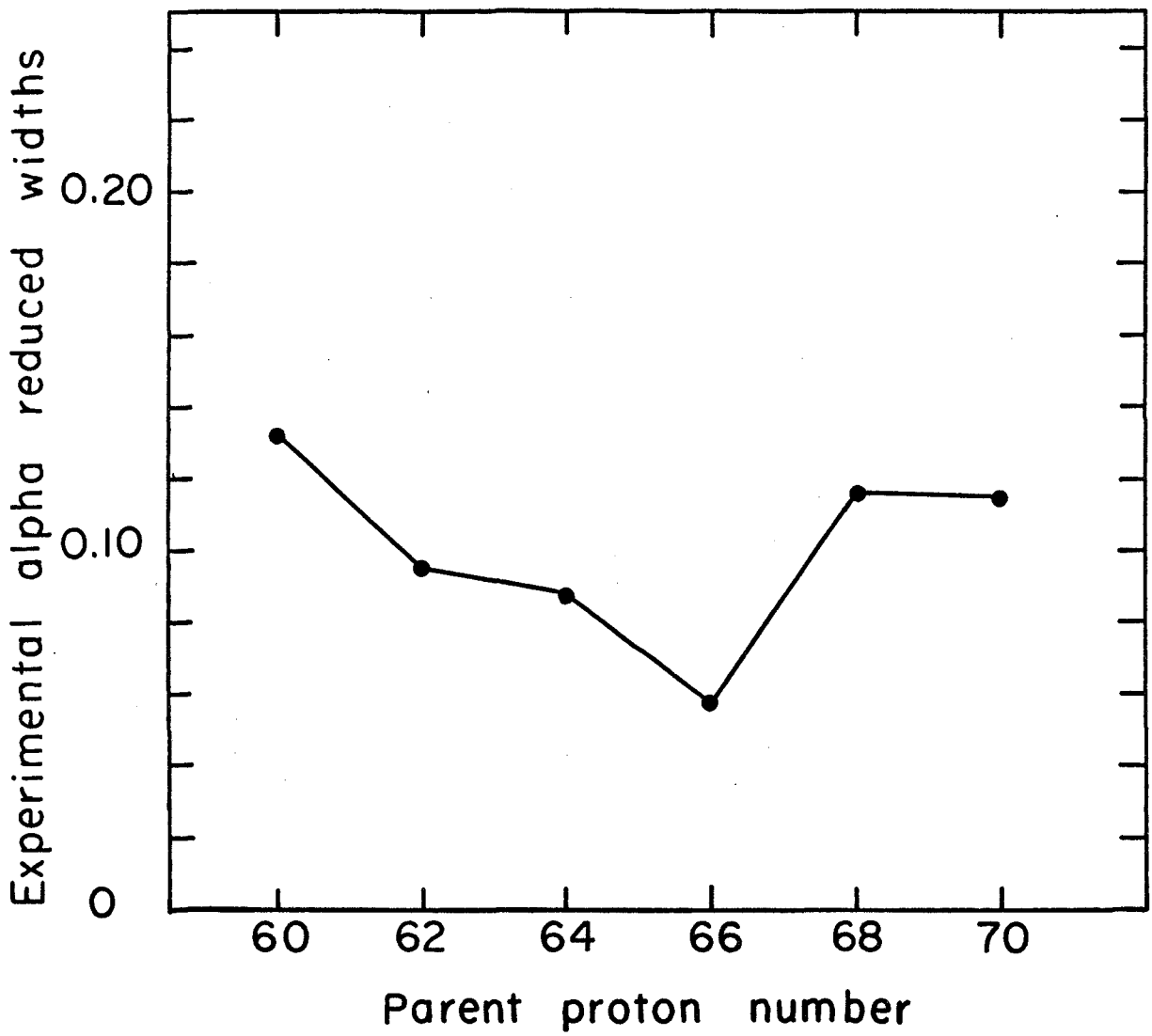
Experimental alpha reduced widths
0.20
0.10
0
60
62
64
66
68
70
Parent proton number

Rasmussen (Ras-63) has used the following formula for Po α's

$$\delta^2_{pair} = C^2 \left| \left[\sum_{jp} (-)^{\ell_p} c(j_p)\ (2j_p+1)^{\frac{1}{2}}\ B_p(\ell_p)\ Y^2_{jp}\ (R) \right] x \right.$$
$$\left. \left[\sum_{jn} (-)^{\ell_n}\ c(j_n)\ (2j_n+1)^{\frac{1}{2}}\ B_n(\ell_n)\ Y^2_{j_n}\ (R) \right] \right|^2 \qquad 7.2$$

where j and l represent the total and orbital angular momentum, B(l) is a correction factor, C is a constant and $y_j(R)$ the orbital wave-function of the valence neutrons or protons. c(j) is defined by Zeh (Zeh-63) as

$$c(j) = (-)^{\ell} < P_f\ P \| P_i > . \qquad 7.3$$

where P_i and P_j are the initial and the final state wave-functions and P an operator. In calculations of δ^2_α only c(j) need to be calculated because the values of $y_j(R)$ are taken from Blomquist and Wohlborn (Blo-60) and $B(\ell)$ according to Rasmussen (Ras-63) is given as $\exp(-0.013\ \ell(\ell+1))$. The c(j) terms can be derived from BCS (Bardeen, Cooper and Schiffer) wave-functions and are taken from Macfarlane et. al. (Mac-64 b)

For pure shell model calculations, as given by Zeh for one orbital j with n pairs in the parent and (n - 1) pairs in the daughter

$$c(j) = \left[\frac{n(\Omega-n+1)}{\Omega} \right]^{\frac{1}{2}} \qquad 7.4$$

where Ω is the degeneracy, $\Omega = j + \frac{1}{2}$.

Zeh also derived c(j) by considering Kisslinger and Sorensen type product wave-functions and arrived at the result

Figure 7.2 Plot of relative reduced alpha width as a function of parent proton number calculated from:

(i) Pure shell model (equation7.4)

(ii) BCS product wave-function (equation 7.5).

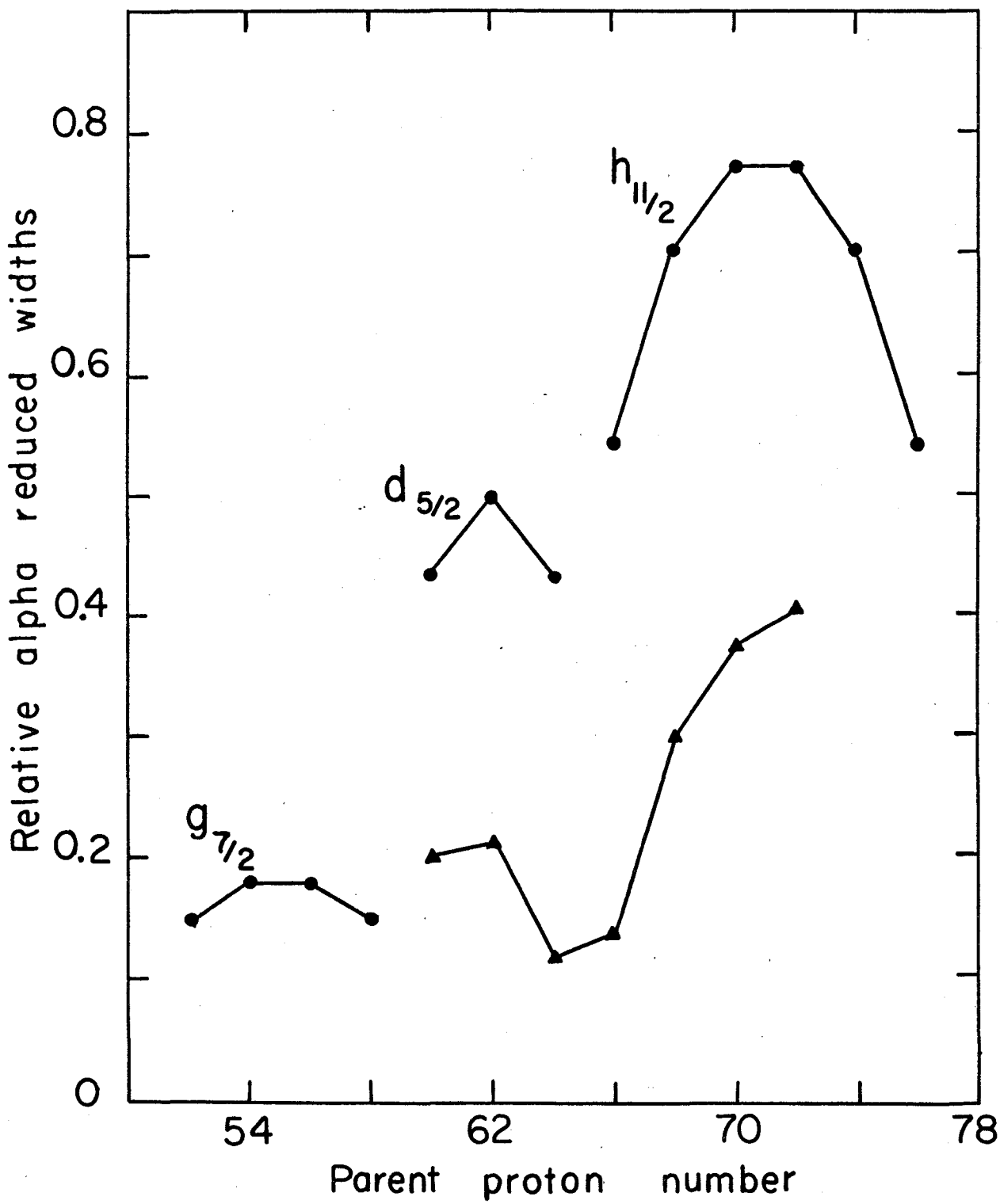
0.8
0.6
0.4
0.2
0
Relative alpha reduced widths
h11/2
d5/2
g7/2
54
62
70
78
Parent proton number

$$< P_f \; P \,||\, P_i > = \frac{U_j' V_j \Omega_j^{\frac{1}{2}}}{U_j U_j' + V_j' V_j} \; \pi_\nu \; (U_\nu U_\nu' + V_\nu V_\nu')^{\Omega_\nu} \qquad 7.5$$

where V_ν^2 is the probability of the νth orbital being occupied by a pair and $U_\nu^2 + V_\nu^2 = 1$. The primes are for final states. The results of the calculations for 84 neutron system from equation 7.2, by using 7.4 and 7.5, are shown in figure 7.2. In these calculations where the neutron number is a constant, the neutron contribution factor can be neglected.

The dip at Z = 64 and 66 may be qualitatively associated with a rate decrease caused by lowered core overlap. The theoretical calculations do reproduce the experimental feature of the dip at Z = 66.

The calculations were also carried out including neutron contribution factor for 84 and 86 neutrons. In the pure shell model calculations the reduced widths for 86 neutron nuclei are 1.22 times the reduced widths for 84 neutron nuclei while by using BCS wave-functions this factor is 2.54. The experimental reduced width for Sm^{148} is 1.86 tines that of Sm^{146} and for Gd^{150} it is 1.40 times the reduced width of Gd^{148}.

In summary (1) the use of different alpha nuclear potentials do not yield any better result than the Igo potential as far as the relative reduced widths are concerned. (2) Theoretical δ^2 shows a dip between Z = 64 and 66 which is consistent with the experimental observations.

Figure 7.3 Plot of Q as a function of parent neutron number for fixed Z.

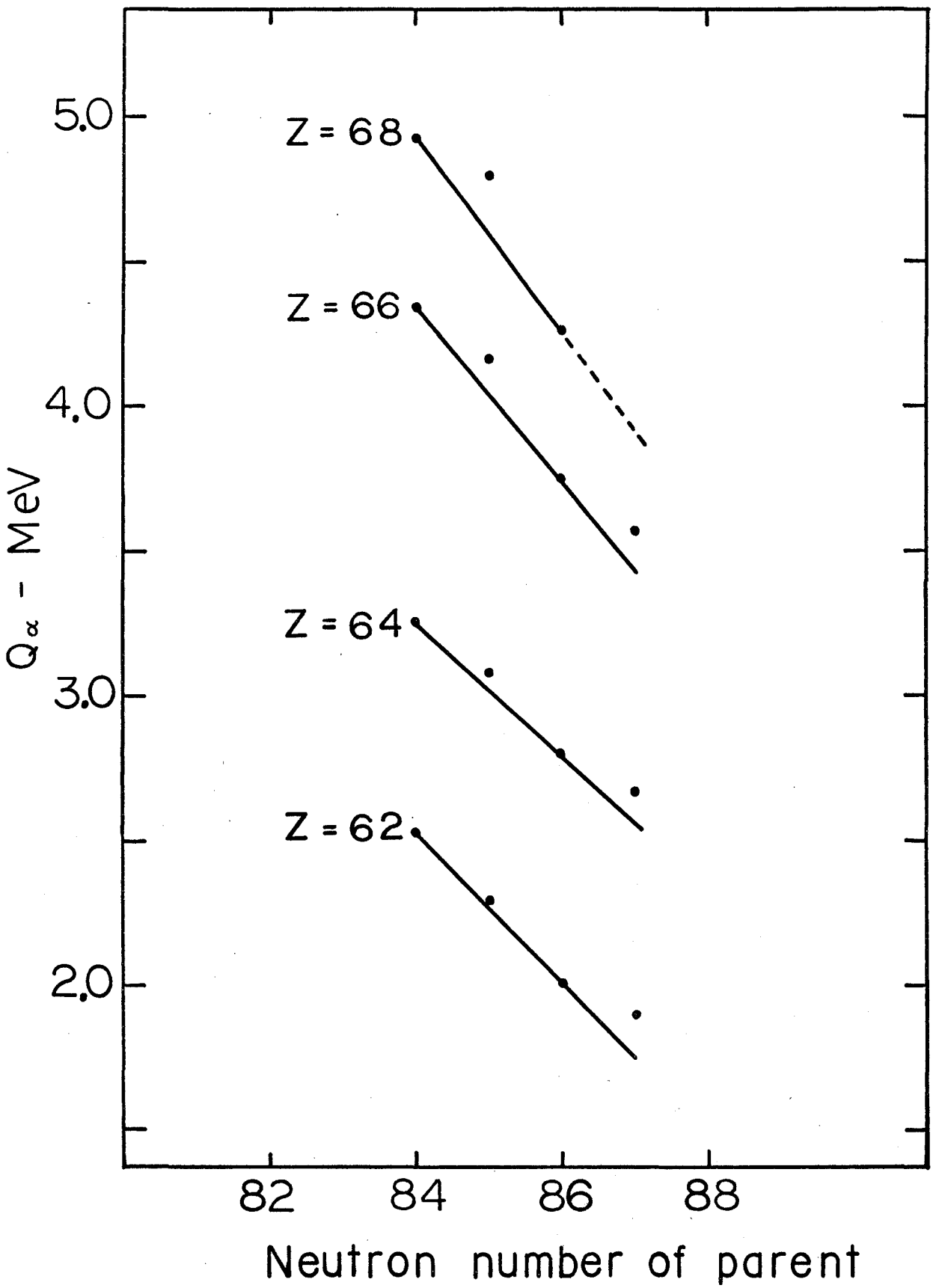
5.0
4.0
3.0
2.0
Z = 68
Z = 66
Z = 64
Z = 62
Qα - MeV
82
84
86
88
Neutron number of parent

7.2.2 Alpha-decay Energy Systematics.

In the heavy element region it is well known that alpha-decay energies for a given Z increase with decreasing neutron number. This trend is also observed in the rare earth region. The behaviour is because of a gain in binding energy associated with increasing A as well as a slight decrease in Coulomb energy. The effect of the closed shell N = 82 is similar to that observed near the closed shell N = 126. The maximum α-decay energy is observed at 84 neutrons for a fixed Z, but no isotope with neutron number less than 84 is known to emit alpha-particles in rare earth region because the energy available for alpha-emission is too low.

If one plots Q_α as a function of the neutron number of the parent, N, for fixed Z (shown in figure 7.3), Q_α for odd N falls systematically higher than that for even N. This effect is apparently because of a rather strong neutron pairing energy where the parent pairing energy is greater than the daughter. This behaviour can be seen in case of Sm, Gd, and Dy isotopes where Q_α values are well established.

7.3 Summary of the Properties of the Gridless Ion-Chamber

It has been established in this work that a cylindrical ionization chamber is in many respects better than a gridded ionization chamber. The total capacitance for the system without grid is less than that of with grid which improves the signal to noise ratio. Also the possibility of electron collection by the grid is

eliminated by removing the grid and charge collection is almost complete.

The use of high pressure reduces the 'positive ion effect' because the alpha track length is reduced. The background is less in ungridded ion chamber than gridded because the natural contaminations of the grid wires is not present.

By employing argon, acetylene and nitrogen gas mixture the total ionization efficiency is increased and electron attachment to oxygen or other electro-negative impurities is reduced.

The low background, high resolution and large sample area have made it possible to investigate natural alpha-decay in the rare earth region using an instrument vastly superior to any that have been employed in previous similar investigations.

Finally, this study has yielded data on the alpha-decay properties of very long lived nuclear species. These data make it possible to test alpha-decay theory over a range of alpha penetrability factors varing more than 23 orders of magnitude.

SECTION B

A SEARCH FOR NEUTRONIC NUCLEI

CHAPTER I

INTRODUCTION

1.1 General Considerations

Recently results have been obtained on the properties of light nuclei which are far on the neutron excess side of the beta stability. Of particular interest has been the question of the possible particle stability of neutron cluster such as n^2, n^3, n^4 etc. Further highly neutron excess light nuclei such as Li^{11} (Pos-66), He^8 (Loz-61, Nef-63, Det-65), Be^{12} (Pos-66, Whe-65, Cer-66) have also been discovered. Neutron separation energies obtained for these nuclei can be used to estimate the binding energy of some of the Z = 0 nuclei. There is some experimental evidence which shows that the dineutron (n^2) does not exist. The data on n^3 and n^4 are non-conclusive. The possibility that bound states might exist for heavier neutronic nuclei such as n^6 and n^8 is considered unlikely, but cannot be ruled out completely.

If such nuclei exist, their density would be less than that of an ordinary nucleus and to a first approximation they could be considered to be a fermi gas of low density. In such a gas the kinetic energy of the colliding particles would be small and the major scattering would be an s-state interaction occuring for pairs of neutrons with opposite spin.

Because of surface tension effects, there might be a

minimum critical size below which the neutronic nucleus is unstable. This implies that if the existence of the dineutron, trineutron and tetraneutron is experimentally disproved, it does not by itself exclude the possible existence of heavier neutronic nuclei. The neutron shell closure at 8 neutrons might give rise to a more tightly bound system so that n^8 might be expected to have extra stability. If n^8 were stable, the possibility that many different kinds of neutronic nuclei are particle stable would exist. These nuclei would be unstable toward β^--emission but would have half-lives not less than 10^{-3} seconds.

Nuclei such as He^6 and He^8 have been observed as fission products. Since a nucleus such as n^8 is not too much different from He^8 it might be expected to be present as a component of a nuclear reactor flux. He^8 and Li^{11} were also found to be products of high energy proton reactions on heavy element targets. This might be an attractive way to produce n^8 or other clusters as well.

1.2 Previous attempts to Produce Neutronic Nuclei.

1.2.1 Dineutron

Ferguson and Montague (Fer-52) were the first to try to detect the dineutron as a component of a reactor flux by using the $He^4(n^2,\gamma)He^6$ reaction. They obtained a negative result. Saksaka and Tomita (Sak-61) looked for the dineutron as a product of the reaction $H^3(d,n^2)He^3$ with the subsequent capture of a dineutron by radiative capture in Al^{27} and Bi^{209}. On the basis of the results with aluminium they reported the detection of the dineutron and

calculated a binding energy of 3 MeV. The experiment with Bi did not yield any definite result. Katase et. al. (Kat-62) repeated the experiment but obtained negative results.

Schiffer and Vandenbosch (Sch-63) also attempted a search for the dineutron in a reactor core using the reaction $Al^{27}(n^2,p)Mg^{28}$ as the detector. They also obtained negative results and set an upper limit of 5×10^{-9} dineutrons per fission for its existence in a reactor flux.

Experiments were also done by Voitovetski, Kosunskii and Pazhin (Voi-65) using the reaction $n(d,p)n^2$ which could be detected through the characteristics of the proton spectrum. Their experiment showed that if the dineutron does exist, the cross section for its production is less than 10^{-29} cm^2. Willard, Bair and Jones (Wil-64) also reported negative results from the same experiment.

1.2.2 Trineutron

Stojic et.al. (reported in Baz-65) made an unseccessful attempt to detect the particle stable trineutron through the reaction $T(n,p)n^3$ using the reaction $Al^{27}(n^3,d)Mg^{28}$ as a detector.

Ajdacic et. al. (Ajd-65) reported an interesting experiment in which the reaction $T(n,p)n^3$ was studied using 14.4 MeV neutrons. The energy spectrum of the outgoing protons at 0^o showed a peak at 6.4 MeV, kinematically corresponding to an n^3 state with a binding energy of 1.0 MeV and with a production cross-section of 3.8 mb.

Thornton et. al. (Tho-66) attempted to detect bound tri-

neutron by the method of Ajdacic et. al. using 20.8 MeV neutrons. No evidence for the existence of the trineutron was found in this experiment. However, this experiment is not directly comparable with that of Ajdacic et. al. because higher energy neutrons were used. Fuschini et. al. (Fus-67) recently repeated the experiment of Ajdacic et. al. at nearly the same energy. There was no evidence for a peak which could be ascribed to n^3 with binding energy lower than 3 MeV.

1.2.3 Tetraneutron

Argon and Piazzoli (Arg-62) suggested the probable existence of n^4 from their study of the excited states of He^4. Consequently Shciffer and Vandenbosch (Sch-63) searched n^4 among the fission products of a nuclear reactor using the reactions $N^{14}(n^4,n)N^{17}$ and $Al^{27}(n^4,T)Mg^{28}$. Assuming reasonable values for the reaction cross section the number of n^4 produced in the fission was found to be less than 5×10^{-9} per fission.

Brill et. al. (Bri-64) tried to detect light nuclei in a two body break-up reaction of the type

$$Ca^{48} + C^{12} \rightarrow n^4 + Fe^{56}$$

where the Fe^{56} energy spectrum would be monoenergetic if the neutrons were emitted as a correlated cluster. They set an upper limit for the n^4 cross-section of about 1 μb. Davis et. al. (Dav-65) studied the reaction $H^4(\pi^-,\pi^+)n^4$ with incident pions of momenta 200 and 270 MeV/C using a two inch diameter liquid helium target. No evid-

hence for the existence of a tetraneutron was found and an upper limit for the production cross-section at 90^{o} for both incident momenta was given a value of about 1μb. Cohen et. al. (Coh-64) searched for a particle stable tetraneutron by observing the spectum of He^{3} from the capture of π^{-}-mesons by Li^{7} i.e. $Li^{7}(\pi^{-},He^{3})n^{4}$ but obtained negative results.

Recently Burmestrove et. al. (Bur-67) searched for bound states of n^{3} and n^{4} in fission products using an activation method to detect the induced activity particularly by neutron cluster capture. The following reactions were used:

$Al^{27}(n^{3},d)Mg^{28}$ $\qquad$ $Al^{27}(n^{4},T)Mg^{28}$

$Sc^{45}(n^{3},n\alpha)K^{43}$ $\qquad$ $Sc^{45}(n^{4},2n\alpha)K^{43}$

$Sc^{45}(n^{3},p)Ca^{47}$ $\qquad$ $Sc^{45}(n^{4},d)Ca^{47}$

They concluded that n^{3} or n^{4} are not produced in fission. The upper limit for the product of the flux of the corresponding neutronic nuclei and the cross-section for the production of Mg^{28} from Al^{27} was found to be 8×10^{-22} sec^{-1}. For K^{43} and Ca^{47} from Sc^{45} the limit was set at 2×10^{-18} and 3×10^{-18} sec^{-1} respectively.

1.3 Theoretical Background

It appears from the experiments reported that the existence of particle stable n^{2}, n^{3} and n^{4} is rather unlikely.

Zeldovich (Zel-60) in a theoretical study considered the system of a very large nucleus consisting of neutrons alone. He

suggested the possibility of the existence of an all neutron nucleus whose size would be governed by the surface tension of the neutron liquid. The theoretical considerations of Mitra and Bhasin (Mit-66) using a separable non-local potential for the trineutron show its possible existence with a binding energy of 1 MeV. But the variational calculations of Barbi (Bar-67) and Okamoto and Davies (Oka-67) led them to conclude that the existence of a bound trineutron is most unlikely.

Goldanskii et. al. (Gol-60) has pointed out from the neutron pairing energy considerations that if a trineutron exists, then the tetraneutron would certainly exist. Variational calculations done by Tang and Bayman (Tan-65) indicate that there is neither a bound nor a resonant n^4 system. From this they have speculated that n^6 is also unbound and have ventured to conclude that a system containing only neutrons does not form a bound state. For a system to be bound there must be the presence of other strongly interacting particle like a proton, Λ-particle etc.

No attempt has been made to detect heavier neutronic nuclei. So it was felt that the theoretical basis for Tang and Bayman's work needed experimental verification. The work described in this section is an attempt to detect particle stable neutron clusters in the range of mass 6-10.

CHAPTER II

METHOD OF DETECTION

2.1 General

Previous work on the detection of neutron cluster are so far based on either a specific nuclear reaction or a detector. The reaction product is chosen on the basis of its decay properties and sensitivity for detection. In our experiments lead isotopes were chosen as the detector because the polonium end product could be detected by α-activity. β^- and γ active interferance from other reaction products is removed. If we consider the case for n^8 only, the following reactions might occur:

$$Pb^{207}(n^8,3n)Pb^{212} \qquad Pb^{208}(n^8,4n)Pb^{212}$$
$$Pb^{207}(n^8,2n)Pb^{213} \qquad Pb^{208}(n^8,3n)Pb^{213}$$

Pb^{212} and Pb^{213} with half-lives of 10.6 hours and 10.0 minutes are β^--emitters and decay to Bi^{212} and Bi^{213} respectively. Bi^{212} and Bi^{213} with half-lives of 60.6 and 47 minutes decay to Po^{212} and Po^{213}. Po^{212} and Po^{213} are alpha-emitters and their alpha particle energies are 8.78 MeV and 8.38 MeV respectively.

The alpha activity of these Po isotopes was detected by the following methods:

2.1.1 Ionization Chamber

A large area ionization chamber was used to detect the alpha-activity of Po^{212}. The ion chamber and its operation has been discussed in Chapter II of Part A of this thesis.

Because of the large alpha-particle energy the ionization chamber was operated at a pressure of 400 cm of Hg. This system was used for counting large samples of neutron-irradiated lead.

2.1.2 Solid State Surface Barrier Detector

For experiments involving the detection of Pb^{213} -Bi^{213} which has a much shorter half-life than Pb^{212}, a gold surface barrier detector with an area of 50 mm^2 was used. Samples consisted of small quantitites of lead and chemically separated bismuth.

2.1.3 Radio-chemical Separation of Bismuth Isotopes from Lead

A very large improvement in sensitivity was achieved when Bi^{212} and Bi^{213} were radio-chemically separated from the bulk lead target. The separation technique for bismuth involved two exchange steps: (Orb-63)

In the first, radioactive bismuth exchanges with inactive bismuth dissolved in mercury. The exchange can be represented by the following reaction:

$$Bi(Hg) + Bi^{3+*} \longrightarrow Bi^{*}(Hg) + Bi^{3+}$$

where the asterisk denotes a radioactive isotope of bismuth.

The concentration of the bismuth in the amalgam must be much greater than that in the aqueous phase for effective exchange.

In the second step, the radioactive bismuth is selectively back-extracted into the aqueous phase by replacing the bismuth in the amalgam with copper. The separation of the bismuth and the remaining copper can be achieved by cation exchange separation using a halogen acid (Hydrobromic acid).

CHAPTER III

SAMPLE PREPARATION

3.1 Source of Sample

Natural lead: A sample of lead metal shot of 99.9999 % (69 grade) purity was obtained from the Consolidated Mining and Melting Company of Canada Limited, Montreal, P.Q., Canada (Cominco, Montreal, Canada).

3.2 Sample Deposition

Several methods were used to detect Pb^{212} and Pb^{213} produced by the capture of a neutron cluster in lead. In the first method a large area ionization chamber was used. Sample preparation for this was accomplished by a simple evaporation method. It consisted of spreading of an alcoholic solution of lead nitrate over the area of the sample backing (1500 cm^2). Samples up to 450 mg were used. As the area of the sample was much smaller in the experiments using the solid state surface detector, vacuum evaporation of lead metal was used to obtain a thin uniform sample. For the bismuth experiment an electroplating technique was found to be convenient.

3.3 Specific Sample Deposition Technique

3.3.1 Evaporation of an Alcoholic Solution - Procedure

(1) A weighed amount of irradiated lead was dissolved in 3 M nitric acid in a 50 ml beaker.

(2) The solution was evaporated to dryness using an infrared heat lamp. About 5 ml of distilled water was added and the solution was again evaporated to dryness. The process was repeated until the excess of nitric acid was removed.

(3) The residue (lead nitrate) was dissolved in 40 ml of anhydrous methyl alcohol and a small amount of polyethylene glycol (Carbowax) was added to it.

(4) The solution of lead nitrate was spread over a stainless steel backing and deposited in the same manner as described in Part A, Section 4.3 of this thesis.

3.3.2 Vacuum Evaporation Method

The apparatus consisted of a vacuum chamber in which a molybdenum boat was situated with a collector plate located 2.54 cm from the boat. A 0.02 cm thick mylar film was placed over the collector to give a source area of 3 cm^2.

The boat was filled with lead and the vacuum chamber was closed. The system was evacuated to a pressure of 10^{-6} mm of Hg. The Mo boat was heated electrically, and lead was evaporated to form a deposit on the mylar film. The mylar film was weighed before and after deposition to determine the weight of the deposited lead.

3.3.3 Radio-chemical Separation of Bismuth from Lead

(1) Preparation of bismuth amalgam

One percent by weight of bismuth metal (99.9999% pure) was amalgamated in triple distilled mercury by heating and agitation.

(2) Preparation of ion-exchange resin column

Dowex-50W-X8 cation exchange resin (200-400 mesh) was used in the separation. The commerical resin was washed prior to use by placing the resin in a beaker and decanting off the distilled water. Afterwards the resin was washed with 10 % ammonium citrate solution. The slurry in ammonium citrate solution was poured into a 12 mm glass tube to give a column height of 10 cm. The resin bed was washed with 3 M HCl and finally with distilled water until all of the chloride was removed. This procedure left the resin bed in the hydrogen form.

(3) Procedure:

(i) A quantity of irradiated lead (up to 20 gm) was dissolved in 3 M nitric acid in a 250 ml beaker and the volume was reduced to 5 ml by evaporation. Some of the lead crystalized out as the nitrate and was removed by decanting the solution.

(ii) The excess of nitric acid was neutralized with 8M NaOH solution and a small amount of acid was then added to prevent the precipitation of lead hydroxide.

(iii) A weighed amount of bismuth amalgam was added to the nitrate solution in a small polyethylene bottle. The air above the solution was removed by purging with nitrogen gas for 1 minute. The solution was shaken vigorously while hot for 3 minutes.

(iv) The solution was decanted off and the amalgam was washed with distilled water. The amalgam was transferred to another polyethylene bottle and 1 ml of saturated $CuSO_4$ solution

in 1M nitric acid was added to it. The bottle was then shaken vigorously for 5 minutes.

(v) The solution from step (iv) containing bismuth and copper sulphate was then passed through the cation exchange resin column where both were absorbed.

(vi) A solution of 0.3M hydrobromic acid (HBr) was then passed through the column which eluted the bismuth leaving the copper behind.

(4) Deposition of bismuth

The solution (from step (vi)) was transferred to an electroplating cell and the bismuth was deposited on a copper foil at 6 volts and 1 amp current.

The yield of the separation process was determined by separating Bi^{212} from a solution of Th^{228}. The yield of Bi was 51% and took 50 minutes to separate Bi^{212} from the solution.

Figure 4.1 Plot of alpha-pulses in the enrgy range 8.4 MeV to 9.0 MeV as a function of time for an unirradiated sample.

A - without washing the surface of lead

B - after washing with nitric acid solution.

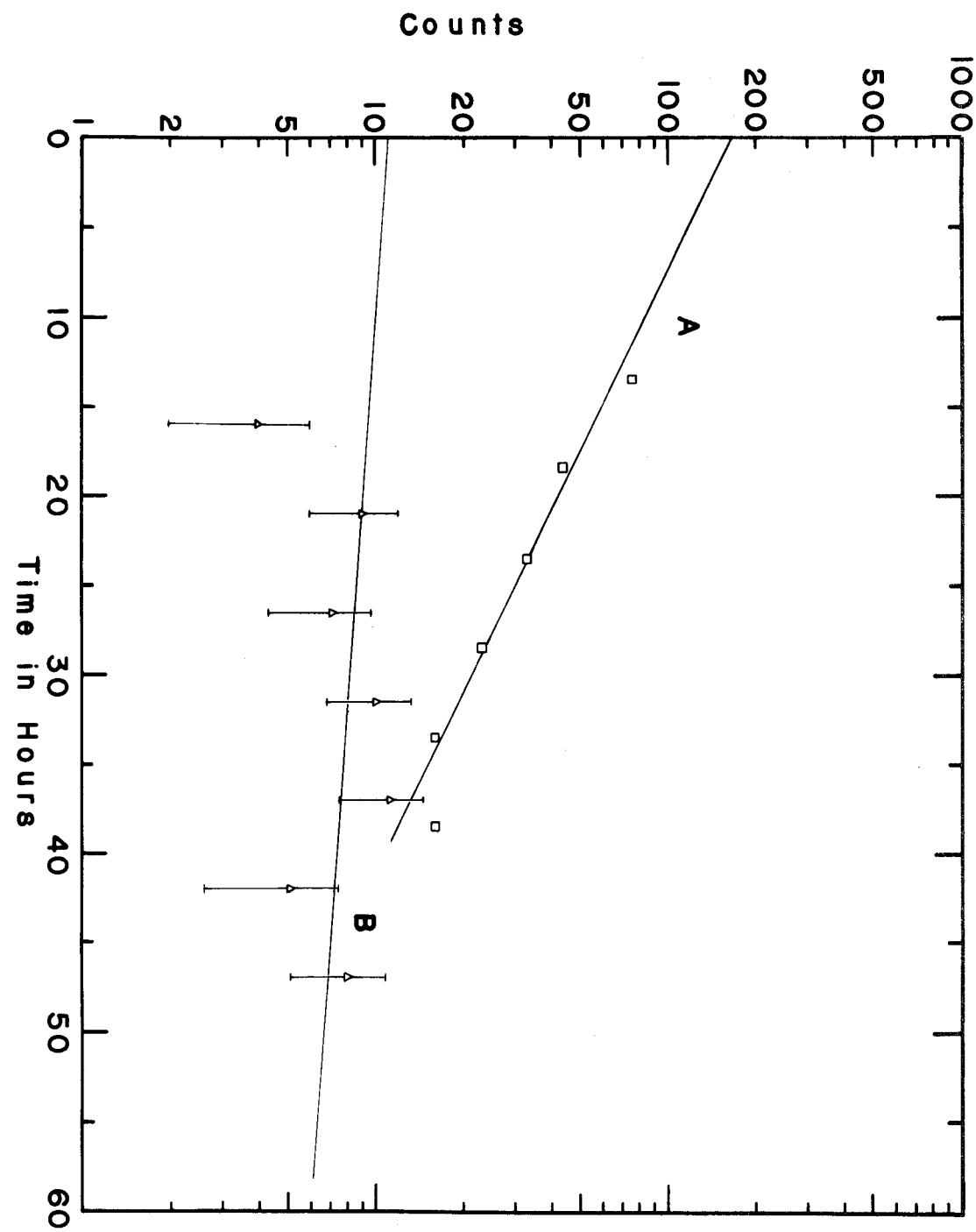
Counts
1
2
5
10
20
50
100
200
500
1000
0
10
20
30
40
50
60
Time in Hours
A
B

CHAPTER IV

EXPERIMENTAL RESULTS

4.1 Reactor Experiments

A search was made for n^8 as a fission product by irradiating a sample of lead at a position close to the core of the McMaster reactor. If n^8 clusters were produced they could be captured at MeV energies or as thermalized species.

4.1.1 Ion-chamber Measurements

(a) Experimental

A 400 mg sample of pure lead metal shot enclosed in a quartz tube was irradiated in the reactor at a neutron flux of 1.8×10^{13} neutrons per second, for 24 hours. After a 5 hour cooling period, the shots were washed with boiling hot nitric acid solution and then dissolved in 3M nitric acid. The lead nitrate was desposited over a stainless steel backing, as described in Chapter III.

(b) Results

The results are shown in Figure 4.1 and Figure 4.2. The sample, after irradiation was washed with nitric acid and the lead nitrate was deposited on a stainless steel sheet. The activity of the sample in the region of the Po^{212} alpha-energy did not decay and was at a level corresponding to the background activity as is evident from the above figures.

Figure 4.2 Plot of Alpha pulses over an energy range of 8.4 to 9.0 MeV vs. time for the irradiated sample.

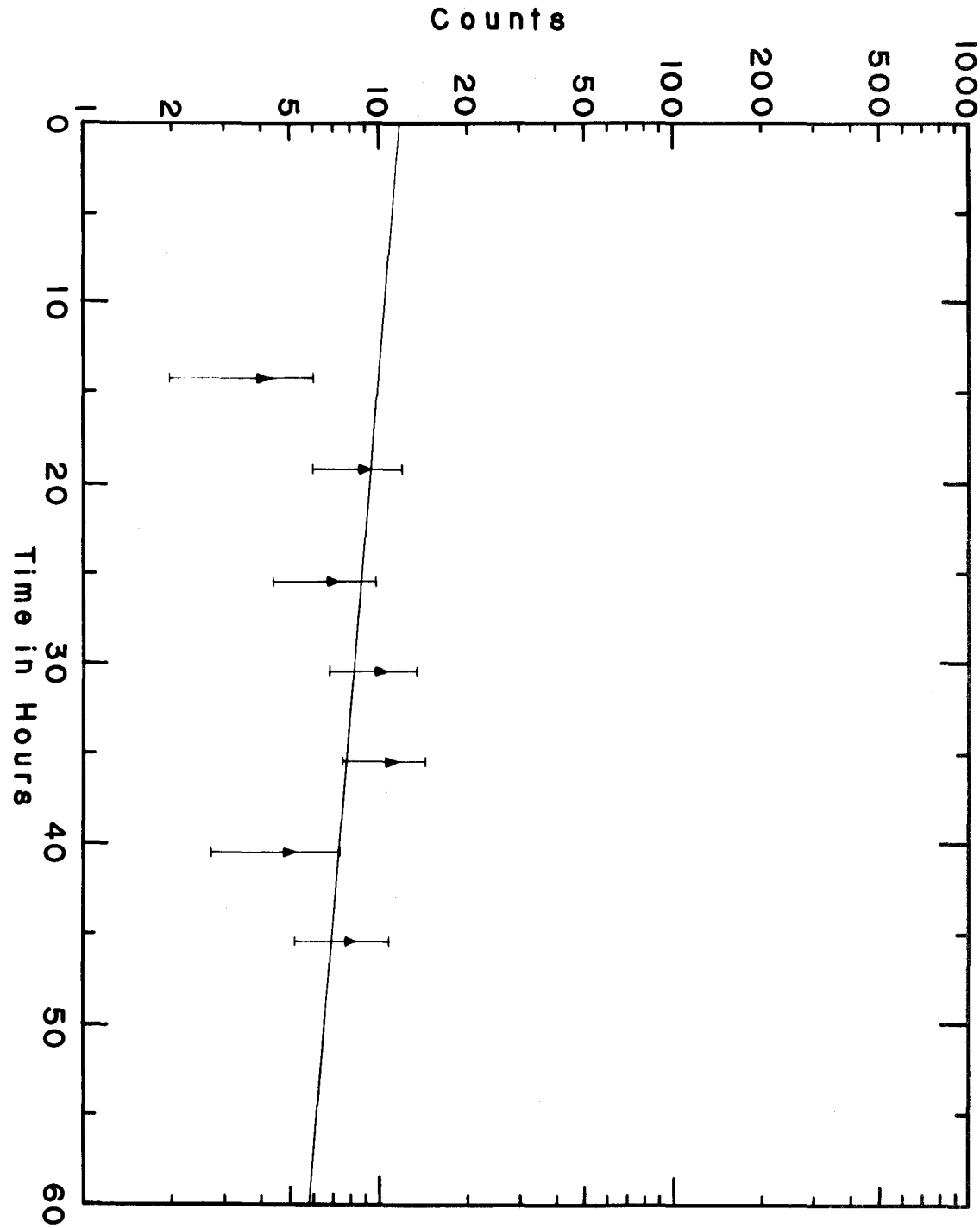
Counts
1
2
5
10
20
50
100
200
500
1000
0
10
20
30
40
50
60
Time in Hours

From the background activity, the upper limit of $(\sigma\varphi)_{n.n}$ (the product of the flux of the neutronic nuclei and the reaction cross-section for the formation of Pb^{212} by them) was estimated to be 1.26×10^{-24} sec^{-1}. If the reaction cross-section for the formation of Pb^{212} is assumed to be 50 mb then the upper limit of the flux of the neutronic nuclei would be one per 7×10^{11} neutrons.

4.1.2 Solid state detector measurements

(a) Experimental

A 3 mg sample of lead deposited on a thin mylar film was irradiated in the reactor core in a neutron flux of 1.8×10^{13} neutrons per cm^2 x sec for two hours. The sample was removed immediately and counted using a solid state surface barrier detector with an area of 50 mm^2.

(b) Results

No alpha-activity which could be attributed to Po^{213} was observed $(\sigma\varphi)_{n.n}$ for the formation of Pb^{213} was found to be 1.44×10^{-22} sec^{-1}. Assuming the reaction cross-section to be 50 mb, the upper limit for the existence of neutronic nuclei in the reactor flux was estimated to be 1 in $6, \times 10^8$ neutrons.

4.1.3 Radio-chemical Separation of Bismuth Isotopes from Lead

(a) Experimental

A 21.4 gm sample of lead metal was placed in an irradiation cell and was irradiated for a period of 5 hours in the reactor core at a neutron flux of 2×10^{13} neutrons per cm^2 x sec. The

irradiated sample was sliced and washed with hot nitric acid solution. From this the isotopes of Bi were extracted and deposited on a copper foil as described in Chapter III. The counting was done as in 4.1.2.

(b) Results

No alpha-activity corresponding to Po^{212} or Po^{213} was observed. The upper limit of $(\sigma\varphi)_{n\cdot n}$ was found to be 7.6×10^{-27} sec^{-1}. This gives the flux of neutronic nuclei to be less than 1 in 10^{14} neutrons per cm^2 x sec.

4.2 High Energy Proton Reactions

The feasibility of employing the high energy proton spallation reactions on lead isotopes for the production of neutronic nuclei was also investigated. From the earlier work on the production of light nuclei with mass numbers 6 to 24 it appeared that the cross-section for n^8 production would be quite large. Experiments were done using 680 MeV and 6.2 GeV energy protons. For the 680 MeV protons the 184" synchrocyclotron and for the 6.2 GeV proton experiments the Bevatron were used. Both of these machines are located at the Lawrence Radiation Laboratory, University of California at Berkeley, California, (U.S.A).

4.2.1 680 MeV Proton Experiments

(a) Experimental

Lead ingots were bombarded for 30 minutes in the proton beam at a current which gave a total flux of 10^{15} protons. After

the irradiation the ingots were cut into pieces and washed with hot nitric acid solution. Each ingot was dissolved in 20 ml of 3M HNO_3 and bismuth isotopes were radio-chemically extracted and electro-plated onto a copper foil. The sample was counted as in 4.1.2.

(b) Results

No α-activity was observed in the range of Po^{212} or Po^{213} α-energy. The sample, however, had Bi^{199m} and Bi^{201m} α-activities. Therefore, it was possible to set an upper limit of the cross-section for the production of neutron clusters in 660 Mev proton reactions with lead.

An upper limit of $(\sigma\varphi)_{n.n}$ was calculated to be 9.3×10^{-25} sec^{-1} and that of the flux of neutronic nuclei was 19 per cm^2 x sec (assuming a capture cross-section of 50mb). At the instant of the termination of bombardment the ratio of the number of neutronic nuclei ($A_{n.n}$) to the total number of Bi^{199}($A_{Bi}199$) formed would be

$$\frac{A_{n.n}}{A_{Bi}199} = \frac{\sigma_{n.n}}{\sigma_{Bi}199}$$

Bi^{199} activity corresponds to the formation of 1.2×10^8 atoms. From these data $\sigma_{n.n}$ (cross-section for the production of neutronic nuclei) was estimated to be

$$\sigma_{n.n} \leq 2.8 \times 10^{-4} . \sigma_{Bi}199$$

The value of $\sigma_{Bi}199$ is taken 10 mb, (Hun-59) which means

$$\sigma_{n.n} < 2.8 \ \mu b.$$

4.2.3 6.2 GeV Proton Reactions

(a) Experiment

This experiment was performed at Bevatron using 6.2 GeV proton beam impinged on a series of five lead ingots (0.5 x 0.5 x 2 cm^3). Beam pulses, 0.8 second long and containing on the average of 6 x 10^{11} protons bombarded the target every five seconds. The ingots were irradiated for a period of 30 minutes. The proton beam was monitored using Au foils. After irradiation, the ingots were washed and a sample of Bi was prepared as described in Chapter III.

(b) Results

The ingot next to the primary target ingot was chosen for the experiment and α-activities of Po^{212} and Po^{213} were observed. The total number of counts of Po^{212} and Po^{213} observed at the end of irradiation were (166 ± 18) and (280 ± 24) respectively. Therefore, the total number of atoms of Bi^{212} and Bi^{213} formed in the target during the 30 minutes irradiation was (364 ± 39) and (434 ± 37) respectively.

With this positive result, other experiments were performed to determine whether these activities were indeed formed by neutronic nuclei. The role of secondary fragments was immediately considered and it was ascertained that the only secondary fragment which could interfere would be Li^{11}, a nuclide discovered by Poskanzer et. al. (Pos-66) which could produce At^{217} from a Li^{11}, 2n reaction on Pb^{208}.

Mekhedov (Mek-64) has studied the formation of At isotopes by secondary reactions in lead. In our experiments

astatine activities were also observed presumably formed by (Li,xn) reactions. Since lead is a multi-isotope element, a large number of reactions are possible. The main contribution to the astatine activities could come from (Li^6,xn), (Li^7,xn), (Li^8,xn), (Li^9,xn) and (Li^{11},xn) reactions. The observed Po^{213} and Po^{212} activities could very well be ascribed to (Li^{11},xn) reaction. Apart from this, nuclear reactions of the type Pb^{208} (He^6,π^+n)Bi^{213}, Pb^{207}(He^6,π^+)Bi^{213} or the emission of $2\pi^+$ to produce the lead isotopes are also possible, but the probability with which they would occur would be very small (Mek-64). Whether the observed activities of $Po^{212,213}$ could be attributed to the formation of $At^{217,216}$ by Pb(Li^{11},xn) reaction was verified by calculating the cross-section for the production of Li^{11} from the the experimental data of this work and comparing it with the result of Paskanzer et. al. (Pos-66).

If the reaction cross-section of the Pb(Li^{11},xn) reaction were 3 μb then from the Po^{212} and Po^{213} activities the flux of Li^{11} would be 8.8×10^6 sec^{-1}. From the alpha-activity of the gold monitor foil (because of Tb^{149}) the proton flux was calculated to be 4.62×10^{11} sec^{-1}. Therefore, the cross-section for the production of Li^{11} by 6.2 GeV protons would be 1 mb.

The experimental results of Poskanzer et. al. (Pos-66) also gave the production cross-section of Li^{11} from U^{238} spallation as 1 mb. This means that the Po^{212} and Po^{213} observed in our experiments is essentially caused by secondary reactions

involving Li^{11}. It also means that our method of detecting neutron clusters in high energy proton reactions cannot be used because of the interference of secondary reactions.

4.3 Conclusion

On the basis of the experimental results obtained in this investigation, we conclude that the neutronic nuclei component in the neutron flux of the reactor is less than 1 in 10^{14} neutrons. The possibility of the existence of heavier neutronic nuclei, however cannot be excluded. On the basis of the theoretical as well as all of the experimental results including the present work it appears that light neutronic nuclei up to approximately mass 10 are not particle stable.

The cross-section ($\sigma^{p}_{n.n}$) for the formation of neutronic nuclei by 680 MeV protons was estimated to be less than 2.8 μb. For higher proton energies $\sigma^{p}_{n.n}$ would be expected to increase. However, our results at higher energies do not provide any information because of the interference of Li^{11} which is also produced in greater yield at the higher bombarding energies.

APPENDIX I

IONIZATION OF ARGON MIXTURES

When an alpha-particle passes through a gas like argon, it loses its energy mainly in ionizing and exciting the gas.

$$Ar \xrightarrow{\alpha} Ar^{+} + \bar{e} \qquad \text{Ionization}$$

(Ionization potential 15.5 eV.)

$$Ar \xrightarrow{\alpha} Ar^{*} \qquad \text{Excitation}$$

The process of excitation leaves the argon atoms in two states of excitation (Mel-54), each of which has sufficiently long life that transfers of energy in collisional processes can take place. One of the states occur at 15.0 eV and the other at 11.6 eV.

These states may be de-excited by either of the following ways:

$Ar^{*} \longrightarrow Ar + h\nu$. Spontaneous radiation emission

$Ar^{*} + Ar \longrightarrow Ar + Ar^{*}$ Transfer of energy with radiation less collision.

If an impurity gas or additive gas X is present then another type of collision can take place:

$Ar^{*} + X \longrightarrow Ar + X^{*}$. Transfer of energy in a collision with another molecule.

If the ionization potential of X is less than the excitation

energy of the meta-stable states then addition of X will increase the ionization substantially. If it is higher, then there will be a small increase in ionization.

The additive gases used in this work were methane and acetylene for which the ionization potentials are 13.1 eV and 11.40 eV respectively. Therefore, addition of acetylene to argon will result in a substantial increase in ionization compared to methane. The processes that can take place are:

$$CH_4^* \longrightarrow CH_4^+ + \bar{e} \qquad \text{Ionization}$$

$$CH_4^* \longrightarrow CH_4 + h\nu \qquad \text{De-excitation}$$

and

$$C_2H_2^* \longrightarrow C_2H_2^+ + \bar{e} \qquad \text{Ionization.}$$

In the case of CH_4 addition, the slight increase in ionization may be due to the second-excited state of Ar. But for acetylene addition, collisional energy transfer from both excited states of Ar to C_2H_2 will take place followed by break-up of the C_2H_2 into an ion-pair.

APPENDIX II

INFLUENCE OF SOURCE THICKNESS ON THE RESOULUTION

When alpha-particles are emitted by a source of finite thickness some of its energy is deposited in the sample. Consequently the alpha-spectral line width increases and a low energy tail develops.

Let us consider an alpha source of thickness h and total area S. If a unit volume emits ν alpha-particles per unit time, then the number of particles, dN impinging on the area ds from a spherical shell between r and r + dr (figure II.1(a)) is given by

$$dN = \frac{ds\,\nu\,dr}{4\pi} \int_0^{2\pi} d\phi \int_{\theta_1}^{\pi/2} \sin\theta\cos\theta\cdot d\theta\cdot$$

$$= \frac{\nu\,ds}{4}\cdot dr\cdot\cos^2\theta_1\cdot$$

where $\theta_1 = 0$ for $r \leq h$

and $\theta_1 = \cos^{-1}\frac{h}{r}$ for $r \geq h$

over the full area the total number of particles $= \frac{\nu\cdot S}{4}\cos^2\theta_1\cdot dr$.

The range of the alpha-particles is proportional to the n^{th} power of the energy, i.e.,

$$R = a\,E^n.$$

where R = Range of alpha-particles of Energy E

a = Proportionality constant

and n = 1.5 for α-particles.

Then these particles should travel a distance r in the source i.e.,

$$r = R_o - R$$

$$= R_o - aE^n$$

$$= R_o(1-\varepsilon^n)$$

where $\varepsilon = \frac{E}{E_o}$

R_o is the range of alpha-particles at full energy E_o. From this after differentiation one gets

$$dr = -n \cdot R_o \cdot \varepsilon^{n-1}\, dE$$

this means that as the thickness increases the energy of the alpha-particles emerging from the sample will decrease. The distribution of particles can be written as a function of energy and is given by

$$dN_\varepsilon = \frac{N_o R_o n}{4h}\ \varepsilon^{n-1} \cdot dE \quad \text{if } \varepsilon \geq \left(1 - \frac{h}{R_o}\right)^{1/n} \qquad \text{II•1}$$

and

$$dN_\varepsilon = \frac{N_o hn}{4R_o} \cdot \frac{\varepsilon^{n-1}}{(1-\varepsilon^n)^2} \cdot dE \quad \text{if } \varepsilon \leq \left(1 - \frac{h}{R_o}\right)^{1/n} \qquad \text{II•2}$$

where $N_o = v \cdot S \cdot h$

The equations I•1 and II•2 for n = 1 are the same as given by Haeberli, Huber and Baldinger (Hae-53). Figure II•1(b) shows the energy distribution of the particles emerging from a source of thickness h.

To determine the shape of the experimental spectra it is

Figure II•1 (a) Diagram for calculating the effect of source thickness on the spectrum shape.

(b) Energy distribution of alpha-particles emitted from a source

1 - curve calculated using equation II•1

2 - curve calculated using equation II•2.

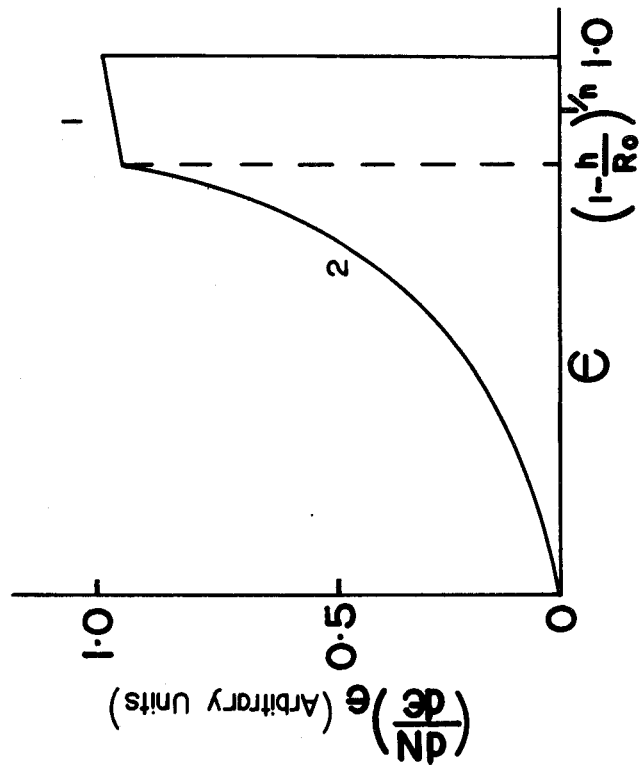
$\left(\frac{dN}{Np}\right)_\epsilon$ (Arbitrary Units)
1·0
0·5
0
2
ϵ
$\left(1-\frac{h}{R_0}\right)^{1/n}$
1·0

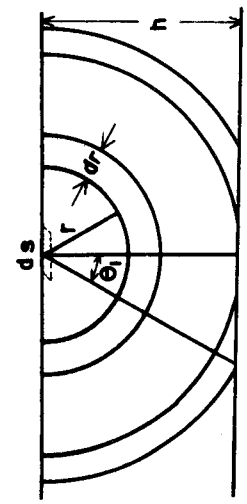
h
dr
r
ds
θ_i

necessary to consider the effect of the detector resolution function. If the resolution function of the detector is $R(\varepsilon_2,\varepsilon_1)$ and the energy distribution $S(\varepsilon_1)$, then the experimentally observed spectrum $M(\varepsilon_2)$ will be given by

$$M(\varepsilon_2) = \int_0^{\infty} R(\varepsilon_2,\varepsilon_1)\cdot S(\varepsilon_1)\, dE_1. \qquad \text{II}\cdot 3$$

Using for the resolution function $R(\varepsilon_2,\varepsilon_1)$ a Gaussian distribution and equations II·1 and II·2 for the energy distribution of the alpha-particles, the experimental spectra can be written as

$$M(\varepsilon_2) = \int_0^{\varepsilon} \frac{N_o nh}{\sqrt{2\pi\sigma}\, 4R_o} \cdot \frac{\varepsilon_1^{n-1}}{(1-\varepsilon_1^n)^2} \cdot \exp(-(\varepsilon_2-\varepsilon_1)^2/2\sigma^2) d\varepsilon_1 +$$

$$\frac{N_o nR_o}{\sqrt{2\pi\sigma}\, 4h} \int_{\varepsilon}^{1} \varepsilon_1^{n-1} \cdot \exp\,(-(\varepsilon_2-\varepsilon_1)^2/2\sigma^2)\, d\varepsilon_1. \qquad \text{II}\cdot 4$$

This equation II·4 describes the influence of source thickness on the resolution. Representative spectum for different source thicknesses are shown in Figure 2.8(a).

REFERENCES

Ajd-65 V. Ajdacic, M. Cerineo, B. Lalovic, G. Paic, I. Slaus and P. Tomas, Phys. Rev. Letters 14, 444, 1965.

Arg-63 P. E. Argan and A. Piazzoli, Phys. Letters 4, 350, 1963.

Bar-67 M. Barbi, Nuclear Phys. A99, 522, 1967.

Bea-54 G. Beard and M. L. Wiedenbeck, Phys. Rev., 95, 1245, 1954.

Bea-58 G. Beard and W. H. Kelly, Nuclear Phys. 8, 207, 1958.

Bet-37 H. Bethe, Revs. Modern Phys. 9, 263, 1937.

Blo-60 J. Blomquist and S. Wahlborn, Arkiv Fysik, 16, No. 46, 1960.

Bor-63 T. E. Bortner, G. S. Hurst, M. Edmunston and J. E. Parks, ORNL-3422, 1963.

Bri-64 O. Brill, N. Venikov, V. A. Kurashov, A. Ogloblin, V. Pankratov and V. Rudakov, Phys. Letters 12, 51, 1964.

Bun-49 O. Buneman, T. E. Cranshaw and J. A. Harvey, Can. J. Research A27, 191, 1949.

Bur-67 V. R. Burmestrove, B. G. Kiselev, V. A. Shilin, and V. L. Kochetkov, Soviet, J. Nuclear Phys. 4, 239, 1967.

Cer-66 J. Cerny, S. W. Casper, G. W. Butler, R. H. Rehl, F. S. Gaulding, D.A. Landis and C. Detraz, Phys. Rev. Letters 16, 469, 1966.

Cha-63 M. L. Chaudhury, Phys. Rev. 130, 2339, 1963.

Coh-64 R. D. Cohen and A. D. Canaris, Reported in Soviet Phys.-Uspekhi, 8, 177, 1965.

Col-57 T. L. Collins, F. M. Rourke and F. A. White, Phys. Rev. 105, 196, 1957.

Con-29 E. U. Condon and R. W. Gurney, Phys. Rev. 33, 127, 1929.

Cra-48 T. E. Cranshaw and J. A. Harvey, Can. J. Research A26, 243, 1948.

Cro-60 T. B. Crockett, T. T. McMillan and J. W. Crowe, NAA-SR-4433 (instruments) 1960.

Cue-46 P. Cuer and C. M. G. Lattes , Nature, 158, 197, 1946.

Cur-34 M. Curie and F. Joliot, Compt rend. 198, 360, 1934.

Don-64 D. Donhoffer, Nucl. Phys. 50, 489, 1964.

Dav-64 R. E. P. Davis, A. Beretvas, N. E. Booth, C. Dalnick, R. J. Esterling, R. E. Hill, H. Raymond and H. Sherden, Bull. Am. Phys. Soc. 9, 627, 1964.

Dem-48 A. J. Dempster, Phys. Rev. 73, 1125, 1948.

Dem-49 A. J. Dempster, ANL-4355, 1949.

Det-65 C. Detraze, J. Cerny and R. H. Pehl, Phys. Rev. Letters 14, 708, 1965.

Dev-61 J. R. Devoe, NAS-NRC-Pub. 895, 1961.

Dun-53 D. C. Dunlavey and G. T. Seaborg, Phys. Rev. 92, 206, 1953.

Fac-56 U. Facchinni, M. Forte, A. Malvicini and J. Rosslini, Energia Nucleare 3, 182, 1956.

Fan-47 U. Fano, Phys. Rev. 72, 86, 1947.

Fer-52 A. J. Feguson and J. H. Montague, Phys. Rev. 87, 215, 1952.

Fri-62 J. S. Fritz and B. B. Garralda, Anal. Chem. 34, 102, 1962.

Fri-63 A. M. Friedman, J. Milstead and A. L. Harkness, Bull. Am. Phys. Soc. II, 8, 525, 1963.

Fri-66 A. M. Friedman, J. Milstead, D. Metta, D. Handerson, J. Lerner, A. L. Harkness and D. J. Rokop, Radio chim. Acta. 5, 192, 1966.

Fus-67 E. Fuschine, C. Maroni, A. Uguzzoni, E. Verondini and A. Vitale, Nuovo Cimento 48B, 190, 1967.

Gam-29 G. Gamow, Z. Physik 52, 510, 1929.

Gol-60 V. I. Goldanskii, Soviet Phys. JETP, 11, 1179, 1960.

Gra-61 G. Graeffe and M. Nurmia, Ann. Acad. Sci., Fennicae Ser. A, VI No. 77, 1961.

Gro-64 Gromov, Makhunka et. al. Materialy XIV. exhegednogo Soveschchaniya po Yadernoispectroskopii v Tbilisi/ 14-22 Febralya, 1964 (in Russian).

Hae-49 C. H. Haenny, M. Najar and M. Gaillourd, Helv. Phys. Acta 22, 611, 1949.

Hae-53 W. Haeberli, P. Huber and E. Baldinger, Helv. Phys. Acta 26, 145, 1953.

Han-50 G. C. Hanna, Phys. Rev. 80, 530, 1950.

Han-59 G. C. Hanna, Experimental Nuclear Physics III, 202, 1959 Edited by E. Segre, John Wiley and Sons, N.Y.

Har-57 B. G. Harvey, H. G. Jackson, T. A. Eastwood and G. C. Hanna, Can. J. Phys. 35, 258, 1957.

Her-34 M. Herzfinkel and A. Wroneberg, Compt rend, 199, 133, 1934.

Hev-32 G. Hevesy and M. Pahl, Nature 130, 846, 1932.

Hev-33 G. Hevesy, M. Pahl and R. Hoseman, Z. Physik 83, 43, 1933.

Hil-61 C. R. Hill, Nuclear Instr. and Methods 12, 299, 1961.

Hof-21 G. Hoffmann, Z. Physik 1, 254, 1921.

Hos-36 R. Hoseman, Z. Physik 99, 405, 1936.

Hun-59 E. T. Hunter and J. M. Miller, Phys. Rev. 115, 1053, 1959.

Igo-58 G. Igo, Phys. Rev. Letters 1, 72, 1958.

Ing-48 M. G. Ingrahm, O. C. Hess and R. J. Hayden, Phys. Rev. 73, 780, 1948.

Jes-50 W. P. Jesse and J. Sadauskis, Phys. Rev. 77, 1, 1950.

Jes-51 W. P. Jesse, AECU-1428, 1951.

Jes-52 W. P. Jesse and J. Sadauskis, Phys. Rev. 88, 417, 1952.

Kar-60a M. Karras, Ann. Acad. Sci. Fennicae Ser. A, VI No. 65, 1960.

Kat-62 A. Katase, M. Seki, Akiyoshi, Yoshimura and Sonoda, J. Phys. Soc. Japan 17, 1211, 1962.

Koh-49 T. P. Kohman, Phys. Rev. 76, 448, 1949.

Koc-61 G. E. Kocharov and G. A. Korolev, Bull. Acad. Sci. USSR Phys. Ser. 25, 227, 1961.

Les-54 G. E. Leslie, Ph.D. Thesis, North Carolina State College, AD-37749, 1954.

Lew-36 L. Lewin, Nature, 138, 326, 1936.

Lib-34 W. F. Libby, Phys. Rev. 46, 196, 1934.

Lon-52 J. K. Long, M. L. Pool and D. M. Kundu, Phys. Rev. 88, 171, 1952

Loz-61 O. V. Lozhkin, Rimskii, A. A. Korsakov, Soviet Phys. JETP 13, 1064, 1960.

Lyf-34 D. Lyford and J. H. Beardon, Phys. Rev. 45, 743, 1934.

Mac-59 R. D. Macfarlane, Doctoral Disseration, Carnegie Inst. of Tech. Pittsburgh, Pa. 1959. NYO-7687.

Mac-60 R. D. Macfarlane, UCRL-9352, 1960.

Mac-61a R. D. Macfarlane and T. P. Kohman, Phys. Rev. 121, 1758, 1961.

Mac-61b R. D. Macfarlane, J. Inorg. and Nuclear Chem. 19, 9, 1961.

Mac-62 R. D. Macfarlane, Phys. Rev. 126, 274, 1962.

Mac-63a R. D. Macfarlane and R. D. Griffioen, Phys. Rev. 130, 1941.

Mac-63b R. D. Macfarlane and R. D. Griffioen, Phys. Rev. 131, 2176, 1963.

Mac-64a R. D. Macfarlane and D. W. Seegmiller, Nuclear Phys. 53, 449, 1964.

Mac-64b R. D. Macfarlane, J. O. Rasmussen and M. Rho, Phys. Rev. 134, B1196, 1964.

Mac-65 R. D. Macfarlane, Phys. Rev. 137, B1448, 1965.

Mac-66 J. D. Macdougall, W. Mclatchie, S. Whineray, and H. E. Duckworth, Z. Naturforsch, 21a, 63, 1966.

Mad-34 M. Mader, Z. Physik 88, 601, 1934.

Mat-65 J. H. E. Mattauch, W. Thiel and A. H. Wapstra, Nuclear Phys. 67, 1, 1965.

Mek-64 V. N. Mekhadov, Nuclear Phys. 53, 225, 1964.

Mel-54 C. E. Melton, G. S. Hurst and T. E. Bortner, Phys. Rev. 93, 643, 1954.

Mit-66 A. N. Mitra and V. S. Bhasin, Phys. Rev. Letters 16, 523, 1966.

Nef-63 B. M. K. Nefkens, Phys. Rev. Letters 10, 243, 1963.

Nob-62 R. A. Nobles, Phys. Rev. 126, 1508, 1962.

Kar-60b M. Karras and M. Nurmia Nature 185, 601, 1960.

Nur-63 M. Nurmia and M. Karras Geophysica, 7, 83, 1963.

Nur-64 M. Nurmia, G. Graeffe, K. Valliand and J. Aaltonen, Ann. Acad. Sci. Fennicae Ser. A, VI No. 148, 1964.

Oka-67 K. Okamoto and B. Davies, Phys. Rev. Letters 24B, 18, 1967.

Orb-63 F. E. Orbe, I. H. Qureshi and W. W. Meinke, Anal. Chem. 35, 1436, 1963.

Ort-34 G. Ortner and J. Schintelmeister, Z. Physik, 90, 698, 1934.

Osb-64 R. V. Osborne and C. R. Hill, Nuclear Instr. Methods 29, 101, 1964.

Pet-62 K. A. Petrzhak and M. I. Yakunin, Soviet Phys. JETP, 14, 1265, 1962.

Pic-49 E. Picciotto, Compt rend. 229, 117, 1949.

Pog-65 J. K. Poggenburg, Ph.D. Thesis, UCRL-16187, 1965.

Por-54 W. Porschen and W. Riezler, Z. Naturforsch, 9a, 701, 1954.

Por-56 W. Porschen and W. Riezler, Z. Naturforsch. 11a, 143, 1956.

Pos-66 A. M. Poskanzer, S. W. Casper, E. K. Hyde and J. Cerny, Phys. Rev. Letters 17, 1271, 1966.

Ras-50 J. O. Rasmussen, F. L. Reynolds, S. G. Thompson, and A. Ghiorso, Phys. Rev. 80, 475, 1950.

Ras-53 J. O. Rasmussen, S. G. Thompson and A. Ghiorso, Phys. Rev. 89, 33, 1953.

Ras-59a J. O. Rasmussen, Phys. Rev. 113, 1593, 1959.

Ras-59b J. O. Rasmussen, Phys. Rev. 115, 1675, 1959.

Ras-63 J. O. Rasmussen, Nuclear Phys. 44, 93, 1963.

Rie-57 W. Riezler and G. Kauw, Z. Naturforsch 12a, 665, 1957.

Rie-57 W. Riezler and G. Kauw, Z. Naturforsch 12a, 665, 1957.

Rie-58 W. Riezler and G. Kauw, Z. Naturforsch 13a, 904, 1958.

Rie-59 W. Riezler and G. Kauw, Z. Naturforsch 14a 196, 1959.

Sak-61 M. Sakisaka and N. Tomita, J. Phys. Soc. Japan 16, 2597, 1961.

Sch-63 J. O. Schiffer and R. Vandenbosch, Phys. Letters 5, 215, 1963.

Sii-62 A. Siivola, Ann. Acad. Sci. Fennicae Ser. A, VI No. 109, 1962.

Sii-64 A. Siivola and G. Graeffe, UCRL-11828, 20, 1964.

Sii-66 A Siivola, Nuclear Phys. 84, 385, 1966.

Szt-53 D. Szteinsznaider, J. Phys. radium 14, 465, 1953.

Taa-61 R. Taagepera and M. Nurmia, Ann. Acad. Sci. Fennicae Ser. A, VI No. 78, 1961.

Tan-65 Y. C. Tang and B. F. Bayman, Phys. Rev. Letters 15, 165, 1965.

Tay-35 H. J. Taylor, Nature 136, 719, 1935.

Tho-49 S. G. Thompson, A. Ghiorso, J. O. Rasmussen and G. T. Seaborg, Phys. Rev. 76, 1406, 1949.

Tho-49 S. T. Thornton, J. K. Bair, C. M. Jones and H. B. Willard, Phys. Rev. Letters 17, 701, 1966.

Tot-60 K. S. Toth and J. O. Rasmussen, Nuclear Phys. 16, 474, 1960.

Val-65 K. Valli, J. Aaltonen, G. Graeffe, M. Nurmia and R. Poyhonen, Ann. Acad. Sci. Fennicae Ser. A, VI No. 177, 1965.

Voi-65 V. K. Voitovetskii, I. L. Korsunskii and Yu F. Pazhin, Soviet Phys. JETP 20, 1084, 1965.

Vor-60 A. A. Vorobev, A. P. Komar, V. A. Korolev and G. E. Solyakin, Soviet Phys. JETP, 37, 386, 1960.

Vor-63 A. A. Vorobev, A. P. Komar and V. A. Korolev, Soviet Phys. JETP 16, 306, 1963.

Wea-50 B. Weaver, Phys. Rev. 80, 301, 1950.

Weg-61 H. E. Wegner, Bull. Am. Phys. Soc. 6, 307, 1961.

Whe-65 S. L. Whetstone and T. D. Thomas, Bull. Am. Phys. Soc. 10, 722, 1965.

Whe-67 S. L. Whetstone and T. D. Thomas, Phys. Rev. 154, 1174, 1967.

Wil-38 J. R. Wilkins and A. J. Dempster, Phys. Rev. 54, 315, 1938.

Wil-50 D.H. Wilkinson, Ionization Chamber and Counters. Cambridge University Press, 1950.

Wil-65 H. B. Willard, J. K. Blair and C. M. Jones, Phys. Letters 9, 339, 1964.

Wri-61 P. M. Wright, E. P. Steinberg and L. E. Glendnin, Phys. Rev. 123, 205, 1961.

Zeh-63 H. D. Zeh, Z. Physik, 175, 490, 1963.

Zel-60 Ya. B. Zeldovich, Soviet Phys. JETP 11, 812, 1960.

Baz-65 A. I. Baz, V. I. Goldanskii and Ya. B. Zeldovich, Soviet Phys. Uspekhi 8, 445, 1965.